



HAL
open science

Low-temperature formation of pyridine and (iso)quinoline via neutral–neutral reactions

Zhenghai Yang, Chao He, Shane Goettl, Alexander M. Mebel, Paulo Velloso, Márcio Alves, Breno Galvão, Jean-Christophe Loison, Kevin Hickson, Michel Dobrijevic, et al.

► **To cite this version:**

Zhenghai Yang, Chao He, Shane Goettl, Alexander M. Mebel, Paulo Velloso, et al.. Low-temperature formation of pyridine and (iso)quinoline via neutral–neutral reactions. *Nature Astronomy*, 2024, 10.1038/s41550-024-02267-y . hal-04627228

HAL Id: hal-04627228

<https://hal.science/hal-04627228>

Submitted on 19 Jul 2024

HAL is a multi-disciplinary open access archive for the deposit and dissemination of scientific research documents, whether they are published or not. The documents may come from teaching and research institutions in France or abroad, or from public or private research centers.

L'archive ouverte pluridisciplinaire **HAL**, est destinée au dépôt et à la diffusion de documents scientifiques de niveau recherche, publiés ou non, émanant des établissements d'enseignement et de recherche français ou étrangers, des laboratoires publics ou privés.

Low-temperature formation of pyridine and (iso)quinoline via neutral–neutral reactions

Zhenghai Yang,¹ Chao He,¹ Shane J. Goettl,¹ Alexander M. Mebel,^{2*} Paulo F. G. Velloso,³ Márcio O. Alves,³ Breno R. L. Galvão,^{3*} Jean-Christophe Loison,^{4*} Kevin M. Hickson,⁴ Michel Dobrijevic,⁵ Xiaohu Li,^{6,7*} Ralf I. Kaiser^{1*}

¹ Department of Chemistry, University of Hawaii at Manoa, 2545 McCarthy Mall, Honolulu, HI 96822 (USA)

² Department of Chemistry and Biochemistry, Florida International University, Miami, Florida 33199, USA

³ Centro Federal de Educação Tecnológica de Minas Gerais, CEFET-MG, Av. Amazonas 5253, 30421-169 Belo Horizonte, Minas Gerais, Brazil

⁴ Institut des Sciences Moléculaires, CNRS, Univ. Bordeaux, 351 Cours de la Libération, 33400 Talence, France

⁵ Laboratoire d'Astrophysique de Bordeaux, Univ. Bordeaux, CNRS, B18N, Allée Geoffroy Saint-Hilaire, 33615 Pessac, France

⁶ Xinjiang Astronomical Observatory, Chinese Academy of Sciences, Urumqi, Xinjiang 830011, P. R. China

⁷ Key Laboratory of Radio Astronomy, Chinese Academy of Sciences, Urumqi, Xinjiang 830011, P. R. China

* Correspondence to:

ralfk@hawaii.edu, mebela@fiu.edu, brenogalvao@gmail.com, jean-christophe.loison@cnrs.fr, xiaohu.li@xao.ac.cn

The file includes:

Main text: 4880 words

Methods: 840 words

Legends: 465 words

Number of main text references: 76

Number of methods references: 8

Number of figures: 6

Aromatic molecules represent fundamental building blocks in prebiotic chemistry and are contemplated as vital precursors to DNA and RNA nitrogen bases. However, despite the identification of some 300 molecules in extraterrestrial environments, the pathways to pyridine (C_5H_5N), pyridinyl ($C_5H_4N^\bullet$), and (iso)quinoline (C_9H_7N) – the simplest representative of mono and bicyclic aromatic molecule carrying nitrogen – are elusive. Here, we afford compelling evidence on the gas-phase formation of methylene amidogen (H_2CN^\bullet) and cyanomethyl (H_2CCN^\bullet) radicals via molecular beam studies and electronic structure calculations. The modeling of the chemistries of Taurus Molecular Cloud (TMC-1) and Titan's atmosphere contemplates a complex chain of reactions synthesizing pyridine, pyridinyl, and (iso)quinoline from H_2CN^\bullet and H_2CCN^\bullet at levels of up to 75%. This study affords unique entry points to precursors of DNA and RNA nitrogen bases in hydrocarbon-rich extraterrestrial environments thus changing the way we think about the origin of prebiotic molecules in our Galaxy.

Since the very first discovery of biorelevant, heteroaromatic molecules such as vitamin B3 (niacin)^{1,2} and nucleobases (pyrimidines, purines)³ in carbonaceous chondrites including Murchison^{3,4}, critical questions have arisen on their formation routes in extraterrestrial environments. The identification of a series of terrestrially rare nucleobases such as 6-diaminopurine along with the ¹⁵N/¹⁴N isotope enrichment suggests an interstellar origin⁴ thus providing a vital link between cold molecular clouds as their origin and their identification in our solar system. However, well defined formation routes of these molecules are still lacking. Their stem compounds - polycyclic aromatic hydrocarbons (PAHs) along with their cations and (partially) hydrogenated counterparts⁵⁻⁷ - have been proposed to be associated with the synthesis of these biorelevant molecules in the interstellar medium (ISM), though not having unraveled how a stable C-H moiety in PAHs can be replaced by an isoelectronic nitrogen atom (N) in NPAHs. The 6.2 μm (1613 cm^{-1}) infrared emission band in deep space has been linked to protonated PAHs⁸, but has also been discussed as the result of NPAHs⁹ with PAHs and NPAHs accounting for up to 30 % of the cosmic carbon budget¹⁰. Whereas well-defined low-temperature (cold molecular clouds; TMC-1) and high-temperature routes (circumstellar envelopes; IRC +10216) to PAH formation in interstellar and circumstellar environments have begun to emerge¹¹, surprisingly little is known on the gas-phase synthesis of their nitrogen-substituted counterparts (NPAHs). This lack of knowledge is rather staggering considering that these aromatics carry the cyclic nitrogen-carbon skeletons of a key class of astrobiologically important molecules: nitrogen bases of deoxyribonucleic acid (DNA) and ribonucleic acid (RNA)^{9,12}.

Recent astrochemical models advocated that the carbon – nitrogen chemistries in molecular clouds can be linked with complex reaction networks¹³ of gas phase ion–molecule¹⁴ and neutral–neutral reactions¹⁵ of aromatic (AR) and resonantly stabilized free radicals (RSFR) such as phenyl ($\text{C}_6\text{H}_5^\bullet$) and propargyl ($\text{C}_3\text{H}_3^\bullet$) along with their nitrogen counterparts pyridinyl ($\text{C}_5\text{H}_4\text{N}^\bullet$) and cyanomethyl ($\text{H}_2\text{CCN}^\bullet$)^{14,16-18}. Further, the synthesis of pyridine ($\text{C}_5\text{H}_5\text{N}$) has been proposed to be driven by radical mediated reactions of hydrogen cyanide (HCN)¹⁹ and via de-facto methylidyne radical (CH) insertion into pyrrole ($\text{C}_4\text{H}_5\text{N}$)²⁰. These reaction networks have been ‘borrowed’ from the planetary science community attempting to rationalize the existence of both stratospheric PAHs and NPAHs in Titan’s atmosphere determined from Cassini’s Visual and Infrared Mapping Spectrometer (VIMS) measurements at 3.28 μm ($3,049\text{ cm}^{-1}$)²¹ and Composite Infrared

Spectrometer (CIRS) measurements at $71.43\ \mu\text{m}$ ($140\ \text{cm}^{-1}$)^{22,23}, and through Cassini's Plasma Spectrometer (CAPS)²⁴. The latter detected positively and negatively charged particles with molecular weights less than 8,000 amu containing (N)PAHs along with their fundamental building blocks benzene (C_6H_6 ; $m/z = 78$) and pyridine ($\text{C}_5\text{H}_5\text{N}$; $m/z = 79$)^{14,24,25}. Overall, to date, an understanding of the synthesis of benzene along with aromatics carrying up to six rings such as corannulene ($\text{C}_{20}\text{H}_{10}$)²⁶ and helicenes ($\text{C}_{26}\text{H}_{16}$)²⁷ is beginning to emerge¹¹. However, the underlying elementary processes even leading to the simplest representative of mono- and bicyclic aromatic molecule carrying nitrogen, i.e. pyridine ($\text{C}_5\text{H}_5\text{N}$; **1**) and (iso)quinoline ($\text{C}_9\text{H}_7\text{N}$; **2/3**) – together with their cyanomethyl ($\text{H}_2\text{CCN}^\bullet$; **4**) and methylene amidogen ($\text{H}_2\text{CN}^\bullet$; **5**) precursors is still in its infancy (Figure 1). The understanding of these gas phase reactions and the formation of the first carbon – nitrogen bonds from the ‘bottom up’ is fundamental to our knowledge of how nitrogen containing aromatics can be produced abiotically in low temperature interstellar and solar system environments from the simple closed shell nitrogen containing hydride (ammonia; NH_3) and reactive carbon-based reactants in form of atomic carbon (C) and dicarbon (C_2).

Here, we report on the gas phase preparation of the methylene amidogen radical ($\text{H}_2\text{CN}^\bullet$, X^2B_2) and of the resonantly stabilized cyanomethyl radical ($\text{H}_2\text{CCN}^\bullet$, X^2B_1) via bimolecular reactions of atomic carbon (C, ^3P) and of dicarbon (C_2 , $\text{X}^1\Sigma_g^+/\text{a}^3\Pi_u$) with ammonia (NH_3 , X^1A_1) exploiting crossed molecular beams experiments. The role of the methylene amidogen and the cyanomethyl radicals in the formation of pyridine ($\text{C}_5\text{H}_5\text{N}$; **1**), pyridinyl ($\text{C}_5\text{H}_4\text{N}$; **9-11**), and (iso)quinoline ($\text{C}_9\text{H}_7\text{N}$; **2/3**) are also elucidated. These data are combined with electronic structure calculations and modeling of the chemistries of hydrocarbon rich environments of cold molecular clouds and atmospheres of planets of their moons exploiting the Taurus Molecular Cloud (TMC-1) and Titan as benchmarks. And a complex chain of exoergic, barrierless routes is contemplated with $\text{H}_2\text{CN}^\bullet$ and $\text{H}_2\text{CCN}^\bullet$ radicals representing fundamental molecular building blocks of pyridine and pyridinyl radicals ($\text{C}_5\text{H}_4\text{N}^\bullet$, **9-11**) synthesized through successive barrierless reactions involving propargyl ($\text{C}_3\text{H}_3^\bullet$, X^2B_1 , **6**) and 1-butene-3-yne-2-yl/1-butene-3-yne-1-yl (*i/n*- $\text{C}_4\text{H}_3^\bullet$, $\text{X}^2\text{A}'$, **7-8**) under low temperature conditions of molecular clouds (10 K) and Titan's atmosphere (70-180 K) (Figure 1)²⁸. Since pyridinyl radicals are isoelectronic to the phenyl radical ($\text{C}_6\text{H}_5^\bullet$), pyridinyl may play a critical role in the gas phase formation of (iso)quinoline upon reaction with vinylacetylene (C_4H_4) via the low-temperature hydrogen abstraction – vinylacetylene addition (HAVA)

pathway²⁹. These results thus offer fundamental knowledge on the previously elusive reaction routes to prototype nitrogen heteroaromatics in low-temperature extraterrestrial environments from cold molecular clouds such as TMC-1 to atmospheres of planets and their moons like Titan. These mechanisms are not constrained to Titan, but may present a versatile strategy for the synthesis of nitrogen heteroaromatics in low temperature, hydrocarbon and nitrogen-rich atmospheres of outer Solar System bodies such as Triton³⁰ and Pluto³¹. Hence, the present work sheds light on sensible processes coupling the carbon and nitrogen chemistries eventually leading to the formation of molecular nitrogen – carbon motives of astrobiological relevance as found in, e.g., nucleobases²⁹ in our Universe.

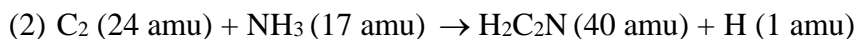
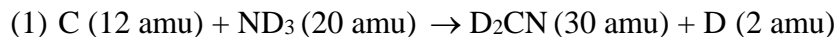
Results

Carbon – D3-Ammonia and Dicarbon – Ammonia Systems: Laboratory Frame

Exploiting a crossed molecular beams machine (Figure S1)³², reactive scattering signal of the reaction of ground state atomic carbon (C , 3P) with D3-ammonia (ND_3 , X^1A_1) was observed at $m/z = 30$ (D_2CN^+) after electron impact ionization of the neutral reaction products. Within our signal-to-noise, no signal was monitored at 32 (D_3CN^+) indicating that no D_3CN adducts were formed. These data alone indicate the existence of the atomic deuterium loss channel (reaction (1)). Note that for technical reasons, the reaction was conducted with D3-ammonia, but not with ammonia (NH_3 , X^1A_1) since this would have shifted reactive scattering signal to $m/z = 28$ (H_2CN^+). Signal at $m/z = 28$ is obscured by significant background counts from carbon monoxide, which outgasses from stainless steel even under our ultra-high vacuum (UHV) conditions of 6×10^{-12} Torr. Therefore, angular resolved TOF spectra were recorded at 30 (D_2CN^+) in 5° intervals within the scattering plane, integrated, and scaled with respect to the TOF recorded at the center-of-mass (CM) angle of $35.9 \pm 0.5^\circ$ leading to the laboratory angular distribution (LAD) (Table S1). This distribution holds a maximum around the CM angle and is nearly forward-backward symmetric (Figure 2, A-B) implying that the carbon – D3-ammonia reaction proceeds through indirect reaction dynamics involving the formation of D_3CN collision complex(es).

Reactive scattering signal of the reaction of dicarbon (C_2 , $X^1\Sigma_g^+/a^3\Pi_u$) with ammonia (NH_3 , X^1A_1) was detected at $m/z = 40$ ($C_2NH_2^+$) and 39 (C_2NH^+) (reaction (2)) with signal at 39 collected at level of $66 \pm 5\%$ compared to signal at 40. The TOF spectra at 40 and 39 are identical after

scaling (Figure S2) suggesting that signal at 39 originates from dissociative ionization of the nascent product (40 amu) in the electron impact ionizer. Further, signal at 40 indicated the existence of a dicarbon versus atomic hydrogen loss and inherent formation of a molecule with the molecular formula C_2NH_2 via reaction (2). Consequently, data were collected at 40 in 2.5° steps (Figure 2, C-D). The derived LAD is also nearly forward-backward symmetric revealing the existence of C_2H_3N intermediate(s) and indirect scattering dynamics.



Carbon – D3-Ammonia and Dicarbon – Ammonia Systems: Center-of-Mass Frame

Having provided compelling evidence on the formation of D_2CN and H_2C_2N isomers in reactions (1) and (2), respectively, we are turning attention to elucidating the nature of the structural isomer(s) and the underlying reaction mechanism(s). This information is obtained by transforming the laboratory data (TOFs, LAD) into the CM reference frame³². This forward convolution approach yields the CM translational energy ($P(E_T)$) and angular ($T(\theta)$) flux distributions as detailed in Figure 3 (A-C). For $C(^3P) - ND_3(X^1A_1)$ system, signal at 30 could be replicated with a single reaction channel of an atomic deuterium loss channel (reaction (1)) with a product mass combination of 30 amu (D_2CN) plus 2 amu (D). A detailed inspection of the $P(E_T)$ reveals a high-energy cutoff of $237 \pm 25 \text{ kJ mol}^{-1}$, which denotes the sum of the collision energy E_c ($28.1 \pm 0.9 \text{ kJ mol}^{-1}$) plus the reaction exoergicity for molecules generated without internal excitation. Therefore, reaction (1) is suggested to be exoergic by $209 \pm 26 \text{ kJ mol}^{-1}$. Further, the $P(E_T)$ display a distribution maximum at $26 \pm 3 \text{ kJ mol}^{-1}$ suggesting a tight exit transition state upon unimolecular decomposition of the D_3CN intermediate to the separated products and a significant electron density reorganization. The $T(\theta)$ function depicts flux across the complete angular range together with a forward-backward symmetric scattering pattern. These findings reveal indirect scattering dynamics through long-lived D_3CN complex(es) holding lifetime longer than the(ir) rotational periods³².

Considering the $C_2(X^1\Sigma_g^+/a^3\Pi_u) - NH_3(X^1A_1)$ system, the laboratory data can be replicated with a single atomic hydrogen loss channel with a mass combination of 40 amu (H_2C_2N) and 1 amu (H) (reaction (2)) (Figure 3, D-F). The $P(E_T)$ as depicted in Figure 3D shows an E_{max} of 327

$\pm 26 \text{ kJ mol}^{-1}$; this results in an exoergicity of $310 \pm 26 \text{ kJ mol}^{-1}$ or $318 \pm 26 \text{ kJ mol}^{-1}$ considering the E_c of $17.0 \pm 0.3 \text{ kJ mol}^{-1}$ for dicarbon reactants in ground $X^1\Sigma_g^+$ or excited $a^3\Pi_u$ state. It should be noted that the $P(E_T)$ peaks only slightly away from zero translational energy at $9 \pm 1 \text{ kJ mol}^{-1}$ indicating a loose exit transition state with only a minor rearrangement of the electron density, which contrasts to the results in C-ND₃ system. Finally, the $T(\theta)$ function exhibits a forward-backward symmetry with sideway scattering and hence a distribution maximum at 90° . These results propose indirect scattering dynamics via the formation of long-lived C₂NH₃ intermediates³³.

Electronic Structure Calculations and Reaction Mechanisms

We are merging now our experimental data with electronic structure calculations (Figures 4 and 5). *First*, our computations on the triplet CND₃ potential energy surface (PES) reveal four reaction intermediates (**i1-i4**), four product channels (**p1-p4**), and ten transition states. These high-level calculations predict relative energies of the transition states, local minima, and products within 8 kJ mol^{-1} .^{34,35} Four deuterium atom (D) loss pathways lead to D2-methylene amidogen (**p1**, D₂CN•, C_{2v}, X²B₂), trans-D2-iminomethyl (**p2**, DCND, C_s, X²A'), cis-D2-iminomethyl (**p3**, DCND, C_s, X²A'), and D2-aminomethylidyne (**p4**, D₂NC, C_{2v}, X²B₂). The relative energies of these isomers are within 3 kJ mol^{-1} compared to two previous studies^{36,37}. A comparison of the theoretically predicted reaction energies (Figure 4A) with our experimentally derived exoergicity of $209 \pm 26 \text{ kJ mol}^{-1}$ reveals that at least the thermodynamically most stable product **p1** is formed. Contributions from high energy isomers **p2-p4** might be masked in the low-energy section of the $P(E_T)$ and cannot be eliminated. How can **p1** be formed? Our calculations predict that the reaction is initiated via a barrierless addition of the carbon atom to the non-bonding electron pair at the nitrogen atom of ammonia. This reaction can be seen as an acid-base reaction and leads to **i1** (CND₃, D3-ammoniamethylidyne) bound by 103 kJ mol^{-1} . This collision complex may eliminate a deuterium atom forming **p4** by passing a transition state located only 2 kJ mol^{-1} below the separated reactants, or isomerizes to **i2** (DCND₂, D3-aminomethylidene) via deuterium migration from nitrogen to carbon. The transition state resides 11 kJ mol^{-1} below the separated reactants and hence can be accessed preferentially compared to the unimolecular decomposition of **i1** to **p4** plus D. The calculations suggest that **i2** can fragment via D loss to **p2** or **p3** through tight transition states residing 34 and 27 kJ mol^{-1} above the separated products; **p4** may be formed barrierlessly, too. Alternatively, **i2** may isomerize to **i3** (D₂CND, D3-methanimine) via a deuterium shift. This intermediate can undergo three distinct decomposition pathways through deuterium loss leading

to **p3**, **p2**, and/or the thermodynamically most stable isomer **p1** involving tight exit transition states (**i3**→**p3** 20 kJ mol⁻¹; **i3**→**p2** 22 kJ mol⁻¹; **i3**→**p1** 29 kJ mol⁻¹; the numbers indicate barrier with respect to the products). Finally, **i3** may undergo a deuterium shift to **i4** (D₃CN, D₃-methylnitrene), the global minimum of the D₃CN PES, followed by unimolecular decomposition to **p1** through a tight exit transition state located 13 kJ mol⁻¹ above the separated products. These considerations reveal that the experimentally detected D₂-methylene amidogen (**p1**) can be formed via **i1**→**i2**→**i3**→**p1**+D and/or **i1**→**i2**→**i3**→**i4**→**p1**+D.

Statistical Rice–Ramsperger–Kassel–Marcus (RRKM) calculations were also conducted to predict the branching ratios of **p1**–**p4** theoretically³⁴. Within the limit of a complete energy randomization, **p1**, **p2**, **p3**, and **p4** contribute 7 %, 33 %, 29 %, and 31%, respectively, at the experimental collision energy of 28.1 kJmol⁻¹ (Table S1). At the low temperature conditions of TMC-1 and Titan, fractions of 8 %, 41 %, 33 %, and 18 % are predicted (Table S2-3). Under the atmospheric conditions of Titan, one peculiarity exists. Suprathermal hydrogen atoms with excess kinetic energies of a few electron volts can be formed via photodissociation of hydrides like methane (CH₄) by solar photons, via neutral-neutral reactions of, e.g., methyldyne (CH) with methane, and/or electron recombination reactions of with abundant ions (CH₅⁺, CH₃⁺, and C₆H₇⁺)^{14,38,39}. These suprathermal hydrogen atoms are not in thermal equilibrium with the surrounding low-temperature atmosphere and their kinetic energies can easily exceed 100 kJ mol⁻¹ (1.04 eV)^{38,40}. Thus, rapid suprathermal hydrogen-atom assisted isomerization processes can efficiently convert the high-energy isomers **p3** and **p4** to **p1**^{41,42}. These processes are very efficient due to absence of a barrier of **p4** + **H** → **i2** and a small barrier of only 20 kJmol⁻¹ for **p3** + **H** → **i3**. As depicted in Figures S3-4, the elevated rate constants of **p3** + H of a few 10⁻¹⁰ cm³s⁻¹ can be reached with suprathermal hydrogen atoms possessing high kinetic energies.

Second, for the C₂-NH₃ system, the primary reactant beam contains dicarbon in its electronic ground state (X¹Σ_g⁺), but also in its first electronically excited state (a³Π_u). The calculations reveal that C₂ (a³Π_u) does not form any bound intermediates upon collision with ammonia, but rather reacts in a direct fashion via hydrogen abstraction forming the ethynyl radical (C₂H•, X²Σ⁺) plus the amino radical (NH₂•, X²B₁) in an exoergic reaction (-36 kJmol⁻¹) through a barrier of 22 kJmol⁻¹. However, on the singlet surface, dicarbon adds barrierlessly to the non-bonding electron pair of the nitrogen atom of ammonia to **i1'** (CCNH₃, ammoniaethynyl). Overall, nine intermediates (**i1'**-**i9'**), seven products (**p1'**-**p7'**), and nine transition states were identified. Among the product

isomers, **p1'** ($\text{H}_2\text{CCN}^\bullet$; cyanomethyl; C_{2v} ; 2B_1) represents the thermodynamically most stable isomer followed by **p2'** (H_2CNC ; isocyanomethyl; C_{2v} ; 2B_1) and **p3'** (HCCNH ; imidogenacetylene; C_s ; $^2A''$). The calculated relative energies of the $\text{C}_2\text{H}_2\text{N}$ isomers agree well with previous calculations⁴³. A comparison of these energies with the experimentally extracted exoergicity of $310 \pm 26 \text{ kJ mol}^{-1}$ proposed that at least **p1'** is formed under single collision conditions. Contributions from high energy isomers **p2'**-**p5'** might be hidden in the low-energy section of the $P(E_T)$ and cannot be eliminated. **i1'** can isomerize to an exotic cyclic intermediate **i2'** ($\text{HC}(\text{NH}_2)\text{C}$) via ring closure along with a hydrogen shift from the nitrogen to the carbon or to **i4'** (HCCNH_2 , aminoacetylene) through hydrogen migration. Our calculations also identify a loose H loss channel to **p7'** (CCNH_2 ; aminoethynyl; C_{2v} ; 2B_1) from **i1'**. Extensive hydrogen migration and ring opening pathway access intermediates **i3'** to **i9'**, with all transition state to isomerization residing well below the energy of the separated reactants. The experimentally detected product **p1'** can eventually be accessed via H loss from **i6'** (H_2CCNH , aminovinyl) and/or **i7'** (CH_3CN , acetonitrile) through loose transition states. Note that **i6'** and **i7'** are connected through a hydrogen migration barrier of 262 kJmol^{-1} . Overall, the experimentally predicted loose exit transition state agrees well with the computational predictions of two open channels to **p1'** ($\text{H}_2\text{CCN}^\bullet$; cyanomethyl) via simple bond rupture processes on the singlet surface (Figure 4B).

From the Laboratory to Hydrocarbon-Rich Atmospheres of Planets and their Moons

We are now conveying our findings to the atmosphere of Saturn's moon Titan. *First*, the carbonaceous reactants (atomic carbon, dicarbon) originate from photolysis of methane (CH_4) and acetylene (C_2H_2), respectively^{14,44}. Carbon can also be generated from dissociative electron – ion (CH_2^+ , CH_3^+) recombination in atmospheric layers above $1,200 \text{ km}^{18}$. The mole fraction of ammonia (NH_3) in Titan's atmosphere is still a tricky question. Ammonia abundances have been inferred indirectly via the Cassini's Ion and Neutral Mass Spectrometer (INMS) detection of the ammonium cation (NH_4^+) predicting high mole fraction of ammonia of $(3-4) \times 10^{-5}$ at around 1000 km^{45} . However, photochemical models cannot replicate these findings and underestimate mole fractions by up to two orders of magnitude^{46,47}. In the stratosphere, the calculated ammonia mole fraction is consistent with upper limits derived from Composite Infrared Spectrometer (CIRS) and Herschel^{47,48}. *Second*, the absence of entrance barriers in the exoergic bimolecular reactions

signifies the crucial prerequisite for reaction operating in Titan's low temperature atmosphere (70–180 K), which would prohibit reactions with significant entrance barrier. Therefore, chemical reactions relevant to Titan's atmospheric chemistry must be exoergic, proceed without an entrance barrier, and involve transition states with lower energy than the separated reactants. All these benchmarks are fulfilled in the formation of the $\text{H}_2\text{CN}^\bullet$ and the $\text{H}_2\text{CCN}^\bullet$ radical holding rate constants of, e.g., a few $10^{-10} \text{ cm}^3 \text{ s}^{-1}$ for the carbon – ammonia system at 50 K⁴⁹. *Third*, the aforementioned radicals are isoelectronic with the vinyl ($\text{C}_2\text{H}_3^\bullet$, $\text{X}^2\text{A}'$) and propargyl ($\text{C}_3\text{H}_3^\bullet$, X^2B_1) radical. Therefore, both the methylene amidogen and the cyanomethyl radical are involved in fundamental molecular mass growth processes in Titan's atmosphere. These processes are in strong analogy to the $\text{C}_2\text{H}_3^\bullet\text{-C}_4\text{H}_3^\bullet$ ^{16,50} and $\text{C}_3\text{H}_3^\bullet\text{-C}_3\text{H}_3^\bullet$ ⁵¹ systems, respectively, which access the phenyl radical ($\text{C}_6\text{H}_5^\bullet$) under single collision conditions and benzene along with its isomers, if the collision complexes can be stabilized through collision with a third body. This conclusion is verified through electronic structure calculation for the $\text{H}_2\text{CN}^\bullet\text{-C}_4\text{H}_3^\bullet$, and $\text{H}_2\text{CCN}^\bullet\text{-C}_3\text{H}_3^\bullet$ systems synthesizing three distinct pyridinyl radicals (o, m, p; $\text{C}_5\text{H}_4\text{N}^\bullet$) under single collision conditions (Figure 5A). Three distinct entrance channels lead barrierlessly to **i1''** to **i3''**. Extensive hydrogen shifts, and cyclization accompanied by aromatization to pyridine ($\text{C}_5\text{H}_5\text{N}$, **i12''**), which undergoes three barrierless hydrogen loss pathways to distinct pyridinyl radicals. It is interesting to point out that analogous barrierless pathways are identified in the *cis*- $\text{HCNH-C}_4\text{H}_3^\bullet$ system, in which two distinct entrance channels lead barrierlessly to **i14''** and **i19''** followed by hydrogen shifts and cyclization to pyridine and pyridinyl radicals (Figure 5B). In the presence of a dense atmosphere such as of Titan, pyridine can be stabilized by a third body with the bath molecule such as molecular nitrogen. Once stabilized, pyridine can be photolyzed to pyridinyl radicals (o, m, p; $\text{C}_5\text{H}_4\text{N}^\bullet$) (Figure 1) followed by barrierless reactions with vinylacetylene (C_4H_4) to (iso)quinoline ($\text{C}_9\text{H}_7\text{N}$)²⁹. *Finally*, previous photochemical models suggest that $\text{H}_2\text{CN}^\bullet$ is produced via the reaction of atomic nitrogen with the methyl radical (CH_3)^{52,53}. However, this modeling study did not include reactions of atomic carbon and dicarbon with ammonia due to the foregoing lack of reliable laboratory and computational data of the C/NH_3 and C_2/NH_3 systems, whereas extensive computational and experimental data exist for the N/CH_3 system^{37,54,55}. Here, we prove that both $\text{H}_2\text{CN}^\bullet$ and *cis*- HCNH radicals can react barrierlessly with *i/n*- C_4H_3 isomers forming pyridine and pyridinyl radicals indicating the potential significant role of C/NH_3 in the prebiotic chemistry of

Titan. Overall, we depict evidence that in Titan's atmosphere, where abundant suprathermal hydrogen atoms exist, **p3** can efficiently undergo suprathermal hydrogen atom – assisted isomerization to **p1**, the most stable isomer, followed by the reactions with *i/n*-C₄H₃ isomers to pyridine and pyridinyl radicals. Even **p3** itself can itself react with *i/n*-C₄H₃ isomers barrierlessly leading to pyridine and pyridinyl radicals.

The aforementioned findings are implemented into a one-dimensional photochemical atmospheric model of Titan to evaluate the eventual formation of pyridine (C₅H₅N) and (iso)quinoline (C₉H₇N) (Supplementary Information). This model incorporates an unbiased chemistry of neutrals and cations along with the coupling between them from the lower atmosphere to the ionosphere^{56,57}. The chemical scheme operated in the present model has been enhanced with the new reactions studied included⁵⁷⁻⁵⁹. To evaluate the uncertainties of the nominal model profiles, a Monte Carlo simulation was performed according to the method described in Benne et al.⁵⁸ (Figure 6A, Supplementary Information). These photochemical models yield exciting results. First, these studies reveal that two C₅H₅N isomers, pyridine (C₅H₅N) and ethylcyanoacetylene (C₂H₅CCCN), display significant mole fractions of 1.4×10^{-7} and 2.3×10^{-7} in the ionosphere of Titan, respectively. The maximum mole fraction for (iso)quinoline is predicted to be 1.7×10^{-11} around 1,100 km, which should be observable spectroscopically. These models also predict maximum mole fractions of C₅H₅NH⁺ and C₂H₅C₃NH⁺ of 1.5×10^{-10} and 3.9×10^{-10} at around 1,100 km, respectively. Accounting for the uncertainties, the mole fraction of $(1.5 \pm 0.3) \times 10^{-9}$ at *m/z* = 80 (C₅H₅NH⁺) derived from the Cassini INMS data^{18,60} agrees within the error limits well with the sum of mole fractions of C₅H₅NH⁺ and C₂H₅C₃NH⁺ of the atmospheric models ranging between 2.5×10^{-9} to 5.4×10^{-10} . Although the atmospheric models provide compelling constraints on the abundances of pyridine and (iso)quinoline, we have to concede that the uncertain abundances of ammonia in Titan's atmosphere, which may vary over at least two orders of magnitude, make it difficult to quantify the contributions of distinct pathways to the H₂CN• radical. With a low predicted ammonia mole fraction of a few 10^{-7} , the carbon – ammonia reaction hardly competes with the nitrogen-methyl system providing small fractions of up to one percent at most. However, considering the bimolecular nature of the carbon – ammonia system, an increase of the fractional abundance of ammonia will lead to an enhancement of H₂CN• radicals. Only future direct spectroscopic measurements of ammonia can resolve this issue. In fact, based on the nominal model results, it can be determined that at least 10% of H₂CN• radicals are produced by the carbon

– ammonia reaction under conditions of high ammonia mole fraction derived from the INMS data of Cassini mission⁴⁵. Therefore, fundamental bimolecular reactions including atomic carbon and dicarbon with ammonia may initiate a chain of barrierless reactions ultimately to pyridine and (iso)quinoline, i.e. the two simplest mono- and bicyclic aromatic molecules. These processes are not limited to Titan, but represent versatile pathways eventually leading to NPAHs in hydrocarbon and nitrogen containing atmospheres of planets and their moons in the outer Solar systems such as on Triton³⁰ and Pluto³¹ with organic haze layers recently detected by the *New Horizons* mission⁶¹. Only recently, NPAH product quinolizinium⁺ (C₉H₈N⁺) was formed via reaction of the pyridine cation with acetylene in low-temperature pathways, highlighting the role of ion-molecule reactions in the NPAH formation in Titan's atmosphere⁶². Here, the low-temperature neutral-neutral formation pathways to pyridine and (iso)quinoline are revealed. The combined ion-molecule and neutral-neutral reaction network may finally reproduce the astronomical detected abundances of PAHs which are drastically underestimated in the current modeling⁶³. Thus our understanding of fundamental low-temperature molecular mass growth processes to nitrogen substituted aromatics and their radicals is deepened.

From the Laboratory to Cold Molecular Clouds: TMC-1

The low temperature chemical mass growth processes in cold molecular clouds such as TMC-1 is fundamentally distinct from those in atmospheres of planets and their moons with both interstellar (TMC-1) and solar system (Titan) low-temperature environments require the absence of any entrance barriers to overall exoergic reactions⁶⁴. However, the low number densities of molecules in molecular clouds ranging from 10⁴ to 10⁶ cm⁻³ necessitate bimolecular reactions; third body collisions, in which collisions of the reaction intermediate with a bath molecule divert the internal energy of the intermediate and hence stabilize the latter, are absent. This requires changes to the reaction network from Titan's atmosphere (Figure 1) to TMC-1 thus implementing a reaction network of barrierless and exoergic bimolecular reactions (Figure S5, Table S4) such as reactions (1) and (2). To explore the implications of our findings to the chemistry leading eventually to pyridine (C₅H₅N), pyridinyl (C₅H₄N[•]), and (iso)quinoline (C₉H₇N), we untangled the role of the cyanomethyl (H₂CCN[•]) and methylene amidogen (H₂CN[•]) radicals in the formation of nitrogen heteroaromatics (pyridine (C₅H₅N), pyridinyl (C₅H₄N[•]), (iso)quinoline (C₉H₇N)) using the *University of Manchester Institute for Science and Technology* Database (RATE2012)⁶⁵

operated with the single-point time-dependent astrochemical models²⁷. Physical parameters were modernized according to Markwick et al.⁶⁶, McElroy et al.⁶⁵, and Yang et al.³³ with a temperature of 10 K, a cosmic ray ionization rate of $1.3 \times 10^{-17} \text{ s}^{-1}$, a visual extinction of 10 Mag, and a number density of molecular hydrogen of 10^4 cm^{-3} . The predictive capabilities of the model are verified by comparing the relevant species observed with modeled fractional abundances.

These models revealed fascinating findings (Figure 6B). First, the remarkable performance of the astrochemical model for TMC-1 can be benchmarked for the methylene amidogen radical ($\text{H}_2\text{CN}^\bullet$)⁶⁷, the cyanomethyl radical ($\text{H}_2\text{CCN}^\bullet$)⁶⁸, vinyl cyanide ($\text{C}_2\text{H}_3\text{CN}$)⁶⁹, and methyl cyanide (CH_3CN)⁷⁰ with astronomically observed fractional abundances of $(1.1 \pm 0.9) \times 10^{-10}$, $(3.5 \pm 1.5) \times 10^{-9}$, $(7.0 \pm 1.0) \times 10^{-10}$, and $(6.0 \pm 3.0) \times 10^{-10}$ relative to molecular hydrogen. Predicted peak abundances of methylene amidogen ($\text{H}_2\text{CN}^\bullet$) and of the cyanomethyl radical ($\text{H}_2\text{CCN}^\bullet$) of $(3.3 \pm 0.3) \times 10^{-10}$ at 1.3×10^5 years and $(6.0 \pm 0.4) \times 10^{-9}$ at 2.0×10^5 years replicate the astronomical observations nicely. Here, the carbon – ammonia system can account for 30 % to 75 % of the observed methylene amidogen radicals; generally spoken, as the initial abundances of nitrogen increase or carbon decreases, the fraction of methylene amidogen rises. For example, the contribution from the carbon – ammonia system rises to 50 % when the fraction of nitrogen increases to 10^{-2} and even to 75 % with at a fraction of 10^{-1} ; these cases operate in those regions of TMC-1 where nitrogen-rich species are injected into the gas phase from the icy grains^{71,72}. Even for standard abundances of carbon versus nitrogen in TMC-1 without grain ejection, the reaction of dicarbon with ammonia contributes up to 75 % to the peak abundance of the cyanomethyl radical ($\text{H}_2\text{CCN}^\bullet$). Model outputs of the closed shell nitriles vinyl cyanide ($\text{C}_2\text{H}_3\text{CN}$) and methyl cyanide (CH_3CN) are reported to be $(8.6 \pm 0.6) \times 10^{-10}$ after 3.2×10^5 year and $(1.0 \pm 0.2) \times 10^{-9}$ after 2.5×10^5 years also close to the observed data with important routes of barrierless reactions of the cyano radical (CN) with ethylene (C_2H_4)⁷³ and of the vinyl radical (C_2H_3) with the imidogen radical (NH)⁷⁴. Second, a complex chain of reactions initiated by barrierless reactions of the cyanomethyl ($\text{H}_2\text{CCN}^\bullet$) and methylene amidogen ($\text{H}_2\text{CN}^\bullet$) radicals (Figure S5) drive molecular mass growth processes to pyridine ($\text{C}_5\text{H}_5\text{N}$), pyridinyl ($\text{C}_5\text{H}_4\text{N}^\bullet$), and (iso)quinoline ($\text{C}_9\text{H}_7\text{N}$) with predicted peak fractional abundances of $(6.0 \pm 0.3) \times 10^{-9}$ (6.3×10^5 years), $(1.2 \pm 0.1) \times 10^{-10}$ (3.2×10^5 years), and $(6.0 \pm 0.4) \times 10^{-12}$ (6.3×10^5 years), respectively. The $\text{H}_2\text{CN}^\bullet/\text{C}_4\text{H}_3^\bullet$ and $\text{H}_2\text{CCN}^\bullet/\text{C}_3\text{H}_3^\bullet$ reactions produce 46 % and 54 % of the predicted abundances of pyridinyl ($\text{C}_5\text{H}_4\text{N}^\bullet$), respectively. These results suggest that at least pyridine ($\text{C}_5\text{H}_5\text{N}$) and pyridinyl ($\text{C}_5\text{H}_4\text{N}^\bullet$) might be

detectable by radio telescopes such as the Green Bank Observatory and Yebes Radio Telescope in TMC-1.

Conclusion

To conclude, our combined crossed molecular beam and electronic structure studies provided persuasive evidence on the formation of the methylene amidogen radical ($\text{H}_2\text{CN}^\bullet$, X^2B_2) and of the resonantly stabilized cyanomethyl radical ($\text{H}_2\text{CCN}^\bullet$, X^2B_1) via bimolecular reactions of atomic carbon (C ; ^3P) and of dicarbon (C_2 ; $\text{X}^1\Sigma_g^+/\text{a}^3\Pi_u$) with ammonia (NH_3 ; X^1A_1) in low temperature extraterrestrial environments such as in the cold molecular cloud TMC-1. Combined with modeling, these findings reveal further that both the methylene amidogen and the cyanomethyl radicals can initiate a complex chain of reactions leading to pyridine (**1**) and pyridinyl radicals (**9-11**) and eventually to (iso)quinoline (**2/3**) as the simplest prototype NPAHs and potential feedstock for more complex nitrogen-based aromatics in deep space. Whereas the elementary reactions of carbon and dicarbon with ammonia can account for up to 75 % of the methylene amidogen and of the cyanomethyl radical in TMC-1, their contributions in Titan's atmosphere are less constrained; this is predominantly based on the uncertain abundances of atmospheric ammonia diverging by at least two orders of magnitude. This can only be solved through future in situ observations by, e.g., the prospective *Dragon Fly* mission. However, pyridine (**1**) and (iso)quinoline (**2/3**) – the most primitive nitrogen aromatics – have been detected in the Murchison (CM2) carbonaceous chondrite with abundances of up to $0.5 \mu\text{g g}^{-1}$ (ppm)^{75,76} thus providing a critical link between the low temperature chemistry in cold molecular clouds and their delivery to our solar system in form of meteorites. Overall, the present study provides a template for a systematic investigation of elementary reactions so that a comprehensive picture of the low temperature chemistry leading to biorelevant molecules in extraterrestrial environments emerges.

References

- 1 Pizzarello, S., Huang, Y. & Fuller, M. The carbon isotopic distribution of Murchison amino acids. *Geochim. Cosmochim. Acta* **68**, 4963-4969 (2004).
- 2 Smith, K. E., Callahan, M. P., Gerakines, P. A., Dworkin, J. P. & House, C. H. Investigation of pyridine carboxylic acids in CM2 carbonaceous chondrites: potential precursor molecules for ancient coenzymes. *Geochim. Cosmochim. Acta* **136**, 1-12 (2014).
- 3 Martins, Z. *et al.* Extraterrestrial nucleobases in the Murchison meteorite. *Earth Planet. Sci. Lett.* **270**, 130-136 (2008).
- 4 Burton, A. S., Stern, J. C., Elsila, J. E., Glavin, D. P. & Dworkin, J. P. Understanding prebiotic chemistry through the analysis of extraterrestrial amino acids and nucleobases in meteorites. *Chem. Soc. Rev.* **41**, 5459-5472 (2012).
- 5 Andrews, H., Candian, A. & Tielens, A. G. G. M. Hydrogenation and dehydrogenation of interstellar PAHs: Spectral characteristics and H₂ formation. *Astron. Astrophys.* **595**, A23 (2016).
- 6 Tsuge, M., Bahou, M., Wu, Y.-J., Allamandola, L. & Lee, Y.-P. The infrared spectrum of protonated ovalene in solid para-hydrogen and its possible contribution to interstellar unidentified infrared emission. *Astrophys. J.* **825**, 96 (2016).
- 7 Tielens, A. G. G. M. Interstellar polycyclic aromatic hydrocarbon molecules. *Annu. Rev. Astron. Astrophys.* **46**, 289-337 (2008).
- 8 Knorke, H., Langer, J., Oomens, J. & Dopfer, O. Infrared spectra of isolated protonated polycyclic aromatic hydrocarbon molecules. *Astrophys. J.* **706**, L66 (2009).
- 9 Hudgins, D. M., Bauschlicher Jr, C. W. & Allamandola, L. J. Variations in the peak position of the 6.2 μm interstellar emission feature: a tracer of N in the interstellar polycyclic aromatic hydrocarbon population. *Astrophys. J.* **632**, 316 (2005).
- 10 Herbst, E. & Van Dishoeck, E. F. Complex organic interstellar molecules. *Annu. Rev. Astron. Astrophys.* **47**, 427-480 (2009).
- 11 Kaiser, R. I. & Hansen, N. An Aromatic Universe—A Physical Chemistry Perspective. *J. Phys. Chem. A* **125**, 3826-3840 (2021).
- 12 Peeters, Z., Botta, O., Charnley, S. B., Ruitkamp, R. & Ehrenfreund, P. The astrobiology of nucleobases. *Astrophys. J.* **593**, L129 (2003).
- 13 Hörst, S. M. Titan's atmosphere and climate. *J. Geophys. Res.* **122**, 432-482 (2017).

- 14 Vuitton, V., Yelle, R. V., Klippenstein, S. J., Hörst, S. M. & Lavvas, P. Simulating the density of organic species in the atmosphere of Titan with a coupled ion-neutral photochemical model. *Icarus* **324**, 120-197 (2019).
- 15 Loison, J. C. *et al.* The neutral photochemistry of nitriles, amines and imines in the atmosphere of Titan. *Icarus* **247**, 218-247 (2015).
- 16 Kislov, V. V., Nguyen, T. L., Mebel, A. M., Lin, S. H. & Smith, S. C. Photodissociation of benzene under collision-free conditions: An ab initio/Rice–Ramsperger–Kassel–Marcus study. *J. Chem. Phys.* **120**, 7008-7017 (2004).
- 17 Lin, M.-F. *et al.* Photodissociation dynamics of pyridine. *J. Chem. Phys.* **123**, 054309 (2005).
- 18 Vuitton, V., Yelle, R. V. & McEwan, M. J. Ion chemistry and N-containing molecules in Titan's upper atmosphere. *Icarus* **191**, 722-742 (2007).
- 19 Ricca, A., Bauschlicher Jr, C. W. & Bakes, E. A computational study of the mechanisms for the incorporation of a nitrogen atom into polycyclic aromatic hydrocarbons in the Titan haze. *Icarus* **154**, 516-521 (2001).
- 20 Soorkia, S. *et al.* Direct detection of pyridine formation by the reaction of CH (CD) with pyrrole: a ring expansion reaction. *Phys. Chem. Chem. Phys.* **12**, 8750-8758 (2010).
- 21 López-Puertas, M. *et al.* Large abundances of polycyclic aromatic hydrocarbons in Titan's upper atmosphere. *Astrophys. J.* **770**, 132 (2013).
- 22 Anderson, C. M. & Samuelson, R. E. Titan's aerosol and stratospheric ice opacities between 18 and 500 μm : Vertical and spectral characteristics from Cassini CIRS. *Icarus* **212**, 762-778 (2011).
- 23 Sebree, J. A., Trainer, M. G., Loeffler, M. J. & Anderson, C. M. Titan aerosol analog absorption features produced from aromatics in the far infrared. *Icarus* **236**, 146-152 (2014).
- 24 Ali, A., Sittler Jr, E. C., Chornay, D., Rowe, B. R. & Puzzarini, C. Organic chemistry in Titan's upper atmosphere and its astrobiological consequences: I. Views towards Cassini Plasma Spectrometer (CAPS) and Ion Neutral Mass Spectrometer (INMS) experiments in space. *Planet. Space Sci.* **109**, 46-63 (2015).
- 25 Mathé, C., Gautier, T., Trainer, M. G. & Carrasco, N. Detection opportunity for aromatic signature in Titan's aerosols in the 4.1–5.3 μm range. *Astrophys. J. Lett.* **861**, L25 (2018).
- 26 Zhao, L. *et al.* Gas-phase synthesis of corannulene—a molecular building block of fullerenes. *Phys. Chem. Chem. Phys.* **23**, 5740-5749 (2021).

- 27 Kaiser, R. I. *et al.* Gas-phase synthesis of racemic helicenes and their potential role in the enantiomeric enrichment of sugars and amino acids in meteorites. *Phys. Chem. Chem. Phys.* **24**, 25077-25087 (2022).
- 28 Parker, D. S. N. & Kaiser, R. I. On the formation of nitrogen-substituted polycyclic aromatic hydrocarbons (NPAHs) in circumstellar and interstellar environments. *Chem. Soc. Rev.* **46**, 452-463 (2017).
- 29 Zhao, L. *et al.* A molecular beam and computational study on the barrierless gas phase formation of (iso)quinoline in low temperature extraterrestrial environments. *Phys. Chem. Chem. Phys.* **23**, 18495-18505 (2021).
- 30 Broadfoot, A. L. *et al.* Ultraviolet spectrometer observations of Neptune and Triton. *Science* **246**, 1459-1466 (1989).
- 31 Moores, J. E., Smith, C. L., Toigo, A. D. & Guzewich, S. D. Penitentes as the origin of the bladed terrain of Tartarus Dorsa on Pluto. *Nature* **541**, 188-190 (2017).
- 32 Yang, Z. *et al.* Gas-Phase Formation of 1, 3, 5, 7-cyclooctatetraene (C₈H₈) through ring expansion via the aromatic 1, 3, 5-cyclooctatrien-7-yl radical (C₈H₉[•]) transient. *J. Am. Chem. Soc.* **144**, 22470-22478 (2022).
- 33 Yang, Z. *et al.* Gas-phase formation of the resonantly stabilized 1-indenyl (C₉H₇[•]) radical in the interstellar medium. *Sci. Adv.* **9**, eadi5060 (2023).
- 34 Zhang, J. & Valeev, E. F. Prediction of Reaction Barriers and Thermochemical Properties with Explicitly Correlated Coupled-Cluster Methods: A Basis Set Assessment. *J. Chem. Theory Comput.* **8**, 3175-3186 (2012).
- 35 Adler, T. B., Knizia, G. & Werner, H.-J. A simple and efficient CCSD(T)-F12 approximation. *J. Chem. Phys.* **127**, 221106 (2007).
- 36 Bourgalais, J. *et al.* The C(³P) + NH₃ reaction in interstellar chemistry. I. Investigation of the product formation channels. *Astrophys. J.* **812**, 106 (2015).
- 37 Chiba, S., Honda, T., Kondo, M. & Takayanagi, T. Direct dynamics study of the N(⁴S)+CH₃(²A₂^{''}) reaction. *Comput. Theor. Chem.* **1061**, 46-51 (2015).
- 38 Morton, R. J. & Kaiser, R. I. Kinetics of suprathreshold hydrogen atom reactions with saturated hydrides in planetary and satellite atmospheres. *Planet. Space Sci.* **51**, 365-373 (2003).
- 39 De La Haye, V., Waite, J. H., Cravens, T. E., Robertson, I. P. & Lebonnois, S. Coupled ion and neutral rotating model of Titan's upper atmosphere. *Icarus* **197**, 110-136 (2008).

- 40 De La Haye, V. *et al.* Heating Titan's upper atmosphere. *J. Geophys. Res.* **113** (2008).
- 41 Mebel, A. M., Georgievskii, Y., Jasper, A. W. & Klippenstein, S. J. Pressure-dependent rate constants for PAH growth: formation of indene and its conversion to naphthalene. *Faraday Discuss.* **195**, 637-670 (2016).
- 42 Jasper, A. W. & Hansen, N. Hydrogen-assisted isomerizations of fulvene to benzene and of larger cyclic aromatic hydrocarbons. *Proc. Combust. Inst.* **34**, 279-287 (2013).
- 43 Lau, K.-C., Li, W.-K., Ng, C. Y. & Chiu, S.-W. A Gaussian-2 study of isomeric C₂H₂N and C₂H₂N⁺. *J. Phys. Chem. A* **103**, 3330-3335 (1999).
- 44 Willacy, K., Allen, M. & Yung, Y. A new astrobiological model of the atmosphere of Titan. *Astrophys. J.* **829**, 79 (2016).
- 45 Cui, J. *et al.* Analysis of Titan's neutral upper atmosphere from Cassini Ion Neutral Mass Spectrometer measurements. *Icarus* **200**, 581-615 (2009).
- 46 Yelle, R. V. *et al.* Formation of NH₃ and CH₂NH in Titan's upper atmosphere. *Faraday Discuss.* **147**, 31-49 (2010).
- 47 Teanby, N. A. *et al.* Constraints on Titan's middle atmosphere ammonia abundance from Herschel/SPIRE sub-millimetre spectra. *Planet. Space Sci.* **75**, 136-147 (2013).
- 48 Nixon, C. A. *et al.* Upper limits for undetected trace species in the stratosphere of Titan. *Faraday Discuss.* **147**, 65-81 (2010).
- 49 Hickson, K. M. *et al.* The C(³P) + NH₃ reaction in interstellar chemistry. II. Low temperature rate constants and modeling of NH, NH₂, and NH₃ abundances in dense interstellar clouds. *Astrophys. J.* **812**, 107 (2015).
- 50 Pope, C. J. & Miller, J. A. Exploring old and new benzene formation pathways in low-pressure premixed flames of aliphatic fuels. *Proc. Combust. Inst.* **28**, 1519-1527 (2000).
- 51 Zhao, L. *et al.* Gas-phase synthesis of benzene via the propargyl radical self-reaction. *Sci. Adv.* **7**, eabf0360 (2021).
- 52 Pearce, B. K. D., Ayers, P. W. & Pudritz, R. E. A consistent reduced network for HCN chemistry in early earth and Titan atmospheres: Quantum calculations of reaction rate coefficients. *J. Phys. Chem. A* **123**, 1861-1873 (2019).
- 53 Pearce, B. K. D., He, C. & Hörst, S. M. An experimental and theoretical investigation of HCN production in the Hadean Earth atmosphere. *ACS Earth Space Chem.* **6**, 2385-2399 (2022).

- 54 Marston, G., Nesbitt, F. L., Nava, D. F., Payne, W. A. & Stief, L. J. Temperature dependence of the reaction of nitrogen atoms with methyl radicals. *J. Phys. Chem.* **93**, 5769-5774 (1989).
- 55 Marston, G., Nesbitt, F. L. & Stief, L. J. Branching ratios in the N + CH₃ reaction: formation of the methylene amidogen (H₂CN) radical. *J. Chem. Phys.* **91**, 3483-3491 (1989).
- 56 Dobrijevic, M., Loison, J. C., Hickson, K. M. & Gronoff, G. 1D-coupled photochemical model of neutrals, cations and anions in the atmosphere of Titan. *Icarus* **268**, 313-339 (2016).
- 57 Loison, J. C., Dobrijevic, M. & Hickson, K. M. The photochemical production of aromatics in the atmosphere of Titan. *Icarus* **329**, 55-71 (2019).
- 58 Benne, B., Dobrijevic, M., Cavalié, T., Loison, J.-C. & Hickson, K. M. A photochemical model of Triton's atmosphere with an uncertainty propagation study. *Astron. Astrophys.* **667**, A169 (2022).
- 59 Vanuzzo, G. *et al.* Reaction N(²D) + CH₂CCH₂ (allene): An experimental and theoretical investigation and implications for the photochemical models of Titan. *ACS Earth Space Chem.* **6**, 2305-2321 (2022).
- 60 Teolis, B. D. *et al.* A revised sensitivity model for Cassini INMS: Results at Titan. *Space Sci. Rev.* **190**, 47-84 (2015).
- 61 Gladstone, G. R. & Young, L. A. New Horizons observations of the atmosphere of Pluto. *Annu. Rev. Earth Planet. Sci.* **47**, 119-140 (2019).
- 62 Rap, D. B., Schrauwen, J. G., Marimuthu, A. N., Redlich, B. & Brünken, S. Low-temperature nitrogen-bearing polycyclic aromatic hydrocarbon formation routes validated by infrared spectroscopy. *Nat. Astron.* **6**, 1059-1067 (2022).
- 63 McGuire, B. A. *et al.* Detection of two interstellar polycyclic aromatic hydrocarbons via spectral matched filtering. *Science* **371**, 1265-1269 (2021).
- 64 Kaiser, R. I. Experimental investigation on the formation of carbon-bearing molecules in the interstellar medium via neutral–neutral reactions. *Chem. Rev.* **102**, 1309-1358 (2002).
- 65 McElroy, D. *et al.* The UMIST database for astrochemistry 2012. *Astron. Astrophys.* **550**, A36 (2013).
- 66 Markwick, A. J., Millar, T. J. & Charnley, S. B. On the abundance gradients of organic molecules along the TMC-1 ridge. *Astrophys. J.* **535**, 256 (2000).
- 67 Ohishi, M., McGonagle, D., Irvine, W. M., Yamamoto, S. & Saito, S. Detection of a new interstellar molecule, H₂CN. *Astrophys. J.* **427**, L51-L54 (1994).

- 68 Thaddeus, P., Vrtilik, J. M. & Gottlieb, C. A. Laboratory and astronomical identification of cyclopropenylidene, C_3H_2 . *Astrophys. J.* **299**, L63-L66 (1985).
- 69 Cernicharo, J. *et al.* Discovery of CH_2CHCCH and detection of HCCN, HC_4N , CH_3CH_2CN , and, tentatively, CH_3CH_2CCH in TMC-1. *Astron. Astrophys.* **647**, L2 (2021).
- 70 Tennis, J. D. *et al.* Detection and modelling of CH_3NC in TMC-1. *Mon. Not. R. Astron. Soc.* **525**, 2154-2171 (2023).
- 71 Abplanalp, M. J. & Kaiser, R. I. Implications for extraterrestrial hydrocarbon chemistry: analysis of acetylene (C_2H_2) and D2-acetylene (C_2D_2) ices exposed to ionizing radiation via ultraviolet-visible spectroscopy, infrared spectroscopy, and reflectron time-of-flight mass spectrometry. *Astrophys. J.* **889**, 3 (2020).
- 72 Thrower, J. *et al.* Photon- and electron-stimulated desorption from laboratory models of interstellar ice grains. *J. Vac. Sci. Technol. A* **28**, 799-806 (2010).
- 73 Balucani, N. *et al.* Crossed beam reaction of cyano radicals with hydrocarbon molecules. III. Chemical dynamics of vinylcyanide (C_2H_3CN ; X^1A') formation from reaction of CN ($X^2\Sigma^+$) with ethylene, C_2H_4 (X^1A_g). *J. Chem. Phys.* **113**, 8643-8655 (2000).
- 74 Kodama, S. Reactions of imidogen radicals. 6. Reactions of imidogen ($a^1\Delta$) with acetylene and unimolecular decompositions of C_2H_3N . *J. Phys. Chem.* **92**, 5019-5024 (1988).
- 75 Stoks, P. G. & Schwartz, A. W. Basic nitrogen-heterocyclic compounds in the Murchison meteorite. *Geochim. Cosmochim. Acta* **46**, 309-315 (1982).
- 76 Sephton, M. A. Organic compounds in carbonaceous meteorites. *Nat. Prod. Rep.* **19**, 292-311 (2002).
- 77 Dangi, B. B., Maity, S., Kaiser, R. I. & Mebel, A. M. A combined crossed beam and ab initio investigation of the gas phase reaction of dicarbon molecules (C_2 ; $X^1\Sigma_g^+/a^3\Pi_u$) with propene (C_3H_6 ; X^1A'): identification of the resonantly stabilized free radicals 1- and 3-vinylpropargyl. *J. Phys. Chem. A* **117**, 11783-11793 (2013).
- 78 Werner, H. *et al.* MOLPRO, version 2015.1, a package of ab initio programs. *University of Cardiff Chemistry Consultants (UC3): Cardiff, Wales, UK* (2015).
- 79 Knowles, P. J., Hampel, C. & Werner, H. J. Coupled cluster theory for high spin, open shell reference wave functions. *J. Chem. Phys.* **99**, 5219-5227 (1993).
- 80 Dunning Jr, T. H. Gaussian basis sets for use in correlated molecular calculations. I. The atoms boron through neon and hydrogen. *J. Chem. Phys.* **90**, 1007-1023 (1989).

- 81 Peterson, K. A., Adler, T. B. & Werner, H.-J. Systematically convergent basis sets for explicitly correlated wavefunctions: The atoms H, He, B–Ne, and Al–Ar. *J. Chem. Phys.* **128**, 084102 (2008).
- 82 Becke, A. D. Density-functional thermochemistry. III. the role of exact exchange. *J. Chem. Phys.* **98**, 5648-5652 (1993).
- 83 Lee, C., Yang, W. & Parr, R. G. Development of the Colle-Salvetti correlation-energy formula into a functional of the electron density. *Phys. Rev. B* **37**, 785 (1988).
- 84 Frisch, M. J. *et al.* Gaussian 16, revision C.1. (2019).

Correspondence and requests for materials should be addressed to R.I.K., A.M.M., B.R.L.G., J.-C.L., and X.L.

Acknowledgements

This work was supported by the U.S. Department of Energy, Basic Energy Sciences, by Grants No. DE-FG02-03ER15411 to the University of Hawaii at Manoa. The support of Conselho Nacional de Desenvolvimento Científico e Tecnológico (CNPq), Grant 311508/2021-9 and 405524/2021-8, is also acknowledged. We would like to acknowledge fruitful discussions on the fractional abundances of ammonia with Drs. Conor A. Nixon (NASA Goddard) and Karen Willacy (JPL).

Author Contributions

R.I.K. designed the experiments; Z.Y., C.H., and S.J.G. performed the experiments; A.M.M., P.F.G.V., M.O.A., and B.R.L.G. conducted the electronic structure calculations; J.-C.L, K.M.H., and M.D. conducted the atmospheric modeling of Titan; X.L. performed the astrochemical modeling of TMC-1; Z.Y. and R.I.K. analyzed data and wrote the manuscript. All authors discussed the data.

Competing interests

The authors declare no competing financial interests.

Methods

Crossed Molecular Beams

C-ND₃ system

The bimolecular reaction of ground-state atomic carbon (C; ³P) with D₃-ammonia (ND₃; X¹A₁) was explored under single collision conditions employing a crossed molecular beams machine³². A supersonic beam of atomic carbon was produced by ablating a rotating graphite rod at 266 nm (Nd:YAG, 10-12 mJ pulse⁻¹, 30 Hz). The ablated carbon species were seeded in helium gas (99.9999%, 4 atm, 60 Hz). The primary carbon beam was velocity-selected by a chopper wheel (120 Hz) after passed through a skimmer revealing a well-defined v_p (peak velocity) of 2512 ± 49 m s⁻¹ and S (speed ratio) of 2.9 ± 0.3 (Table S1). Carbon atoms in the primary beam are only in the ground state (³P) under these conditions. Operation conditions were optimized that dicarbon in the primary beam was reduced to levels of less than 5%, which does not interfere with the scattering signal. The secondary beam of D₃-ammonia (ND₃; Sigma-Aldrich; 99% D) was released with a backing pressure of 550 Torr and 60 Hz, characterized by a v_p of 1091 ± 25 m s⁻¹ and S of 10.1 ± 1.3 . Finally, the carbon beam crossed the ND₃ beam perpendicularly in the interaction region resulting in a collision energy (E_C) of 28.1 ± 0.9 kJ mol⁻¹ and a CM angle (Θ_{CM}) of $35.9 \pm 0.5^\circ$.

C₂-NH₃ system

A pulsed supersonic dicarbon beam [C₂ (X¹Σ_g⁺/a³Π_u)] was produced exploiting the same ablation source described above. Briefly, the graphite rod was ablated by focusing the 266 nm laser output at 30 Hz and energy of 8-10 mJ pulse⁻¹. The ablated species were seeded in Neon (Ne, 4 atm, 99.9999%). Operation conditions and delay times were optimized to maximize dicarbon concentrations in the primary beam. Laser-induced fluorescence (LIF) of dicarbon revealed both singlet ground state (X¹Σ_g⁺) and the lowest lying triplet state (a³Π_u) along with the ro-vibrational distribution. The rotational temperature (T_{rot}) for the vibrational levels of $v = 0, 1$ of the a³Π_u state were measured to be 240 ± 30 and 190 ± 30 K with fractions of 0.67 ± 0.05 and 0.33 ± 0.05 , respectively, via the Swan band transition (d³Π_g-a³Π_u). The singlet state was detected via the Mulliken excitation (D¹Σ_u⁺-X¹Σ_g⁺) and the bimodal rotational distributions of both $v = 0, 1$ were revealed at fractions of 0.83 ± 0.10 and 0.17 ± 0.04 , respectively. Rotational temperature of the first and second vibrational levels was derived to be 200 K with population fraction of 0.44 ± 0.05 and 0.06 ± 0.02 together with 1000 K with fraction of 0.39 ± 0.05 and 0.11 ± 0.02 , respectively⁷⁷.

The secondary ammonia (NH₃, Matheson, 99.99%) beam was released with 550 Torr backing pressure. The peak velocities, speed ratios of the primary and secondary beam along with the derived collision energy and CM angles of the C₂-NH₃ system are tabulated in Table S1.

For both reactions, the products were detected by a rotatable detection system at ultrahigh-vacuum conditions (6×10^{-12} Torr). In detail, the neutral species were ionized with an electron impact ionizer (80 eV; 2 mA) before they are mass-selected by a quadrupole mass spectrometer (QMS) in the time-of-flight (TOF) mode. The ions at a selected m/z will eventually lead to the signal detected and filtered by a photomultiplier tube (PMT; model 8850; -1.35 kV) and a discriminator (1.6 mV). Finally, a multichannel scaler is used to collect the TOF spectra at different angles. These laboratory data are converted into the CM frame with a forward-convolution method yielding the CM translational energy ($P(E_T)$) and angular ($T(\theta)$) flux distributions, with which the information of the reaction dynamics can be extracted³². The reactive differential cross section, $I(u, \theta) \sim P(u) \times T(\theta)$, which reports the product intensity (I) as a function of the center-of-mass angle θ and the velocity u , represents an overall image of the reaction and contains all the information of the scattering process³².

Electronic Structure Calculations

The electronic structure calculations reported in this work for the carbon and dicarbon reactions with ammonia (Figure 4, Table S5-6) were performed with the MOLPRO⁷⁸ software. The geometry optimizations and harmonic frequencies calculations employed the coupled-cluster singles and doubles plus perturbative triples – CCSD(T) – method⁷⁹. For such optimizations and frequencies, the augmented correlation consistent family basis set aug-cc-pVXZ⁸⁰ was employed, with a quadruple-zeta ($X=Q$) basis being used for the CNH₃ system, and a triple-zeta ($X=T$) for CCNH₃. For both systems, a final single point energy calculation was performed at the optimized geometries with the explicitly correlated CCSD(T)-F12 method³⁵ with the quadruple-zeta basis set cc-pVQZ-F12⁸¹. Using the conventional notation, the reported energies for the carbon-ammonia system are therefore CCSD(T)-F12/cc-pVQZ-F12//CCSD(T)/aug-cc-pVQZ+ZPE(CCSD(T)/aug-cc-pVQZ) and for dicarbon-ammonia CCSD(T)-F12/cc-pVQZ-F12//CCSD(T)/aug-cc-pVTZ+ZPE(CCSD(T)/aug-cc-pVTZ). For the larger C₃H₅N system where the potential energy surface is accessed by the C₃H₃ + H₂CCN, C₄H₃ + H₂CN, and C₄H₃ + cis-HCNH reactions (Figure 5, Table S7), geometry optimizations and harmonic frequencies calculations used the density functional (DFT) B3LYP method^{82,83} with the cc-pVTZ basis and single-point energies refined at

the CCSD(T)-F12/cc-pVTZ-F12 level. Thus, the reported energies for C₅H₅N species are obtained at CCSD(T)-F12/cc-pVTZ-F12//B3LYP/cc-pVTZ+ZPE(B3LYP/cc-pVTZ) employing the Gaussian 16⁸⁴ and MOLPRO⁷⁸ software packages.

Data availability

The data that support the plots within this paper and other findings of this study are available from the corresponding author upon reasonable request.

Supplementary information

Astrochemical modeling details, Figure S1 to S5, Table S1 to S7.

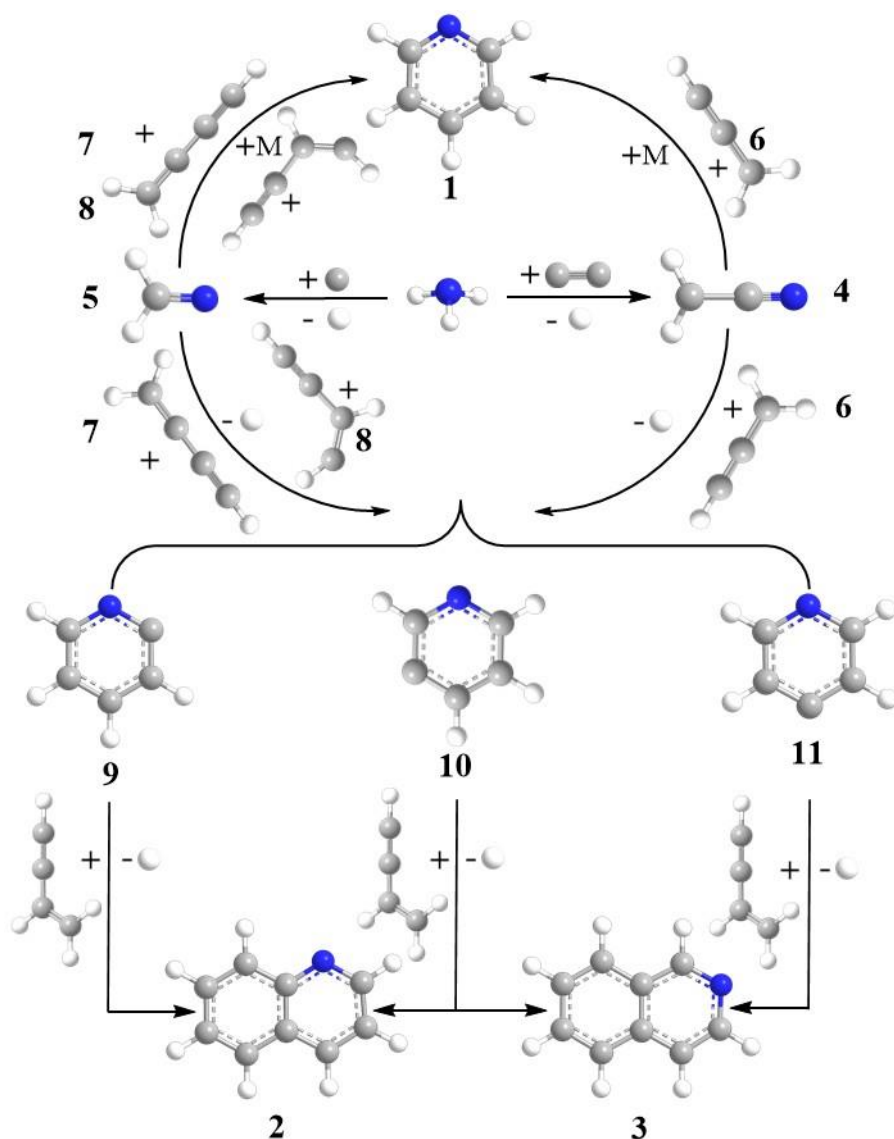


Figure 1. Pathways to pyridine and (iso)quinoline. A chain of reactions initiated through the formation of methylene amidogen radical ($\text{H}_2\text{CN}^\bullet$) and cyanomethyl radical ($\text{H}_2\text{CCN}^\bullet$) lead to the simplest representative of mono and bicyclic aromatic molecules carrying nitrogen. The reactions of atomic carbon and dicarbon with ammonia leading to methylene amidogen radical (5) and cyanomethyl radical (4) are investigated via our crossed molecular beam machine; our calculations also predict the formation of pyridine (1) and pyridinyl radicals (9-11) through the reactions of methylene amidogen with *i/n*-C₄H₃ and of cyanomethyl with propargyl. The reactions of pyridinyl radicals (9-11) with vinylacetylene (C₄H₄) forming (iso)quinoline are depicted in Ref. 29.

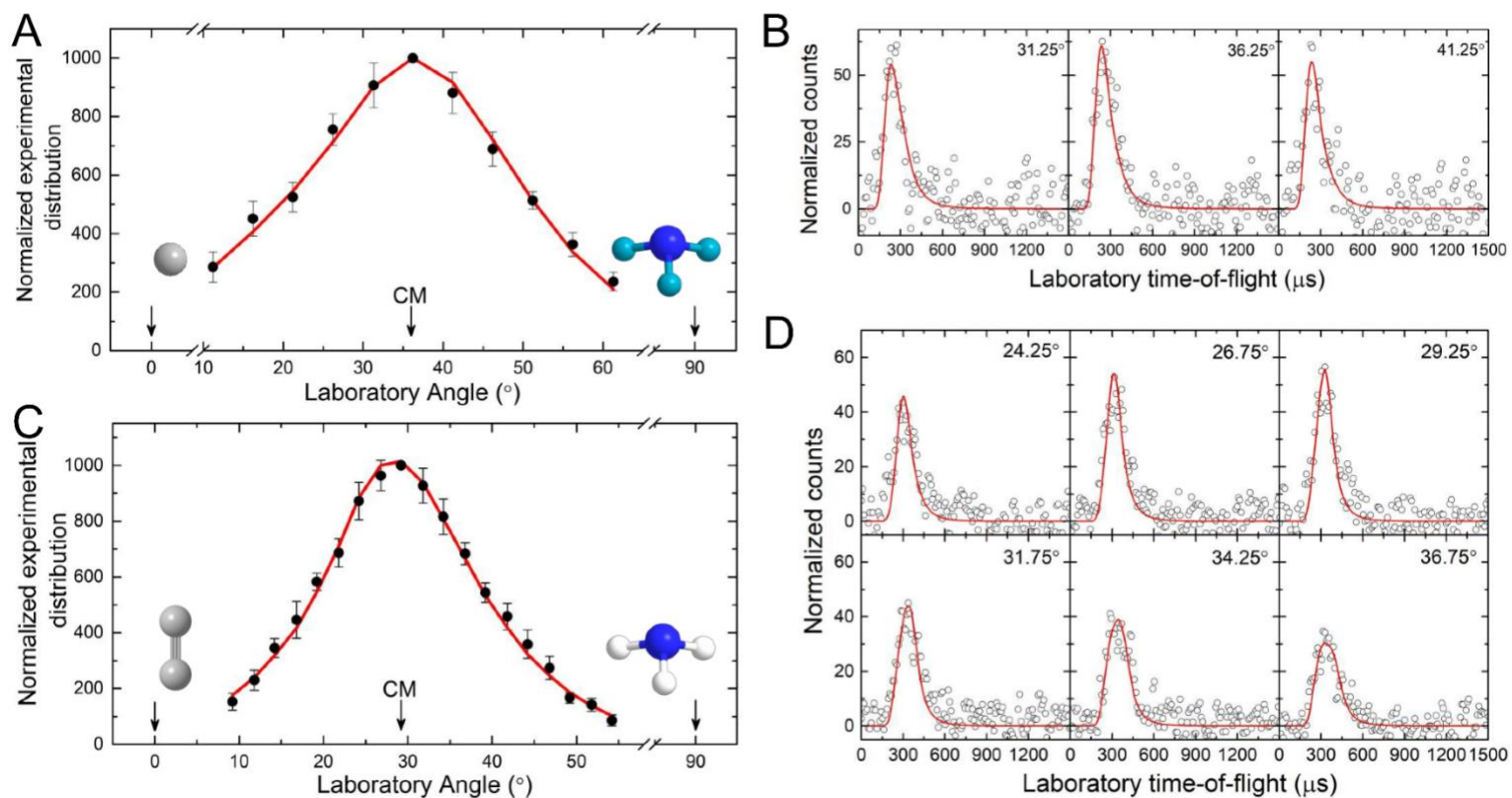


Figure 2. Laboratory data of the C-ND₃ and C₂-NH₃ reactions. Laboratory angular distributions (A, C), and time-of-flights (B, D) for the carbon – D₃-ammonia (A, B) and dicarbon – ammonia (C, D) reactions. The solid circles with their error bars represent the normalized experimental distribution; the open circles indicate the experimental data. The red lines represent the best fits obtained. Atoms are color coded as follows: carbon, gray; nitrogen, blue; deuterium, light blue; and hydrogen, white.

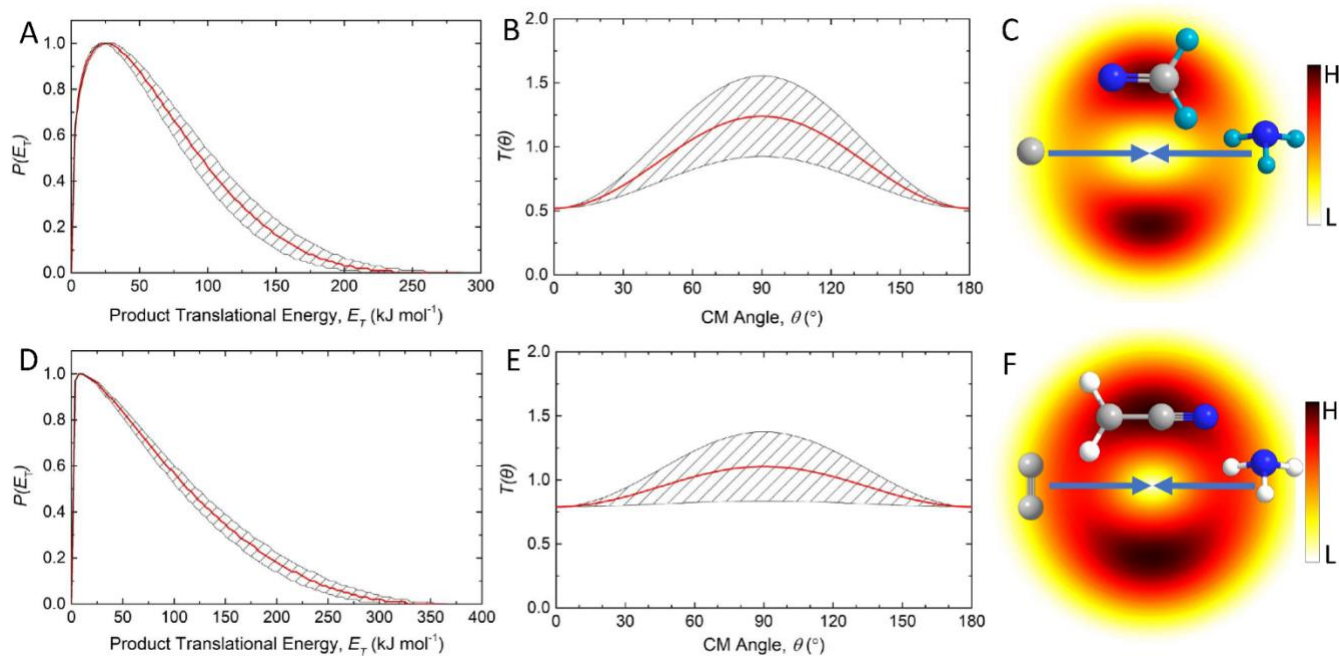
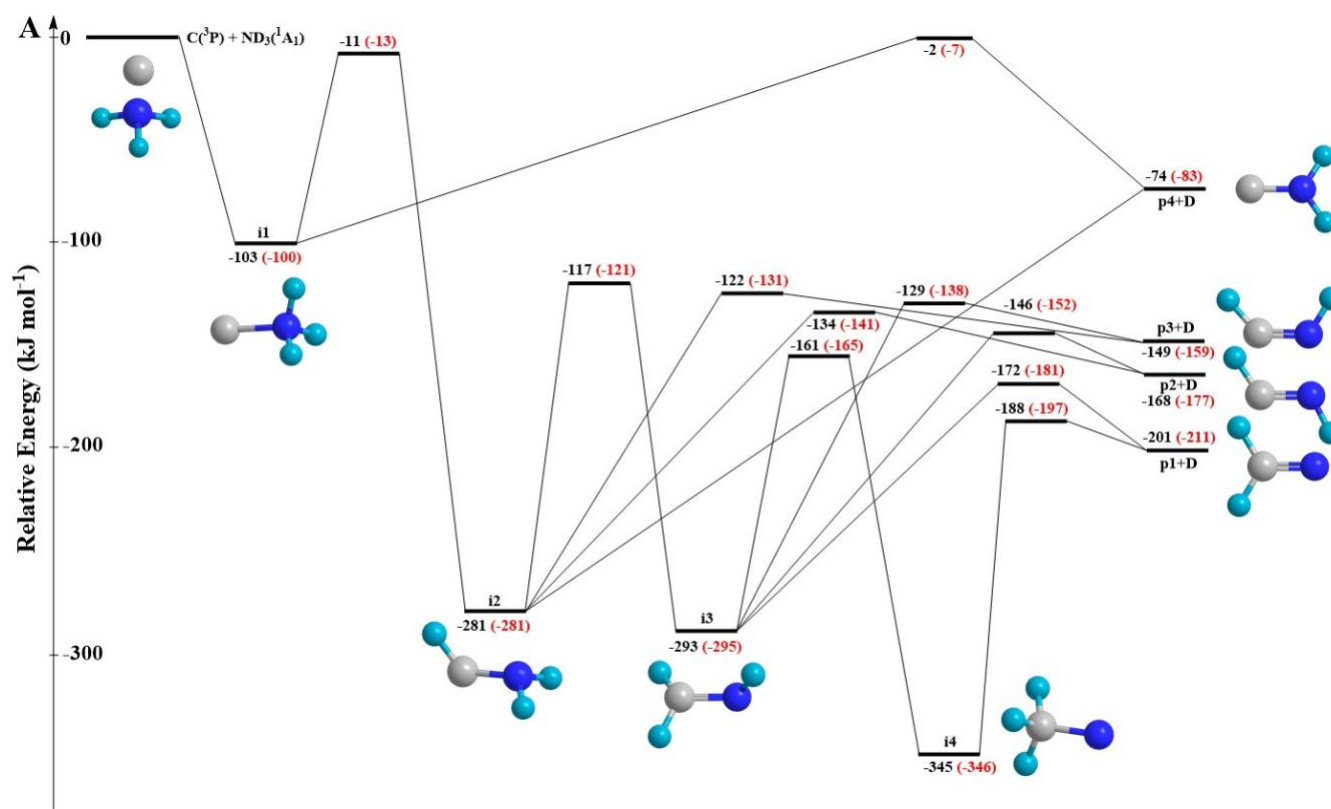


Figure 3. CM functions of the C-ND₃ and C₂-NH₃ reactions. Center-of-mass translational energy distributions ($P(E_T)$; A, D), angular flux distributions ($T(\theta)$; B, E), and the corresponding flux contour map (C, F) for the carbon – D₃-ammonia (A, B, C) and dicarbon – ammonia (D, E, F) reactions. The red lines represent the best-fit; shaded areas depict the error limits of the best fits.



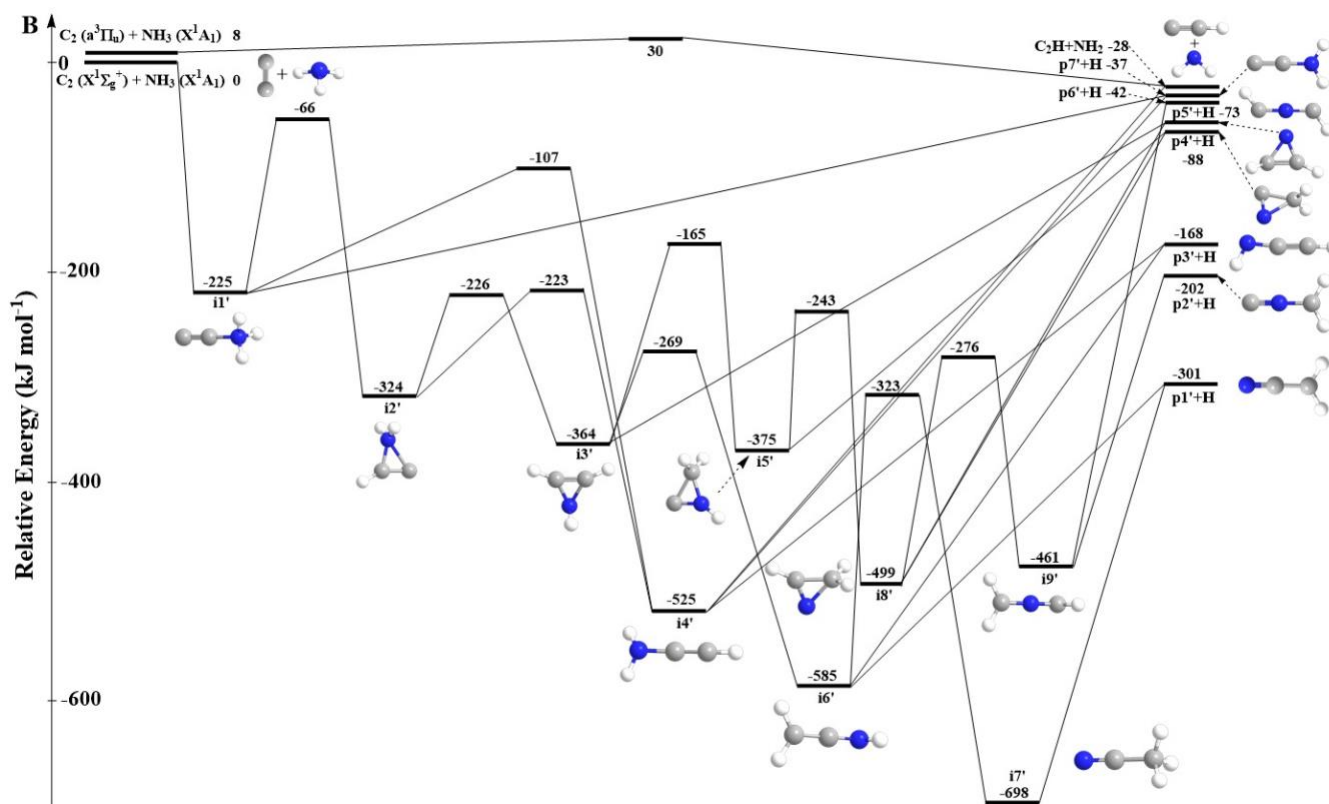
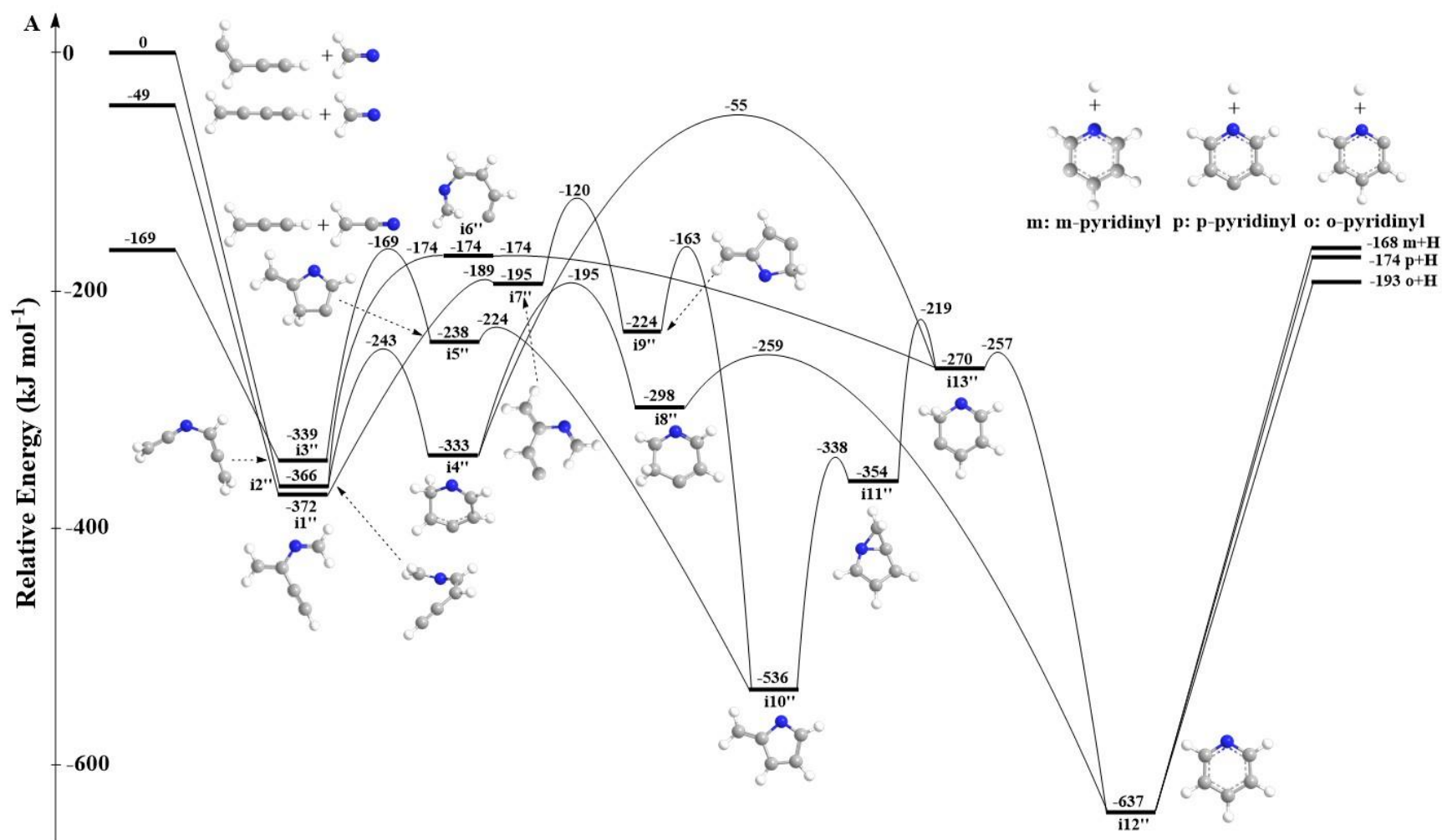


Figure 4. Potential energy surfaces of the reactions of carbon – D3-ammonia (A) and dicarbon – ammonia (B). For the carbon – D3-ammonia reaction, energies provided in black are relative energies for the deuterated reactants, whereas the energies in red refer to the hydrogenated reactants. Corresponding Cartesian coordinates and vibrational modes are compiled in the Supplementary Information.



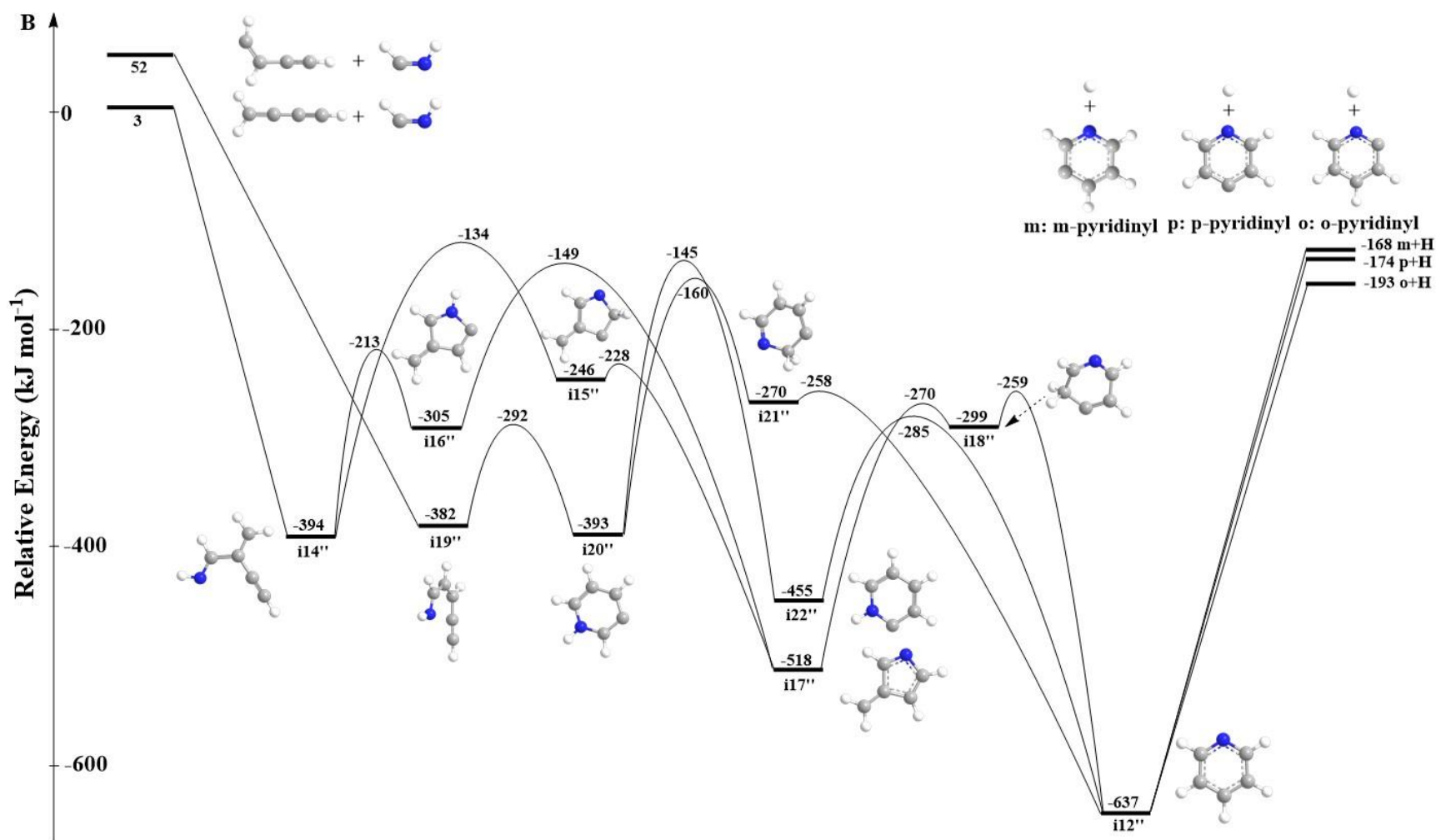
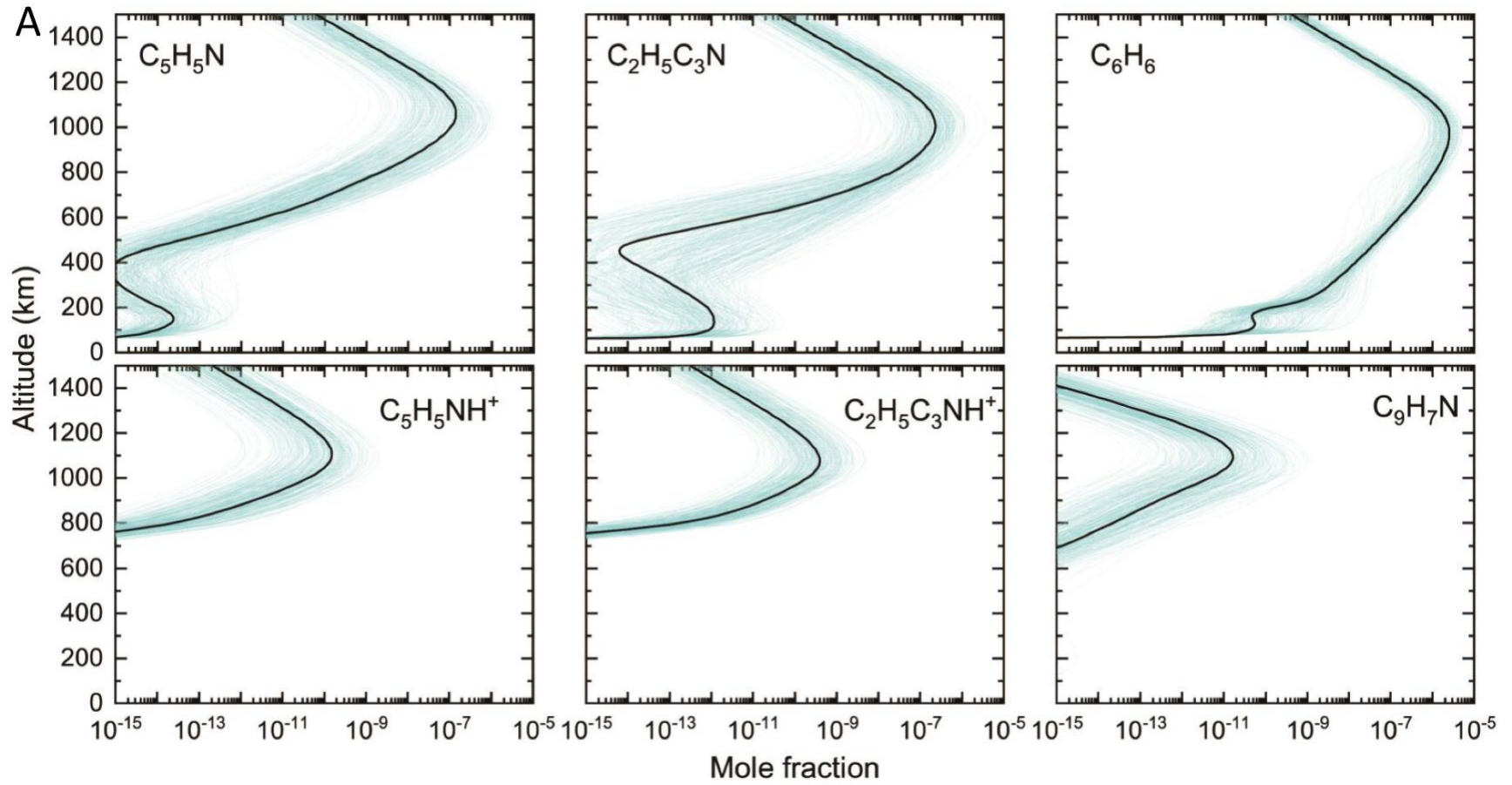


Figure 5. Formation pathways to pyridinyl radicals and the pyridine intermediate. Distinct pyridinyl radicals and pyridine can be formed from reactions of methylene amidogen (H_2CN) with *i/n*- C_4H_3 isomers and the cyanomethyl (H_2CCN) with propargyl (A) and *cis*-iminomethyl (HCNH) with *i/n*- C_4H_3 isomers (B).



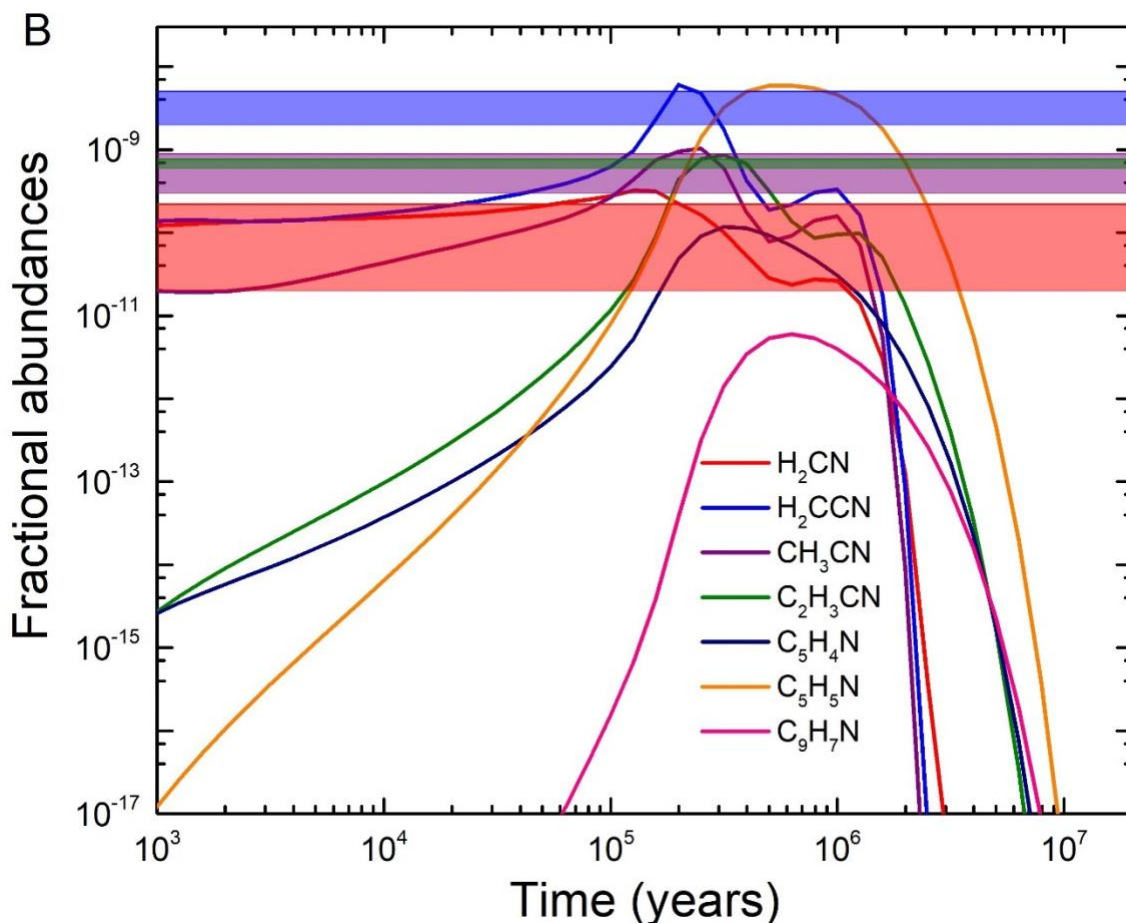


Figure 6. Results of the astrochemical model for Titan’s atmosphere and TMC-1. Mole fraction profiles for six species obtained from a one-dimensional photochemical model of Titan’s atmosphere (A) and the fractional abundance of the gas-phase methylene amidogen (H_2CN , red), cyanomethyl (H_2CCN , blue), methyl cyanide (CH_3CN , purple), vinyl cyanide (C_2H_3CN , olive), pyridinyl (C_5H_4N , navy), pyridine (C_5H_5N , orange), and (iso)quinoline (C_9H_7N , pink) plotted as a function of time (B). The solid black lines in Figure 6A represent the nominal model results, with 280 runs of the Monte Carlo analysis displayed as cyan lines. Please confer to the text for details on the error analysis and the assignment of the species. Astronomically observed fractional abundances of the four species are visualized with the colored horizontal bars in Figure 6B.

Supplementary information

This file includes:

The file includes:

Text: 853 words

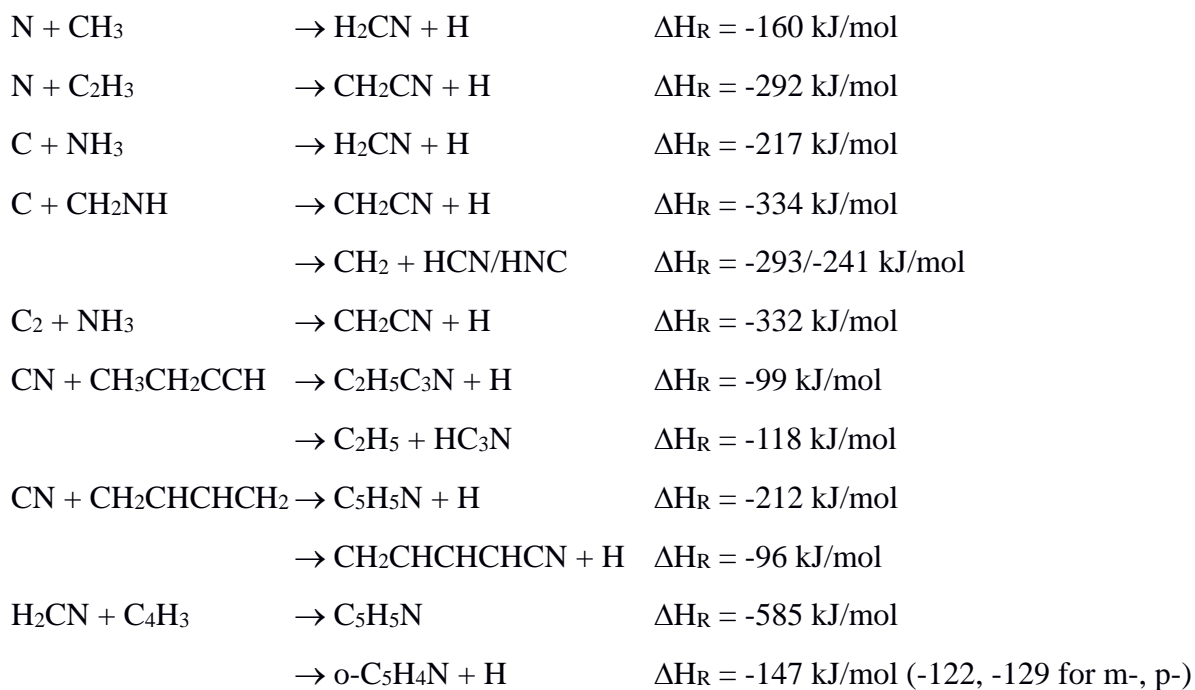
Number of references: 14

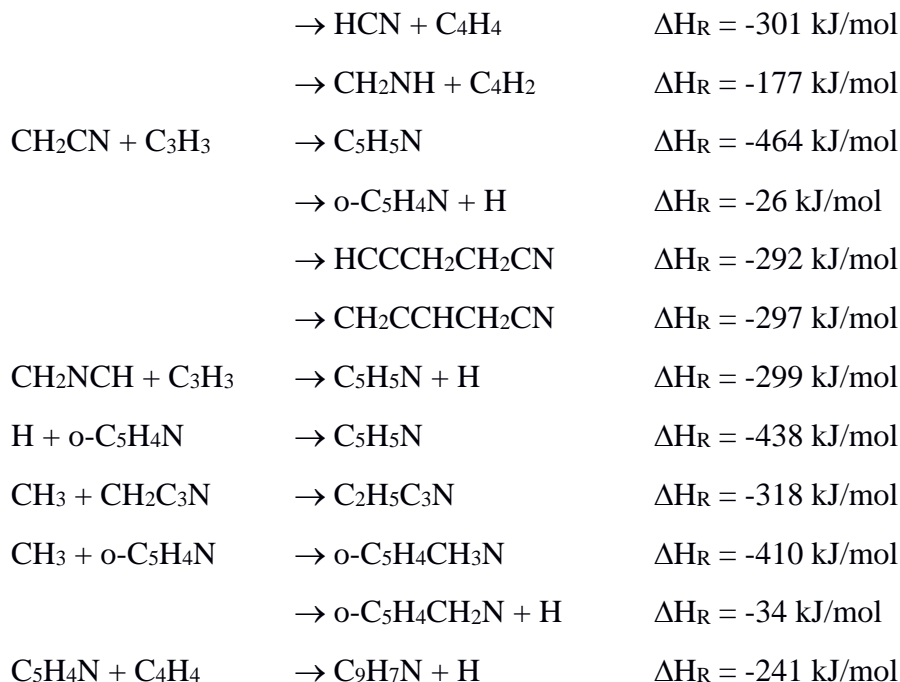
Number of figures: 5

Number of tables: 7

Astrochemical modeling

The main aspects of the chemistry of the formation of pyridine (C_5H_5N) and ethylcyanoacetylene ($C_2H_5C_3N$) (the most abundant linear C_5H_5N isomer deduced from production fluxes) and (iso)quinoline (C_9H_7N) are presented below¹⁻⁵:





The rates of these barrier-free reactions are incorporated from capture theory when no experimental measurements exist, while the rates of the three-body reactions are taken to be equal to similar reactions of benzene derivatives. For some reactions such as $\text{CN} + \text{CH}_2\text{CHCHCH}_2$ (and also $\text{CH}_2\text{CN} + \text{C}_3\text{H}_3$) the formation of pyridine is in competition with the formation of nitriles, see for example^{1,4}. The destruction of pyridine, $\text{C}_2\text{H}_5\text{C}_3\text{N}$ and quinoline occurs mainly through photodissociation, through reactions with $\text{N}(^2\text{D})^6$ and C_2H , and through reactions with ions such as HCNH^+ , C_2H_5^+ , NH_4^+ . Unlike benzene where ionic chemistry plays an important role in its formation through the $\text{C}_4\text{H}_3^+ + \text{C}_2\text{H}_2$ and $\text{C}_4\text{H}_3^+ + \text{C}_2\text{H}_4$ reactions^{7,8}, ionic reactions do not appear to be effective in producing pyridine (nor likely quinoline). Indeed the pyridine forming reaction $\text{C}_4\text{H}_3^+ + \text{HCN}$ is slow, in contrast to the benzene forming reaction $\text{C}_4\text{H}_3^+ + \text{C}_2\text{H}_2^9$, and even if the reaction $\text{C}_4\text{H}_3^+ + \text{CH}_2\text{NH}$ is fast (this reaction has never been studied to the best of our knowledge) the flux will be much smaller than the reaction $\text{C}_4\text{H}_3^+ + \text{C}_2\text{H}_4$ because CH_2NH is much less abundant than C_2H_4 (CH_2NH has not yet been detected in Titan's atmosphere). Moreover, the proton affinity of pyridine (937 kJ mol^{-1}) is very high which will induce a proton transfer from ions (HCNH^+ , C_2H_5^+ , NH_4^+ and so on) to $\text{C}_5\text{H}_5\text{N}$. If the electronic recombination reaction of $\text{C}_5\text{H}_5\text{NH}^+$ does not lead to a 100% yield of $\text{C}_5\text{H}_5\text{N} + \text{H}$, not only will the ionic chemistry not induce the formation of pyridine, but it will promote its destruction instead.

The absorption spectrum of pyridine and quinoline and the products for the photodissociation

of pyridine has been studied. The products for the photodissociation of quinoline are deduced from photodissociation of similar species¹⁰⁻¹³. For pyridine (and quinoline) photodissociation, the rate we use is in fact the maximum limit. Indeed, as for benzene, the lifetime of C₅H₅N** produced after photon absorption is quite long so some of these molecules will stabilize before dissociating¹³. On the other hand, the lifetime of pyridine is shorter than benzene (the pyridine lifetime is 0.1 μs following excitation at 193 nm compared with 10 μs for benzene) so photodissociation will be more efficient for pyridine than for benzene. The absorption of C₂H₅C₃N has not been studied to the best of our knowledge but the photodissociation of this species will be dominated by the absorption of the chromophore -C₃N, so its absorption spectrum is taken to be the same as CH₃C₃N. The photodissociation products of C₂H₅C₃N are assumed to be C₂H₄ + HC₃N and CH₃ + CH₂C₃N.

To evaluate the uncertainties on the nominal model profiles, obtained using the recommended rate constants, a Monte Carlo simulation was performed according to the method described in Benne et al.¹⁴. Briefly, the rate constants for all reactions were recalculated using their associated uncertainty factors, F_i , the temperature-dependent uncertainty factor, and g_i , a coefficient used to extrapolate F_i to lower temperature, allowing $F_i(T)$ to be determined. Each rate constant was considered to be a random variable, k_i , with a log-normal distribution centered on the nominal value, k_{0_i} , with a standard deviation, $\log F_i$. For bimolecular reactions, k_i was given by

$$\log(k_i) = \log(k_{0_i}) + \varepsilon_i \log[F_i(T)]$$

As ε_i is a random number with a normal distribution centered on zero and a standard deviation of one, this led to a 68.3 % probability of finding a k_i value within the interval $\left[\frac{k_{0_i}}{F_i}, k_{0_i} \times F_i\right]$. 280 simulations were performed using this procedure to establish the possible dispersion from the nominal mole fraction profiles displayed in Figure 6.

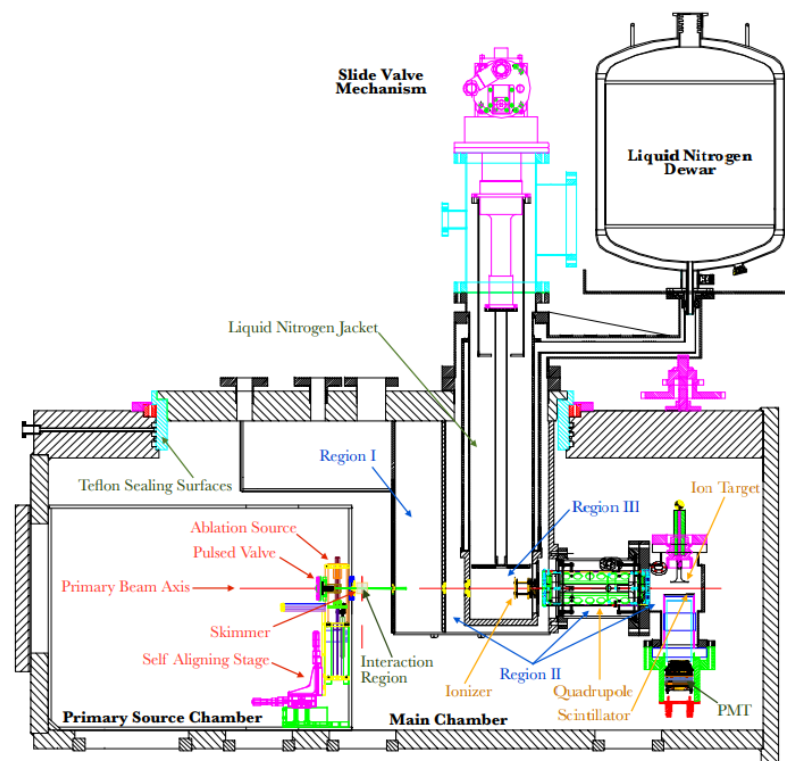
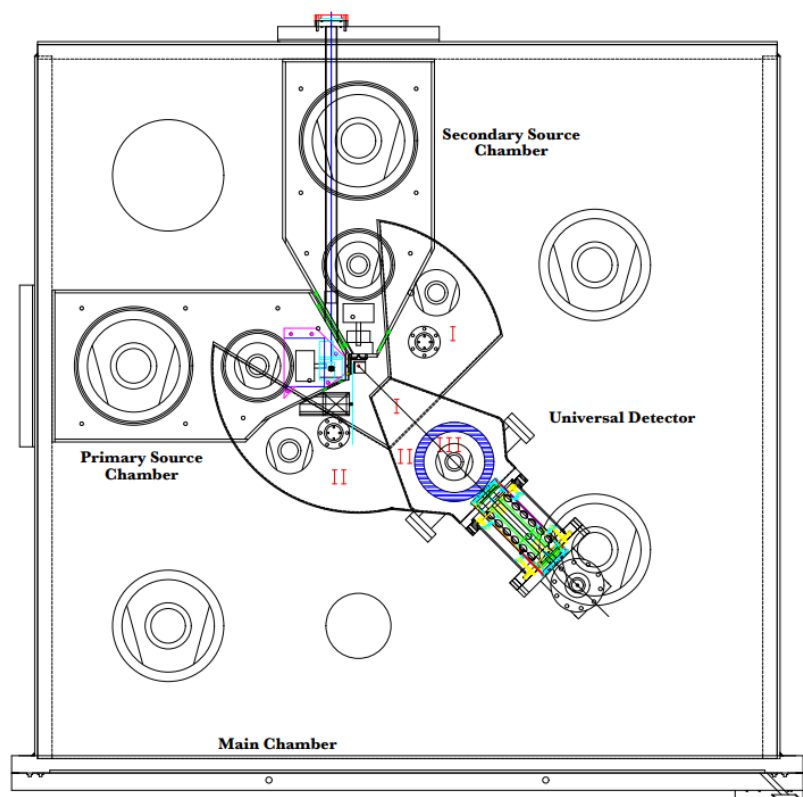


Figure S1. Schematic of the crossed molecular beam machine.

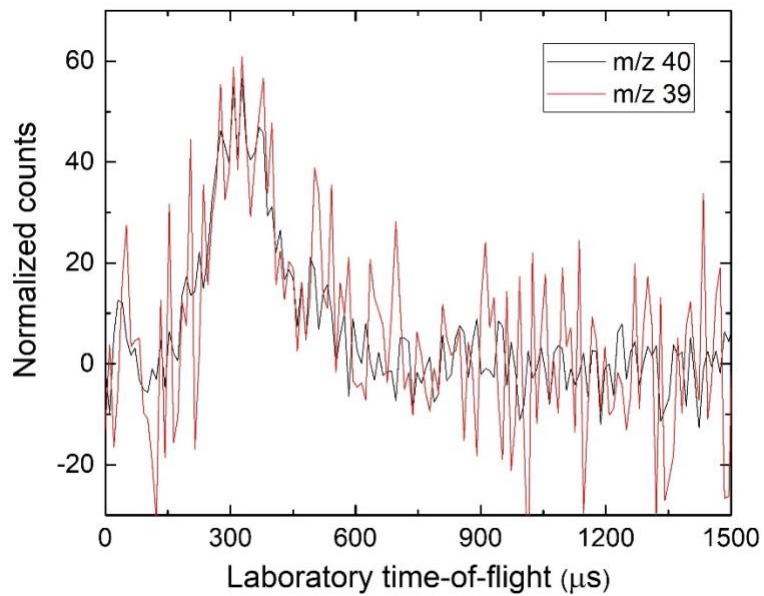


Figure S2. Scaled time-of-flight spectra recorded at the CM angles for $m/z = 40$ and 39 for the C_2-NH_3 reaction.

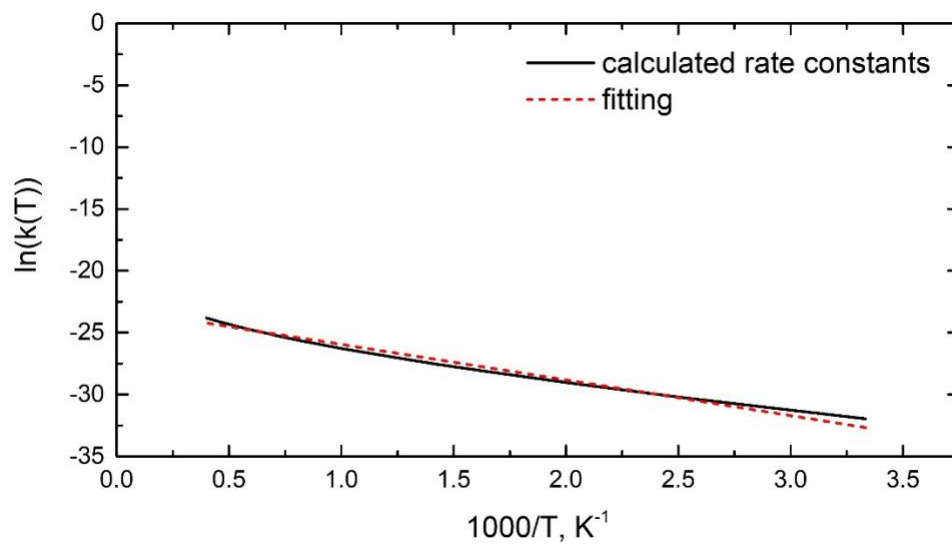


Figure S3. Temperature dependence of the thermal rate constant $k(T)$ for the **p3** + H in the C + NH₃ reaction. The thermal rate constants are obtained using TST calculations.

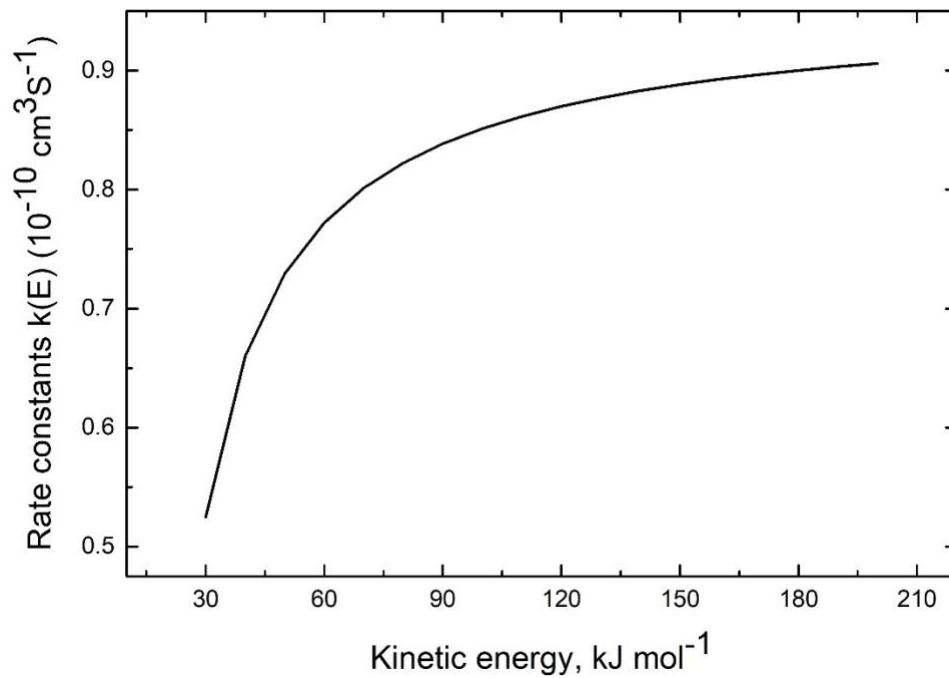


Figure S4. Energy dependence of the suprathermal rate constants $k(E)$ for the **p3** + H in the C + NH₃ reaction. The calculation details are described in Ref. 38.

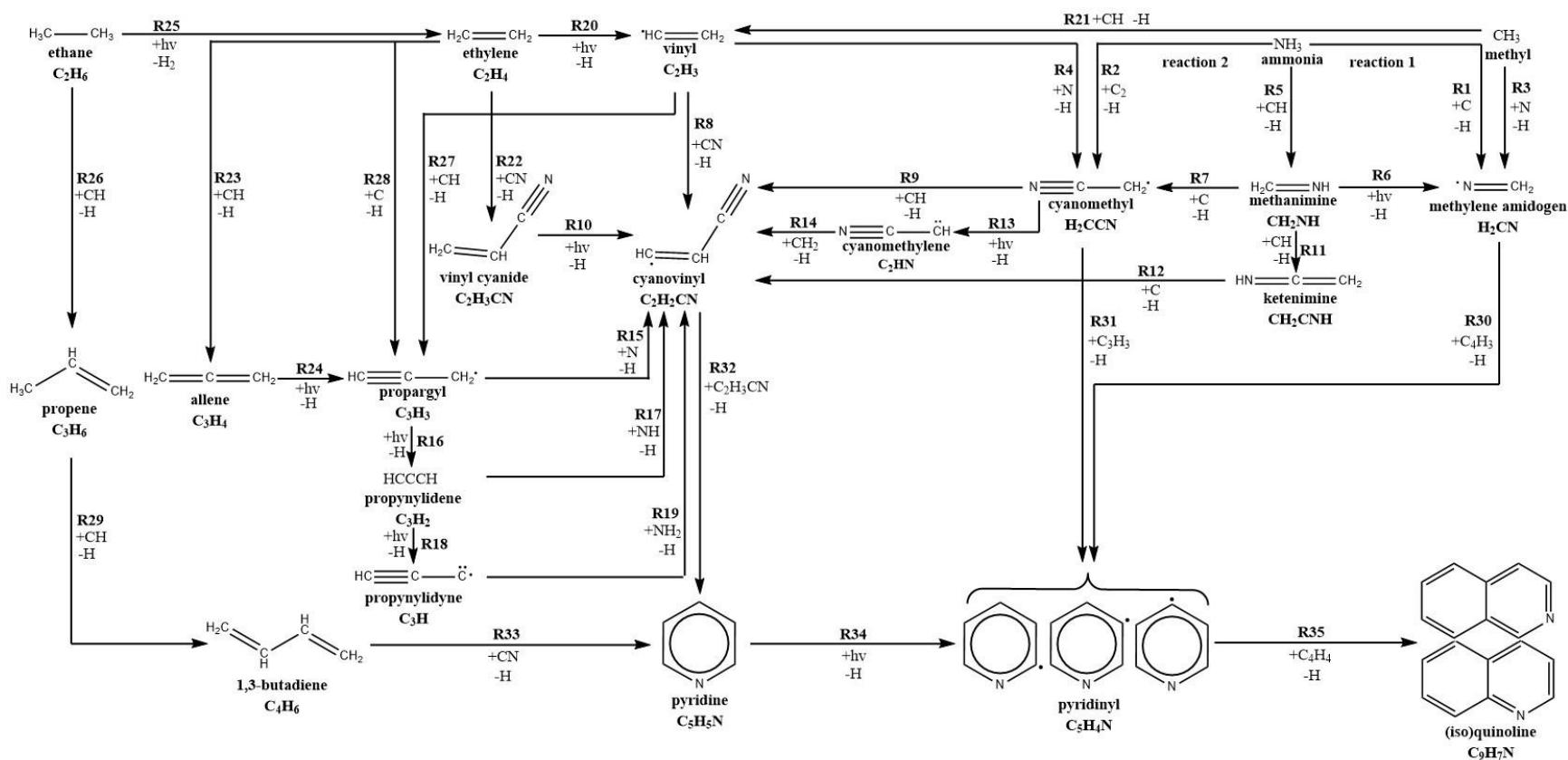


Figure S5. Compilation of key bimolecular reactions and photodissociation processes newly introduced into the astrochemical model for TMC-1 leading to pyridine, pyridinyl, and (iso)quinoline.

Table S1. Peak velocity (v_p) and speed ratios (S) of the atomic carbon (C; 3P), dicarbon (C_2 ; $X^1\Sigma_g^+/a^3\Pi_u$), ammonia (NH_3 ; X^1A_1), and D3-ammonia (ND_3 ; X^1A_1) beams along with the corresponding collision energy (E_c) and center-of-mass angle (θ_{CM}) for each reactive scattering experiment.

beam	v_p (m s $^{-1}$)	S	E_c (kJ mol $^{-1}$)	θ_{CM} (deg)
C	2512 \pm 49	2.9 \pm 0.3		
ND_3	1091 \pm 25	10.1 \pm 1.3	28.1 \pm 0.9	35.9 \pm 0.5
C_2	1451 \pm 19	3.2 \pm 0.1		
NH_3	1143 \pm 34	10.3 \pm 1.4	17.0 \pm 0.3	29.2 \pm 0.3

Table S2. Statistical branching ratios (%) for the reaction of carbon with D3-ammonia (ND_3) at the collision energies (E_c , kJ mol $^{-1}$) of 0 and 28.1 kJ mol $^{-1}$.

E_c	p1	p2	p3	p4
0	8	41	33	18
28.1	7	33	29	31

Table S3. The RRKM rate constants (s^{-1}) for the reaction of carbon with D3-ammonia (ND_3) computed at collision energies of 0.0 and 28.1 kJ/mol.

	0.0	28.1
(i1 \rightarrow i2)	5.27×10^{10}	4.13×10^{11}
(i2 \rightarrow i1)	3.70×10^7	5.36×10^8
(i1 \rightarrow p4)	8.09×10^9	1.37×10^{11}
(i2 \rightarrow i3)	1.56×10^{11}	2.73×10^{11}
(i3 \rightarrow i2)	1.13×10^{11}	2.01×10^{11}
(i2 \rightarrow p2)	5.35×10^{11}	9.16×10^{11}
(i2 \rightarrow p3)	4.36×10^{11}	8.12×10^{11}
(i2 \rightarrow p4)	6.41×10^{10}	1.64×10^{11}
(i3 \rightarrow i4)	5.84×10^{11}	8.16×10^{11}
(i4 \rightarrow i3)	1.64×10^{12}	2.48×10^{12}
(i3 \rightarrow p1)	3.24×10^{12}	4.45×10^{12}
(i3 \rightarrow p2)	7.71×10^{11}	1.26×10^{12}
(i3 \rightarrow p3)	4.60×10^{11}	8.50×10^{11}
(i4 \rightarrow p1)	2.12×10^{13}	2.98×10^{13}

Table S4. Key bimolecular reactions and photodissociation processes associated with the C/C₂ – NH₃ systems newly incorporated into the astrochemical model.

Reactant 1	Reactant 2	Products	α	β	γ	No.
NH ₃	C	H ₂ CN+H	4.00E-10	0	0	R1
NH ₃	C ₂	CH ₂ CN+H	4.00E-10	0	0	R2
CH ₃	N	H ₂ CN+H	4.00E-10	0	0	R3
C ₂ H ₃	N	CH ₂ CN+H	4.00E-10	0	0	R4
NH ₃	CH	CH ₂ NH+H	4.00E-10	0	0	R5
CH ₂ NH	hν	H ₂ CN+H	3.00E-09	0	3.1	R6
CH ₂ NH	C	CH ₂ CN+H	4.00E-10	0	0	R7
C ₂ H ₃	CN	C ₂ H ₂ CN+H	4.00E-10	0	0	R8
CH ₂ CN	CH	C ₂ H ₂ CN+H	4.00E-10	0	0	R9
C ₂ H ₃ CN	hν	C ₂ H ₂ CN+H	3.00E-09	0	3.1	R10
CH ₂ NH	CH	CH ₂ CNH+H	4.00E-10	0	0	R11
CH ₂ CNH	C	C ₂ H ₂ CN+H	4.00E-10	0	0	R12
CH ₂ CN	hν	C ₂ HN+H	3.00E-09	0	3.1	R13
C ₂ HN	CH ₂	C ₂ H ₂ CN+H	4.00E-10	0	0	R14
C ₃ H ₃	N	C ₂ H ₂ CN+H	4.00E-10	0	0	R15
C ₃ H ₃	hν	C ₃ H ₂ +H	3.00E-09	0	3.1	R16
C ₃ H ₂	NH	C ₂ H ₂ CN+H	4.00E-10	0	0	R17
C ₃ H ₂	hν	C ₃ H+H	3.00E-09	0	3.1	R18
C ₃ H	NH ₂	C ₂ H ₂ CN+H	4.00E-10	0	0	R19
C ₂ H ₄	hν	C ₂ H ₃ +H	3.00E-09	0	3.1	R20
CH ₃	CH	C ₂ H ₃ +H	4.00E-10	0	0	R21
C ₂ H ₄	CN	C ₂ H ₃ CN+H	4.00E-10	0	0	R22
C ₂ H ₄	CH	C ₃ H ₄ +H	4.00E-10	0	0	R23
C ₃ H ₄	hν	C ₃ H ₃ +H	3.00E-09	0	3.1	R24
C ₂ H ₆	hν	C ₂ H ₄ +H ₂	3.00E-09	0	3.1	R25
C ₂ H ₆	CH	C ₃ H ₆ +H	4.00E-10	0	0	R26
C ₂ H ₃	CH	C ₃ H ₃ +H	4.00E-10	0	0	R27
C ₂ H ₄	C	C ₃ H ₃ +H	4.00E-10	0	0	R28
C ₃ H ₆	CH	C ₄ H ₆ +H	4.00E-10	0	0	R29
H ₂ CN	C ₄ H ₃	C ₅ H ₄ N+H	4.00E-10	0	0	R30
CH ₂ CN	C ₃ H ₃	C ₅ H ₄ N+H	4.00E-10	0	0	R31
C ₂ H ₂ CN	C ₂ H ₃ CN	C ₅ H ₅ N+CN	4.00E-10	0	0	R32
C ₄ H ₆	CN	C ₅ H ₅ N+H	4.00E-12	0	0	R33
C ₃ H ₅ N	hν	C ₅ H ₄ N+H	3.00E-09	0	3.1	R34
C ₃ H ₄ N	C ₄ H ₄	C ₉ H ₇ N+H	4.00E-10	0	0	R35
CH ₃ CN	hν	CH ₂ CN+H	3.00E-09	0	3.1	R36
C ₂ H ₃	NH	CH ₃ CN+H	4.00E-10	0	0	R37
CN	CH ₃	CH ₂ CN+H	4.00E-10	0	0	R38
C ₂ H	NH ₂	CH ₂ CN+H	4.00E-10	0	0	R39
C ₂ H ₃	hν	C ₂ H ₂ +H	3.00E-09	0	3.1	R40
C ₂ H ₄	hν	C ₂ H ₂ +H ₂	3.00E-09	0	3.1	R41
CH ₃	C	C ₂ H ₂ +H	4.00E-10	0	0	R42
CH ₂	CH	C ₂ H ₂ +H	4.00E-10	0	0	R43
CH ₂	NH	H ₂ CN+H	4.00E-10	0	0	R44
CH	NH ₂	H ₂ CN+H	4.00E-10	0	0	R45
CH ₃	NH	CH ₂ NH+H	4.00E-10	0	0	R46
CH ₂	NH ₂	CH ₂ NH+H	4.00E-10	0	0	R47
C ₄ H ₅ N	CH	C ₅ H ₅ N+H	4.00E-10	0	0	R48
C ₃ H ₆	CN	C ₄ H ₅ N +H	4.00E-10	0	0	R49
CH ₃ CN	C	C ₂ H ₂ CN+H	4.00E-10	0	0	R50

Table S5. Optimized Cartesian coordinates (Angstrom) and vibrational frequencies (cm^{-1}) for the intermediates, transition states, reactants, and products involved in the reactions of carbon (C) with ammonia (NH_3) at the CCSD(T)/aug-cc-pVQZ level.

Reagents

NH_3

H	0.2920763332	0.6431570428	-0.0000000704
N	0.2426306353	-0.3684334478	-0.0000000879
H	0.7606464234	-0.6823617387	-0.8116631239
H	0.7606466082	-0.6823618562	0.8116632825

Frequencies

1059.43	1673.76	1673.79
3476.22	3607.15	3607.31

Products

CNH_2

C	-0.9933203864	-0.9214443079	0.0019111645
N	0.1124136467	-0.2955814902	0.2602648600
H	0.2975499258	0.6506602979	-0.0669802735
H	0.8643903439	-0.7113712499	0.8065141390

Frequencies

729.14	1026.37	1431.05
1627.18	3380.82	3452.96

H_2CN

H	-2.6544106164	0.4788743740	-0.8724769137
H	-2.6544073940	-1.0629837221	0.1942219438
C	-2.1083030395	-0.2077878248	-0.2173258026
N	-0.9021919501	-0.0214978272	0.0519437726

Trans-HCNH

C	-1.2403610158	0.8976528810	0.1235983255
N	-0.0966015804	0.4604591028	-0.0630484877
H	-1.8674903239	1.3560037585	-0.6456500726
H	0.3919166204	0.0540003576	0.7329070547

Frequencies

915.27	975.80	1198.91
1747.93	3057.20	3463.99

Cis-HCNH

H	-1.9207551690	1.3703203969	-0.6286635164
C	-1.2152373401	0.9038689002	0.0673580619
N	-0.0764022072	0.4558729561	-0.0482882515
H	0.3992817164	0.4798667468	-0.9545312940

Frequencies

856.12	895.91	1026.32
1796.26	3008.66	3349.23

Intermediates

i1

C	-1.1894678183	-0.9542707245	0.0851101292
N	0.3105105939	-0.3613889756	0.0178554606
H	0.2937207108	0.6557867370	0.0036902535
H	0.8508218659	-0.6604236666	0.8263574396
H	0.7864481175	-0.6844401806	-0.8213033347

Frequencies

564.20	774.84	775.14
1311.16	1651.71	1651.94
3408.61	3522.57	3522.89

i2

H	-1.6922382002	-1.5923622445	0.3507131705
C	-1.2046714483	-0.8190124445	-0.2381403996
H	0.2700264633	0.4934781122	0.2219812975
N	0.1158154341	-0.4496963491	-0.1096604394
H	0.6980534112	-0.6416152941	-0.9143410390

Frequencies

467.14	642.25	1086.37
1111.59	1261.55	1635.63
3116.57	3503.61	3585.55

i3

H	-1.9526769089	1.3839273143	0.0312517729
H	-1.9522667175	-0.4066837897	0.5091839033
C	-1.4082796893	0.5307877328	0.4277311559
N	-0.0762237674	0.4380610522	0.0791584036
H	0.5575364800	0.6455537103	0.8561111650

Frequencies

597.96	725.46	1022.97
1033.04	1208.50	1407.81
3081.94	3181.15	3388.57

i4

H	-2.5271326402	0.5275089738	0.8455204920
H	-2.5271282332	0.3823144949	-0.9293346016
H	-2.5271189379	-1.0821206285	0.0838181791
C	-2.1449804709	-0.0574401193	-0.0000055465
N	-0.7243634224	-0.0574442745	-0.0000000289

Frequencies

970.68	970.70	1052.49
1388.10	1439.90	1440.07
2966.17	3043.50	3043.74

Transition states

i1-i2

C	-1.2904643133	-0.1622041734	0.0528994377
N	0.2574410299	-0.0943573664	-0.0086854701
H	-0.4716490707	0.8827577429	0.0054427490
H	0.7858269331	-0.3004802937	0.8309508648
H	0.7188444210	-0.3257159094	-0.8806075814

Frequencies

1682.01i	669.38	828.24
837.16	1135.33	1516.26
2214.69	3458.50	3595.22

i2-i3

H	-1.2978772894	-0.6995688413	0.5912701261
C	-0.6602691565	-0.1125924912	-0.0618714970
H	0.0653807966	0.8378001215	0.3924678722
N	0.7399349670	-0.1331852620	-0.0102571205
H	1.1528306823	0.1075474730	-0.9116093807

Frequencies

2020.90i	568.49	885.60
1145.06	1155.40	1252.39
2362.67	3156.27	3455.42

i3-i4

H	-0.6199616799	0.4011258166	-1.0020966152
H	1.0814113318	-0.0349079901	0.0564017817
H	-0.7299868098	-0.9753435963	0.2554958557
C	-0.2111511007	-0.1011742743	-0.1292105004
N	0.4796892585	0.7103000441	0.8194094782

Frequencies			
	2007.75i	808.34	863.01
	1086.54	1108.77	1370.37
	2338.18	3070.11	3186.26
TS4: i4 -H ₂ CN+H			
H	-2.4961864208	0.5206942498	0.8919184391
H	-2.4962626561	0.3678856178	-0.9739658543
H	-2.7882606466	-1.4991596464	0.1179012034
C	-1.9580041580	0.2681002147	-0.0266157351
N	-0.7120101186	0.0552975640	-0.0092390531
Frequencies			
	737.72i	377.59	535.50
	940.38	986.62	1365.80
	1577.32	3003.40	3080.00
TS5: i1 -CNH ₂ +H			
C	-1.0709041950	-1.0215745615	0.0815068427
N	0.1992995094	-0.5514812678	0.0249796829
H	0.4075914569	0.9178384447	-0.0046321396
H	0.7910227493	-0.6624576001	0.8488020870
H	0.7250244794	-0.6870620152	-0.8389464730
Frequencies			
	1677.25i	693.77	908.04
	1093.86	1107.31	1236.49
	1597.59	3373.76	3438.58
TS6: i2 -HNCH-trans+H			
H	-1.7934092894	-1.4433736508	0.4134862479
C	-1.1054579840	-1.0667244438	-0.3437882844
H	0.3372112649	0.7926245217	0.3620798321
N	0.1039854473	-0.7542380077	-0.1412403940
H	0.6446555612	-0.5374964194	-0.9799844017
Frequencies			
	1288.62i	567.37	614.87
	892.88	1034.33	1210.47
	1576.15	3094.54	3436.63
TS7: i3 -HCNH-trans +H			
H	-2.0469895379	1.2516261050	-0.0816561852
H	-2.1449398866	-0.6628754098	0.4781219017
C	-1.2234029792	0.9056857999	0.5507866290
N	-0.0756399919	0.6235325772	0.1335310565
H	0.6590613956	0.4736759277	0.8226535980
Frequencies			
	974.09i	533.61	706.01
	920.00	996.70	1210.30
	1641.00	3051.46	3477.31
TS8: i3 -H ₂ CN+H			
H	-2.0104593049	1.4105545666	0.0854255674
H	-2.0100006747	-0.4028402326	0.5695027994
C	-1.4669167972	0.4700470050	0.2002930435
N	-0.2294788357	0.4022699271	-0.0547783161
H	0.8849456124	0.7116157339	1.1029929059
Frequencies			
	1196.87i	469.21	605.36
	901.92	952.89	1363.78
	1568.83	3022.32	3106.34
TS9: i3 -HCHN-cis +H			
N	-0.0626492823	-0.0578199324	-0.6073326617

C	0.1398712320	-0.0646430046	0.6169361531
H	-0.2603333692	0.8121467167	-1.1067808513
H	0.3959790624	0.7181600998	1.3408320025
H	-1.5188517119	0.0147509759	1.4235729461

Frequencies

932.16i	414.52	631.96
852.59	897.59	975.79
1705.45	2992.14	3371.73

TS10: **i2**-HCHN-cis +H

C	0.0496204860	-0.1001076326	-0.6874776856
N	0.0878062752	0.0911919989	0.5499932305
H	-0.6805889055	0.1387471724	-1.4641976588
H	-0.6197544000	0.7120633340	0.9556393538
H	-0.4015921914	-1.1739958577	1.5316373109

Frequencies

1146.69i	483.01	604.33
838.40	963.20	1087.21
1631.65	3046.70	3349.79

Table S6. Optimized Cartesian coordinates (Angstrom) and vibrational frequencies (cm^{-1}) for the intermediates, transition states, reactants, and products involved in the reactions of dicarbon (C_2) with ammonia (NH_3) at the CCSD(T)/aug-cc-pVTZ level.

Reagents

CC-singlet

C	0.9952159254	2.4895524659	0.0000000000
C	1.8541340746	1.5802375341	0.0000000000

Frequencies

1839.74

CC-triplet

C	0.9714406887	2.5147227080	0.0000000000
C	1.8779093113	1.5550672920	0.0000000000

Frequencies

1626.64

NH_3

N	0.9032657888	1.7990987104	-0.0283246089
H	1.9168543871	1.7731051376	0.0161169887
H	0.5896810578	2.2379536100	0.8313585748
H	0.5896587665	0.8346425420	0.0110690454

Frequencies

1062.66 1672.48 1672.58

3463.43 3592.09 3592.37

Products – Hydrogen loss

p1'- H_2CCN

C	-3.5113218329	0.6957951603	0.0000000000
C	-2.2758036638	1.3417953683	0.0000000000
N	-1.2344952172	1.8863012203	0.0000000000
H	-3.5525242695	-0.3831820446	0.0000000000
H	-4.4208950166	1.2776602956	0.0000000000

Frequencies

361.82 410.91 639.50

1028.14 1032.94 1453.51

2106.03 3176.35 3288.10

p2'- CNCH_2

C	0.2302786477	0.0388504735	-1.1737183331
N	0.0765014478	-0.0300441832	0.1628446127
C	-0.0590572679	-0.0846127020	1.3440269914
H	0.6338526302	-0.8175478564	-1.6908521866
H	-0.0633999503	0.9450738400	-1.6799461854

Frequencies

267.65 351.17 516.29

1082.88 1130.14 1476.20

2014.43 3172.00 3302.50

p3'- HNCCH

C	-0.0000744816	-0.0329406061	0.0594034496
C	-0.0000823576	0.0061864152	1.3036509529
N	0.0000552715	0.0838882631	-1.2183936925
H	0.0000833841	-0.8287540002	-1.6778857414
H	0.0010174992	-0.0181745353	2.3664470687

Frequencies

282.32 409.51 450.54

460.30 1094.69 1167.82

1878.30 3444.31 3452.74

p4'- CNCH_2 -cic-ccsd.out

C	-1.0315761990	1.0726409199	0.4815831706
C	0.4044794514	1.0816451737	0.0562025756
N	-0.9511133655	0.3419132509	-0.5012599035
H	0.7739125694	1.8785380463	-0.5738577767
H	1.1121975438	0.4212326091	0.5373319340

Frequencies

451.03	698.74	914.41
972.08	1053.07	1477.66
1799.62	3147.81	3264.77

p5'-HCNCH-cic

C	-2.7315575846	0.7532997051	0.3325871697
C	-1.3693002226	0.7562223352	0.0316040394
N	-1.8744114271	-0.4253195170	-0.0797057126
H	-0.4075840205	1.2343059149	-0.0899684272
H	-3.6091267453	1.1091715618	-0.1945170694

Frequencies

676.60	806.02	900.98
931.99	1017.71	1263.96
1595.50	3164.78	3228.10

p6'-HCNCH

C	0.1436927101	-0.0459816405	-1.1364480880
N	0.0277999840	-0.1807549654	0.0932931191
C	-0.0452783852	-0.2416461749	1.3355246718
H	0.7674068264	-0.6490795594	-1.7859582321
H	-0.9799064978	-0.1798303414	1.8842323676

Frequencies

418.61	431.84	548.08
645.35	930.91	1268.72
1793.80	3165.51	3187.08

p7'-H₂NCC

C	-3.3943594394	1.4021634927	-0.0330769642
C	-2.1955504586	0.9231724138	-0.0141800666
N	-4.6095313447	1.8872458411	-0.0524795501
H	-4.7745758274	2.8794911116	-0.1298858597
H	-5.4143929298	1.2822671408	0.0106224407

Frequencies

250.95	277.15	457.39
1089.32	1136.16	1643.87
1992.71	3545.24	3655.93

Products – Diatomic loss

CCH₂

C	-4.4936456595	1.0604997146	0.0000000000
C	-5.7991757611	1.0026148420	0.0000000000
H	-3.9909460566	2.0244443888	0.0000000000
H	-3.9076025228	0.1448310545	0.0000000000

Frequencies

334.50	735.53	1218.48
1658.20	3122.94	3212.72

CH₃

C	-3.7439913569	0.9044748851	0.0000000000
H	-3.6827293956	1.9822470432	0.0000000000
H	-2.8412402496	0.3125198490	0.0000000000
H	-4.7080389979	0.4186282227	0.0000000000

Frequencies

496.26	1419.04	1419.32
3114.51	3294.20	3294.52

CN			
C	-3.9235798168	0.0526859896	-0.0505174148
N	-2.7505461210	-0.0086756109	0.0511838882
Frequencies			
2047.02			
HCCH			
C	-2.2659004487	0.7915210348	-0.5489139075
C	-1.4048754979	1.1017278813	0.2430052110
H	-3.0229375347	0.5189936474	-1.2450661960
H	-0.6478374687	1.3743001563	0.9391389024
Frequencies			
592.63	744.05		748.25
1994.29	3394.15		3502.03
NH			
N	-5.0314562212	0.8270822024	0.0000000000
H	-6.0681537788	0.8168677976	0.0000000000
Frequencies			
3316.66			
Products – triatomic loss			
C₂H			
C	-2.1251664279	1.4561036200	0.0000000000
C	-0.9116097073	1.3878936144	0.0000000000
H	0.1513161352	1.3281227656	0.0000000000
Frequencies			
277.84	277.93		2004.03
3444.00			
CH₂			
C	0.5643229808	2.6925678760	0.0000000000
H	1.5382405669	2.1585901950	0.0000000000
H	0.8863651323	3.7555525990	0.0000000000
Frequencies			
1395.37	2911.72		2982.21
HCN			
C	-2.9341609294	1.4371232641	0.0000000000
H	-4.0012095834	1.4232707382	0.0000000000
N	-1.7740994872	1.4521659977	0.0000000000
Frequencies			
717.02	717.04		2107.00
3432.82			
HNC			
H	-3.5816631508	0.0896920456	0.0556058680
N	-2.5926335666	-0.0099767083	-0.0321272858
C	-1.4270769626	-0.1272434672	-0.1351145323
Frequencies			
453.55	2036.73		3805.94
NH₂			
N	-2.2893248185	0.0194787741	0.0000000000
H	-1.9068507422	0.9731738754	0.0000000000
H	-3.3042044392	0.1802273504	0.0000000000
Frequencies			
1539.75	3359.56		3453.36
Intermediates			
il'			
C	-4.9343582319	0.5184036386	-0.1030368723
C	-3.7076291179	0.7389389301	-0.2407041336
N	-6.3357239293	0.2660792143	0.0551349170

H	-6.7458168567	0.8773959426	0.7659701927
H	-6.8433217313	0.4250964786	-0.8191006153
H	-6.5095501328	-0.7008142042	0.3417365115
Frequencies			
868.10	1057.09	1057.19	
1480.33	1661.85	1662.13	
2018.74	3371.28	3442.49	
3442.70			
i2'			
C	0.9349002884	-0.0001857275	0.4189000342
C	-0.3637498793	0.0000851182	0.6439974543
N	-0.3176538573	-0.0001051324	-0.8046253922
H	-1.2138540846	0.0004960622	1.3023129801
H	-0.4366503735	0.8551862482	-1.3228665887
H	-0.4370151917	-0.8554804727	-1.3226433891
Frequencies			
414.40	597.27	645.83	
803.38	1036.24	1110.82	
1135.85	1596.01	1674.95	
3287.21	3553.84	3670.72	
i3'			
C	-3.0316242732	0.1390802675	0.0355302879
C	-1.7491437648	0.1074562676	-0.0128452674
N	-2.4410981845	-1.1663409900	-0.4898229342
H	-0.7535942490	0.5055079132	0.0235402942
H	-4.0008000538	0.5856085706	0.1459827921
H	-2.4276194747	-1.8219920289	0.2976148273
Frequencies			
537.43	556.91	716.09	
879.65	973.32	1059.64	
1147.21	1365.30	1723.66	
3288.42	3342.30	3350.49	
i4'			
C	-2.9969018464	0.6442965597	0.0734523904
C	-1.7898594514	0.6788815786	-0.0258221061
N	-4.3502018494	0.6193080518	0.2609644739
H	-0.7317082326	0.7090581293	-0.1139163400
H	-4.8295219218	1.3519598506	-0.2448121841
H	-4.7585066984	-0.2813441699	0.0501337660
Frequencies			
335.66	381.20	495.32	
651.93	696.26	1053.69	
1215.43	1649.41	2195.72	
3468.12	3535.29	3624.70	
i5'			
C	-1.5915491794	0.0743675121	0.5100854444
C	-0.0594291041	-0.0042577375	0.0875463765
N	-1.1225259530	-0.9377432845	-0.1395598083
H	0.2763211526	0.5856735264	-0.7567187504
H	0.6743481260	-0.2568823608	0.8433776770
H	-1.3753350423	-1.8263976556	-0.5447309394
Frequencies			
428.94	711.07	960.97	
965.30	1030.83	1145.56	
1206.01	1485.16	1587.05	
3116.20	3216.67	3589.33	

i6'

C	-3.5336584338	0.9452242240	0.1434747168
C	-2.2282978370	1.0377713288	-0.0069751689
N	-4.7341358669	0.8686798763	0.4143163364
H	-5.3444076380	0.7680235655	-0.3960908261
H	-1.7677965926	2.0065409788	-0.1369635323
H	-1.6219536317	0.1435100266	-0.0177615257

Frequencies

402.99	457.40	705.10
903.17	996.93	1044.59
1132.94	1437.75	2072.91
3173.21	3268.21	3478.17

i7'

C	-1.3448702716	0.5221913550	-0.1555211309
C	0.1003924279	0.4534726637	0.0799687810
N	-2.4906355389	0.5766588663	-0.3422119556
H	0.4254170455	1.3310641561	0.6387662219
H	0.6284265979	0.4206070286	-0.8729854907
H	0.3388797392	-0.4431640697	0.6519835744

Frequencies

359.03	359.12	920.87
1063.21	1063.22	1416.36
1490.92	1491.09	2291.43
3060.88	3144.47	3144.55

i8'

C	0.1312397935	-0.0273422675	0.8936355675
N	-0.7270848325	-0.2576981029	-0.3841334780
H	0.0732889768	0.9641139028	1.3271505201
H	0.1787200430	-0.8601831883	1.5852918077
H	1.2827312425	-0.2652989951	-1.2663092735
C	0.5284456091	-0.2009850074	-0.4954186625

Frequencies

700.41	772.30	987.40
996.28	1039.35	1106.96
1264.68	1510.77	1684.47
3115.68	3208.15	3226.58

i9'

C	0.2188237836	0.0350389259	-1.1584936983
N	0.0069347177	-0.0494125908	0.1073631491
C	-0.0294278283	-0.0629584557	1.3335387238
H	0.6493078956	-0.8101672039	-1.6764675568
H	-0.0348452538	0.9508938049	-1.6731689524
H	-0.9471891349	-0.4190442406	1.8082663247

Frequencies

332.28	465.08	690.84
903.79	946.16	1140.10
1195.07	1492.92	1952.44
3085.95	3152.93	3267.13

Transition states**i1'-i2'**

C	-0.0000224478	0.7315569642	-0.6999477987
N	0.0000078738	-0.2131191257	0.8006015074
H	-0.0000032176	1.0446573757	0.5807381277
H	-0.8609997040	-0.5015151593	1.2458768708
H	0.8610342858	-0.5015046720	1.2458473465
C	-0.0000170286	-0.5976761089	-0.7801970036

Frequencies			
1510.65i	513.43	654.46	
800.15	847.88	963.18	
1134.38	1526.01	1579.27	
2149.09	3511.20	3643.54	
i1'-i4'			
C	-0.2529780174	-0.0008754995	0.1981897162
C	0.1785624366	-0.0003380137	1.3920151241
N	0.0615389166	0.0001468492	-1.2358851854
H	-0.2009444208	0.8507839909	-1.7169130755
H	0.9308727346	0.0017262380	-0.3319439119
H	-0.1975490456	-0.8512597811	-1.7173722504
Frequencies			
1759.06i	195.48	274.13	
819.44	893.05	922.61	
1128.04	1582.34	1893.70	
2328.51	3502.90	3621.04	
i2'-i3'			
C	0.0448363805	0.8898131938	-0.5404035000
N	0.0872635416	-0.3366935268	0.8994138445
H	0.2089632179	1.0173338244	0.7083085280
H	-0.0357540472	-1.2899873136	-1.1967322541
H	-0.8823848033	-0.3946520806	1.2379218943
C	0.0280379802	-0.4297992173	-0.5592476326
Frequencies			
1416.76i	650.51	689.32	
921.68	937.33	1083.79	
1138.29	1282.63	1602.68	
2281.15	3327.76	3338.81	
i2'-i4'			
C	0.7460718136	-0.0008484134	0.2875963435
C	-0.3196236681	0.0010365390	0.9766882194
N	-0.2478966855	-0.0004215887	-0.9775218373
H	-1.1888487821	0.0012048268	1.6040810095
H	0.0369609750	0.8229815062	-1.4941677273
H	0.0371980701	-0.8232698933	-1.4948207961
Frequencies			
756.30i	320.00	489.03	
626.36	893.82	989.82	
1127.04	1567.13	1704.97	
3365.06	3500.56	3608.21	
i3'-i5'			
C	-0.3216049178	0.1710877088	-0.6577835066
C	0.8956883618	-0.1455110473	-0.1164197254
N	-0.4989883855	-0.1104094931	0.7458525875
H	0.2134383539	-0.9357774491	-0.9649628872
H	-0.9008108393	0.5536032240	-1.4866576269
H	-0.4021987404	0.7840517503	1.2324938414
Frequencies			
876.61i	508.19	878.75	
990.77	1005.94	1086.16	
1161.90	1388.33	1481.90	
2188.82	3226.55	3417.58	
i3'-i6'			
C	-0.3735348985	-0.0338544063	0.0080311260
C	0.1948256843	0.1321644801	-1.3068605764

N	0.2716163410	0.0687364067	1.1209335899
H	0.7706378488	-0.7649202927	-1.5962517444
H	-1.4720391525	-0.1259082484	-0.0657321539
H	-0.3856521880	0.0593289481	1.9001504240
Frequencies			
391.57i	456.39		640.99
948.38	1022.60		1055.92
1171.83	1367.03		1587.79
2950.23	2996.74		3471.31
i3'-i8'			
C	0.3441624285	-0.1048274843	0.7596440336
N	-0.6513021268	-0.1457778301	-0.1255944657
H	-0.6678028412	0.7499824985	0.8026652307
H	0.3110423673	-0.5852570560	1.7372110931
H	0.9108965991	-0.6554080270	-1.2674923173
C	0.6619026486	0.2890835998	-0.7475152404
Frequencies			
2241.42i	317.10		800.63
873.77	1013.42		1056.44
1165.14	1254.33		1374.70
1996.15	2943.23		3112.76
i5'-i8'			
C	-0.8151416221	-0.0010334925	0.1955680092
N	0.5094102063	0.0051654081	0.5842569311
H	-0.3260317015	-0.8154763461	1.0029810384
H	0.4882612246	-0.9019780951	-1.4454982314
H	0.4154263761	0.9424893992	-1.3311765600
C	0.2400444065	-0.0183163736	-0.8715841674
Frequencies			
1412.19i	762.82		811.62
989.44	1013.18		1069.26
1177.60	1314.72		1516.85
2485.80	3143.12		3251.84
i6'-i7'			
C	0.0422766629	-0.0585159724	-0.0443649745
C	-0.0048674323	0.1636868456	1.3592232958
N	-0.0444476319	0.0055481870	-1.2698351051
H	0.0076805630	-1.1954458879	-0.2095180442
H	0.9297972361	-0.0872839651	1.8689138675
H	-0.9124443554	-0.0992440420	1.8237209925
Frequencies			
1083.22i	327.97		329.58
473.90	591.61		998.85
1018.06	1430.86		1892.96
2734.56	3155.23		3259.54
i8'-i9'			
C	0.0499750424	0.1949768750	-0.9930802840
N	0.2894284082	-0.5415881485	0.1538498343
C	-0.1118500962	0.2326341600	1.1166681652
H	0.8707706579	0.2854362009	-1.6976648404
H	-0.7619545692	0.9242909147	-1.0237810089
H	-1.0315171604	0.8476462491	1.0177935396
Frequencies			
482.75i	496.84		693.06
827.26	1027.89		1102.36
1183.70	1383.06		1497.18

2883.13 3057.47 3198.96

Triplet reactants-C₂H+NH₂

C	0.21406831	-0.55043530	1.21402335
C	-0.13445067	0.29974809	2.05287814
H	0.28214970	-0.69848108	-0.08832047
N	0.03155981	-0.06023769	-1.10680139
H	-0.95380658	0.19947821	-1.04096675
H	0.56047946	0.80992776	-1.03081286

Frequencies

1479.449i	164.414	185.358
444.698	571.514	827.791
1290.143	1443.355	1600.149
1857.841	3455.361	3554.673

Van der Waals Minimum

C	-0.4406937533	-0.3234263552	-0.5941362302
C	0.4705218199	0.3564968030	-1.2407949600
N	0.0202666611	-0.0432962812	1.3608243596
H	0.8208029174	0.5774970992	1.3966044248
H	-0.7836959985	0.3718426209	1.8157068741
H	0.2415157759	-0.9464499038	1.7620211911

Frequencies

72.15	238.98	291.73
472.85	489.16	1005.41
1587.60	1639.27	1644.47
3466.06	3625.12	3634.49

Table S7. Optimized Cartesian coordinates (Angstrom) and vibrational frequencies (cm^{-1}) for the intermediates, transition states, reactants, and products involved in the pathways from $\text{H}_2\text{CN}^\bullet$, *cis*- HCNH , and $\text{H}_2\text{CCN}^\bullet$ radicals to pyridine and pyridinyl radicals.

Intermediates

i1''

N	-0.385437	1.299259	0.167033
C	0.787331	1.773708	0.079994
C	-1.863082	-0.540348	0.158601
C	-0.603813	-0.095142	0.059028
C	0.496031	-0.989878	-0.150056
C	1.451701	-1.697261	-0.325122
H	0.913723	2.848672	0.168024
H	1.681512	1.166729	-0.078485
H	-2.095289	-1.591704	0.084763
H	-2.663680	0.167381	0.316134
H	2.281003	-2.341415	-0.479913

Frequencies

131.5830	165.9401	264.8221
336.0832	487.7798	555.2548
632.9441	655.7867	694.0683
729.1735	771.4176	819.6866
935.5021	958.2878	1066.3564
1205.9243	1268.3081	1414.7085
1489.4531	1660.3799	1693.8677
2199.5097	3035.5270	3149.6127
3162.8817	3261.2002	3467.0127

i2''

N	0.4438576679	1.1505584071	-0.4309098078
C	1.3596449225	0.2077985965	0.0086988525
C	-0.7608831099	1.1416076566	-0.0493850848
C	-0.6875494153	-2.4916374783	-1.2059713972
C	0.1987293616	-1.8394121976	-0.7184024829
C	1.2768566614	-1.128066558	-0.1386006873
H	2.2720901289	0.6343490767	0.4080753452
H	-1.4520424298	1.8672561668	-0.4694036441
H	-1.1466666684	0.4428795255	0.6959319629
H	-1.4717914353	-3.0597788639	-1.6390362887
H	2.1336763794	-1.7160243314	0.1673072321

Frequencies

111.2549	155.6359	236.0377
347.0416	415.6753	579.3046
610.2701	631.4413	682.1259
795.1164	840.1914	906.5206
970.9944	1055.7787	1077.9638
1216.9261	1258.5385	1423.4055
1505.9993	1631.4523	1724.7337
2194.7745	3036.1360	3146.4363
3151.7320	3170.0200	3470.4076

i3''

N	0.3209032145	-1.5983031008	0.0236674737
C	1.6024032627	-1.1074968393	-0.3335764311
C	-1.9438180083	-0.5456244821	-0.3252197502
C	-0.7489193153	-1.0470903198	-0.1636461813
C	2.2686961089	1.4092046462	-0.4228595565

C	1.9337404891	0.1549244401	-0.4021729944
H	2.3385884111	-1.8844604064	-0.4919169681
H	-2.3606993856	0.1245493957	0.4125978694
H	-2.5268069396	-0.7853842295	-1.2025963735
H	2.2085983158	1.9957374816	-1.3327669586
H	2.6212788468	1.9166014144	0.46852487043

Frequencies

70.9759	125.8867	245.8180
327.8856	356.5984	504.1446
529.3447	674.3859	702.7065
721.9612	892.0032	898.4185
904.8004	995.1426	1017.6454
1116.4550	1280.3020	1366.5653
1454.8339	1473.1939	2031.5375
2112.9385	3110.5007	3152.2684
3171.1149	3179.9485	3234.5683

i4''

N	-0.6988758407	1.1267296462	-0.1774601689
C	0.5682500143	1.154281835	-0.1619021145
C	-1.4122794543	-0.1378133206	-0.4947422254
C	-0.5620833098	-1.3458232391	-0.1640845948
C	0.6994898319	-1.1377496743	-0.4947863741
C	1.3749682009	-0.0192347218	-0.6559623015
H	1.0601625156	2.0972593193	0.0609501725
H	-1.753908383	-0.0406292022	-1.5295642806
H	-0.8951523952	-2.0719687212	0.5659305601
H	2.2096434071	0.1605588106	-1.3203999596
H	-2.3080365866	-0.171020732	0.1261082866

Frequencies

246.8213	369.9522	478.5709
567.6994	593.9747	716.9793
786.0319	840.5193	869.5373
888.6101	929.9435	969.1541
991.3862	1142.6242	1204.4800
1268.2462	1285.1240	1321.1815
1404.3504	1450.4074	1638.3408
1819.3129	3024.1687	3080.1730
3124.1528	3163.8738	3174.0067

i5''

N	-0.3810283198	1.0165112229	0.3024468279
C	0.9087039471	1.1856420968	0.1400686544
C	-1.9127503971	-0.8033176124	0.1238249184
C	-0.6769963999	-0.3091058572	-0.0094365759
C	0.6089252133	-0.9925425453	-0.4163426467
C	1.6923780152	-0.0174441861	-0.126319208
H	1.3355448665	2.1699258047	0.2878534745
H	-2.1449506564	-1.8211336869	-0.1565246692
H	-2.7038582424	-0.1901712525	0.5315453209
H	0.7732134739	-1.9750929209	0.0295433203
H	0.6558474996	-1.1603920631	-1.5044304166

Frequencies

132.0457	280.4002	360.7234
405.5388	692.5977	712.5371
756.2907	848.8171	869.9720
940.4539	954.4918	961.4774
973.9444	1036.8040	1129.9303

1225.9002	1252.0573	1346.7961
1368.8297	1424.6288	1447.2034
1682.9441	2978.2972	3072.2903
3152.3826	3176.7638	3244.6811

i6''

N	-1.440513	0.168703	-0.292883
C	-0.572181	1.172447	0.069215
C	-1.264781	-1.016243	0.139034
C	1.163742	-1.410815	0.050037
C	1.513044	-0.159311	-0.146926
C	0.773248	1.064131	0.116716
H	-1.023403	2.151383	0.174095
H	-1.858029	-1.834564	-0.254051
H	-0.604927	-1.260777	0.981913
H	2.538667	-0.096021	-0.522514
H	1.352854	1.957807	0.302286

Frequencies

86.1636	176.4700	258.7647
347.4921	423.2845	545.3816
616.0966	713.7198	822.9208
844.0340	947.9610	971.3034
993.1331	1053.1191	1079.6650
1184.1962	1248.8240	1420.5409
1479.6947	1568.9124	1662.0984
1674.6659	2958.0010	3060.8211
3161.0552	3163.4516	3187.6947

i7''

N	-0.325656	1.178499	0.148884
C	0.825181	1.674035	0.066574
C	-1.702139	-0.744909	0.121362
C	-0.479647	-0.209490	0.034025
C	0.741180	-1.015762	-0.180564
C	1.991599	-0.654373	-0.287177
H	0.995142	2.743063	0.148872
H	1.748304	1.041667	-0.098365
H	-1.857816	-1.809823	0.037566
H	-2.558147	-0.106873	0.278806
H	0.622001	-2.096034	-0.269984

Frequencies

195.0156	222.3138	304.2281
395.7098	493.7103	520.6605
626.1489	640.6000	766.0342
794.2101	801.2346	928.0259
946.9070	990.3141	1015.3876
1149.4864	1264.4663	1424.0187
1490.3829	1653.8548	1701.4364
1733.0366	2518.7911	3111.1026
3148.1583	3167.7159	3262.1691

i8''

N	-0.7292145011	1.1458653784	-0.6421200114
C	0.5911327122	1.2000919561	-0.5123567789
C	-1.3503864737	0.0178200226	-0.5872979444
C	-0.6272193001	-1.1892936419	-0.0647640312
C	0.8383711285	-1.079798316	-0.3024108535
C	1.4045805051	0.0451595367	-0.7806193936
H	1.0183638986	2.1187201801	-0.1236424972

H	-2.3190276717	-0.0649873219	-1.0711340439
H	-1.0291569608	-2.0792618149	-0.5615428072
H	-0.7912178821	-1.3706727716	1.0028607772
H	2.4400045451	0.1406307923	-1.0773814159

Frequencies

239.1324	406.3987	442.8284
524.8076	617.7342	755.7827
784.0421	819.1163	858.8821
884.0443	930.0744	993.1080
1074.6735	1163.2201	1199.8168
1248.4787	1279.6555	1325.8255
1370.3485	1391.7727	1526.3940
1604.2493	3009.3741	3042.1096
3133.1478	3143.2087	3173.1282

i9"

N	0.112793	-1.101983	0.010418
C	1.478875	-0.598472	0.029725
C	-2.058297	-0.182799	-0.015805
C	-0.687032	-0.052345	0.075816
C	0.072171	1.263454	0.010626
C	1.324579	0.875721	-0.128973
H	2.084819	-1.137611	-0.703298
H	1.932565	-0.784653	1.007767
H	-2.727263	0.557886	0.398561
H	-2.479662	-0.993945	-0.591413
H	-0.381785	2.238858	-0.012874

Frequencies

209.7937	301.0197	339.3796
411.1292	583.8559	656.8328
693.1627	786.2121	804.3294
866.2269	882.9250	903.5660
969.7584	1049.9006	1128.0107
1192.1379	1207.2359	1291.1352
1389.8395	1455.1981	1550.0055
1591.3609	3027.7601	3059.2289
3154.1627	3244.8736	3252.8396

i10"

N	-0.3984892466	1.0595669939	0.2427558971
C	0.881075444	1.1849419039	0.1001726806
C	-1.8992440879	-0.8237742875	0.0721508462
C	-0.6654819112	-0.3128727266	0.0095638082
C	0.58968907	-1.0079827176	-0.2901709714
C	1.5581631984	-0.0736927105	-0.2333051205
H	1.3695444353	2.1435233327	0.2250157762
H	-2.0822148687	-1.8735395937	-0.1091624369
H	-2.7401774234	-0.1864497137	0.3057695905
H	0.6858786258	-2.0595926349	-0.5068632194
H	2.6166527642	-0.201119846	-0.396295850

Frequencies

215.8776	361.2693	524.2419
656.7713	714.7008	771.6220
804.8083	855.5774	910.1132
927.0609	948.6039	960.3147
982.7142	995.3293	1095.7845
1236.0254	1317.5072	1364.7241
1438.0710	1500.8976	1611.1601

1706.4605	3154.7640	3172.3051
3217.6542	3238.7427	3248.0791

i11"

N	-0.4128560963	-0.9499703571	-0.823772183
C	0.8775819644	-1.1529291594	-0.3702104976
C	-1.6169684187	-0.2530727576	-0.2440794855
C	-0.569414476	0.4122938206	-1.0057193738
C	0.6209357895	1.0655804857	-0.7627440414
C	1.5629422893	0.0422027433	-0.4590315302
H	1.2468197735	-2.1434745015	-0.1606408189
H	-1.6674825309	-0.0921730301	0.8326830741
H	-2.5346880776	-0.5873117863	-0.7091868534
H	0.7953582393	2.1282670884	-0.7613717438
H	2.6213735434	0.1750144541	-0.2926415465

Frequencies

262.8914	398.2524	596.4878
682.9826	775.3911	805.0076
844.1164	860.3412	910.7915
956.2375	966.4662	1028.8614
1044.1842	1076.6567	1133.4898
1149.5762	1232.4524	1324.8803
1401.4021	1450.3796	1501.4291
1582.4501	3062.2408	3179.8226
3207.1971	3234.2922	3242.1391

i13"

N	-0.7035404545	1.150910699	-0.6016999379
C	0.569996411	1.1446064701	-0.4303233198
C	-1.3260999043	-0.117810772	-0.2757175434
C	-0.498594353	-1.3389319302	-0.2538119554
C	0.837314346	-1.2719527284	-0.5646155919
C	1.3773223949	-0.0301150079	-0.235839485
H	1.099808584	2.0877659626	-0.5491258399
H	-2.1796956596	-0.2933024771	-0.946382539
H	-1.8075426329	-0.0182932947	0.7061168766
H	1.4413163462	-2.1383540769	-0.8051844051
H	2.4042369222	0.0852571556	0.0920477409

Frequencies

214.7525	303.9880	442.0225
551.3136	584.7212	778.9524
832.1376	883.3665	910.9268
933.1649	946.0195	989.5555
1018.0630	1162.0432	1179.9352
1260.9375	1307.1619	1342.9664
1364.4234	1381.8756	1495.1358
1607.0779	2988.3159	2997.2003
3108.1051	3146.1260	3159.8011

i12"

N	-0.7359722139	1.2061105275	0.
C	0.5981266297	1.2073644302	0.
C	-1.3472272486	0.0205355566	0.
C	-0.669957128	-1.1933918478	0.
C	0.7181483568	-1.1770787145	0.
C	1.3677129828	0.0498986353	0.
H	1.0742733952	2.1815763129	0.
H	-2.4313680107	0.0426687654	0.
H	-1.2205890411	-2.1238774727	0.

H	1.2816251307	-2.1007559891	0.
H	2.4470424663	0.1136463322	0.

Frequencies

385.0580	421.1848	617.1777
670.6838	720.6418	768.8550
900.1629	963.6626	1011.1029
1012.2452	1022.8882	1051.6637
1080.1513	1095.8266	1172.8986
1243.4233	1282.6877	1390.4050
1477.0811	1517.4330	1620.7286
1627.0112	3145.5433	3148.2899
3171.6967	3188.3994	3195.9953

i14"

C	-0.155584975	1.1258001963	0.0972934457
N	1.0081607036	1.6163262798	-0.0089725479
C	-1.6689545179	-0.7775443367	0.1955595128
C	-0.4091521361	-0.330601499	0.0776780519
C	0.6967173745	-1.2194217619	-0.0665490791
C	1.6257650094	-1.9695639599	-0.1878275458
H	-1.0624442902	1.7293118447	0.2117290345
H	0.9787932647	2.6339834168	0.0266889756
H	-1.9011762181	-1.8318966054	0.18634337
H	-2.4911679911	-0.0828289749	0.303823763
H	2.4535217761	-2.6246175996	-0.2954239807

Frequencies

155.3187	155.6702	260.1579
311.9809	475.1999	534.2345
670.9766	674.7578	679.8206
734.4054	759.8282	863.1626
960.9739	962.4278	1109.5932
1192.6383	1332.2631	1408.8986
1450.1202	1649.2735	1697.2320
2216.9262	3013.8644	3149.7411
3243.3312	3462.3234	3471.3871

i15"

C	-0.5146406869	1.0024750489	0.917546642
N	0.661235018	1.4780399394	0.8035080412
C	-1.6206042789	-1.2933411086	0.9524892429
C	-0.5537421853	-0.4792349362	0.8641956392
C	0.8082377258	-0.9768097089	0.6915978855
C	1.562423995	0.3011315002	0.6563630381
H	-1.3803530044	1.6463090937	1.0399334145
H	-1.4791418424	-2.3639609286	0.8948945671
H	-2.6301496803	-0.9187919145	1.0806658659
H	2.3292484925	0.3064835655	1.4412005219
H	2.1360954469	0.373273449	-0.2762118584

Frequencies

126.0641	278.2498	348.6203
549.3659	621.5931	678.2593
803.3156	804.0417	898.6820
924.1759	933.6198	960.0546
1016.5948	1053.9580	1158.6038
1247.2384	1270.5116	1303.2150
1361.8508	1436.2478	1644.6926
1662.0507	3009.7081	3024.0987
3130.0616	3140.9697	3229.8471

i16"

C	-0.5479631203	1.3582705445	0.1064556861
N	0.6508625964	1.8363209874	-0.0102590296
C	-1.4729096331	-0.9218547931	0.1213267252
C	-0.4167836403	-0.0951764916	0.0348529178
C	1.0089124695	-0.325771122	-0.1343139427
C	1.7426811556	0.829485942	-0.172490844
H	-1.4425141092	1.9517590306	0.2303174431
H	0.8595400707	2.8237733985	0.0045736483
H	-1.3519792129	-1.9956664968	0.0659854637
H	-2.4795354612	-0.5458306894	0.2491024161
H	1.4338418849	-1.3139393103	-0.2205424841

Frequencies

132.5455	303.5686	334.7713
605.6927	676.7597	702.8028
734.2577	813.3894	820.2104
824.3547	910.5704	946.7966
970.0152	990.1267	1160.4473
1188.5396	1286.6489	1398.2481
1436.0355	1494.0619	1552.6028
1673.0249	3140.0503	3200.9534
3208.1957	3226.8313	3597.2696

i17"

C	-0.2162550272	1.0529015843	0.1044361807
N	0.966805281	1.5471159254	-0.0080562418
C	-1.2799285937	-1.2225485004	0.136454034
C	-0.212375471	-0.4230577089	0.0482228905
C	1.2014504235	-0.7491532395	-0.1209631373
C	1.8477860721	0.4306433592	-0.1480399181
H	-1.097185939	1.6704624632	0.2255328782
H	-1.1932683273	-2.3000526209	0.0861077685
H	-2.2742816716	-0.8141290899	0.2622130526
H	1.6195081274	-1.7382983915	-0.2047482334
H	2.9046921258	0.614935219	-0.2583012739

Frequencies

208.3867	335.1508	493.3692
652.7495	691.1667	727.8829
802.2892	831.3998	900.4739
948.5291	949.8403	965.4203
991.7074	999.6659	1121.1981
1261.1888	1307.6438	1343.5292
1458.9608	1544.0775	1605.5293
1705.4387	3138.7221	3176.3439
3219.8309	3223.2182	3244.3470

i18"

C	-1.2717463681	1.4519263728	-0.735551344
N	-0.0081141748	1.5511325065	-0.9693561761
C	-2.0647036922	0.3929190629	-1.443937182
C	-1.2090137499	-0.7760333608	-1.7888368684
C	0.1263244518	-0.7628225822	-1.6102491437
C	0.6437118775	0.5784270591	-1.5955532682
H	-1.6940287427	2.0249411744	0.0845558301
H	-2.5495823334	0.7472951326	-2.3598925171
H	-2.8914710261	0.0833955969	-0.7951923047
H	0.7768660095	-1.6174710767	-1.7356290419
H	1.5322947484	0.8513761144	-2.1553489841

Frequencies

237.2123	406.0228	442.5767
524.3662	617.4667	755.5948
784.2408	819.4467	859.0195
883.8848	929.5247	993.1945
1074.8721	1162.9924	1199.5593
1247.6127	1280.0867	1325.5719
1369.7941	1391.4365	1525.8554
1603.9923	3008.4050	3041.9796
3132.3920	3142.6631	3171.8031

i19"

N	-1.1615262955	-0.5324013648	-0.1944882569
C	-1.2682572799	0.7263624778	-0.0390043289
C	-0.1281879117	1.6182274805	0.1742874634
C	1.1773758941	1.2967980398	0.2426449022
C	1.7704996895	0.0215492889	0.125653045
C	2.3829726262	-1.0105960172	0.0421374688
H	-2.0772051801	-0.9583059077	-0.3278899009
H	-2.2359021138	1.2401465915	-0.0541355402
H	-0.3802088611	2.6651672344	0.2900611935
H	1.8794195662	2.1077666156	0.4081568257
H	2.8764218663	-1.9463264388	-0.0387038716

Frequencies

70.6927	141.9694	268.8271
278.4458	467.9024	501.6666
649.1345	678.7968	745.5298
818.4114	850.6556	882.3810
1006.6841	1024.3301	1116.6376
1237.6138	1267.2272	1416.7194
1462.3331	1632.2349	1698.9888
2196.1259	3004.3147	3132.1995
3167.9687	3458.7031	3471.4914

i20"

N	-0.7602801275	-0.8984451246	0.2250473021
C	-1.1140966009	0.3888143201	0.0544479831
C	-0.1237597465	1.3429198375	0.1031259027
C	1.1973127634	0.9362167593	0.322904806
C	1.6065004275	-0.4031744054	0.5081823232
C	0.5326465619	-1.2807480742	0.4435711609
H	-1.4853131525	-1.6048928449	0.1888958922
H	-2.1594312458	0.5973878696	-0.1120659874
H	-0.3920238676	2.3833405344	-0.0316927456
H	1.9476429644	1.7240069747	0.3485532318
H	0.6280380236	-2.3568198465	0.5620501309

Frequencies

129.8156	382.1494	607.0255
645.4805	672.7497	741.5567
831.7271	893.7848	945.3990
970.3572	1013.3146	1044.9947
1060.0701	1087.7355	1195.7398
1262.2073	1315.1955	1358.5382
1452.1637	1482.0709	1601.6751
1621.1859	3090.4651	3113.3922
3163.0351	3216.9526	3516.5337

i21"

N	-1.0313652824	-0.9688044562	0.1126587621
---	---------------	---------------	--------------

C	-1.2607656365	0.2489442163	-0.2276044545
C	-0.2663782189	1.2820489217	-0.3421885533
C	0.9787909829	1.0777380588	0.2498352056
C	1.3801843649	-0.2305176693	0.1385080381
C	0.3774027527	-1.3112246758	0.0798713378
H	-2.2995337049	0.5558940597	-0.3336674101
H	-0.5315285249	2.2174813991	-0.8220054928
H	1.6398119219	1.885810472	0.5392242628
H	0.6010249812	-2.0306881951	0.8808559446
H	0.5645976395	-1.8967424279	-0.8298630337

Frequencies

215.0134	303.7726	441.7982
551.2716	584.8037	779.3563
832.1040	883.7259	911.1397
933.2786	945.3735	989.8643
1018.3801	1161.9735	1180.1615
1261.2461	1307.3500	1343.2197
1364.0781	1381.8298	1495.3549
1607.2588	2988.3178	2996.6725
3106.6045	3143.8585	3157.7417

i22"

N	-0.6170445952	-1.1824065585	-0.0823793066
C	-1.0013441891	0.1110564795	-0.2584714891
C	-0.058389694	1.0968665664	-0.218623403
C	1.2749130543	0.7145778872	0.00524343
C	1.5908272994	-0.6158605717	0.1751885052
C	0.637438308	-1.6727628624	0.140564373
H	-1.355495545	-1.8713411485	-0.1214403727
H	-2.053933769	0.2950508364	-0.4241011862
H	-0.3413183093	2.1296239805	-0.3558748228
H	2.0455269011	1.476392115	0.0419553942
H	2.6252415388	-0.887820724	0.3465308779

Frequencies

328.7826	399.6054	620.8401
646.0188	677.9736	763.2289
863.2379	898.6014	971.3153
977.1490	1033.3269	1044.6121
1057.5776	1084.4232	1179.3570
1230.2539	1242.5224	1402.1942
1455.5157	1517.2436	1572.2467
1653.9083	3142.7609	3160.8356
3182.7943	3208.9729	3545.9573

Transition states

i13"-i12"

N	-0.7351698553	1.1576358409	-0.1588559638
C	0.5524844988	1.1693709263	-0.0164820846
C	-1.3381647923	-0.114510272	-0.0811487193
C	-0.6675863986	-1.4054543088	-0.1117556207
C	0.7651877367	-1.2372140998	-0.0315679543
C	1.3507389747	-0.0124658128	0.0992107974
H	1.0457027999	2.1373082699	-0.0401356413
H	-2.4071939219	-0.0876993898	-0.2676404689
H	-1.2684287235	-0.5536955815	1.0005813187
H	1.3879260562	-2.1226515052	-0.1005670387
H	2.4223666253	0.0957169328	0.2225433756

Frequencies

550.0235i		
201.3572	371.4614	597.3076
625.2420	701.4467	778.6399
877.1027	918.3343	997.5089
1006.0660	1026.7763	1041.4261
1062.6254	1145.2094	1214.2870
1243.7459	1372.0576	1397.8448
1448.4657	1527.0841	1630.8172
2479.0553	3122.3929	3135.5134
3136.2927	3160.4337	

i8"-i12"

N	-0.7933788696	1.2728390424	-0.1095229789
C	0.5765891892	1.2742962329	-0.0910645812
C	-1.3794083908	0.1185945903	-0.0110150796
C	-0.6406870491	-1.1193315665	0.1322088907
C	0.8068064978	-1.1755922855	0.0943515016
C	1.3513355828	0.15504288	0.0392205792
H	1.0250230618	2.2576501578	-0.189122245
H	-2.466501421	0.107018112	-0.0350047712
H	-1.2035535085	-2.0471851642	0.0688075557
H	-0.1063820078	-1.235071221	1.2028234877
H	2.4292679151	0.2751832219	0.0381876409

Frequencies

822.0571i	137.3827	378.0750
589.4335	659.9247	690.0920
707.8510	849.9117	932.0338
962.0004	1000.3362	1032.9380
1035.8846	1072.1104	1204.8966
1220.0697	1251.4997	1378.0573
1409.4799	1462.4062	1495.6375
1624.3412	2291.2158	3106.4321
3120.3603	3131.4924	3150.7284

i4"-i13"

N	-0.7618752425	1.0458503489	-0.4159834251
C	0.5225210754	1.100550771	-0.2926214624
C	-1.5958604465	-0.1120368561	-0.1633311928
C	-0.5751075438	-1.2386516867	-0.313489258
C	0.6888964836	-1.1429755824	-0.1696632745
C	1.4588556525	0.0271727865	-0.134667549
H	0.953530751	2.0992073436	-0.3446962089
H	-2.3928960151	-0.1967821961	-0.9006397252
H	-2.0526967828	-0.1000063198	0.8336106559
H	0.1717877153	-1.7970662497	0.7374646259
H	2.521732353	0.1522536407	-0.0598141859

Frequencies

1327.7355i		
113.9325	226.7294	426.7299
487.6655	581.0323	621.8820
695.1350	754.4839	810.1230
917.4382	953.1687	1005.4572
1033.8544	1129.7973	1163.5573
1241.8821	1280.1604	1315.8303
1510.7312	1576.5807	1880.2880
2250.4975	2969.6929	3069.5312
3109.3720	3277.8840	

i4"-i8"

N	-0.7986857649	1.2254916837	-0.609325027
C	0.5254314677	1.212212221	-0.4941077512
C	-1.4003167419	0.0226514896	-0.5625973649
C	-0.6351464366	-1.2291915044	-0.4495030857
C	0.7785519143	-1.2436258602	-0.5107822209
C	1.3122679899	0.0496957506	-0.4919824403
H	0.9971377795	2.1917718039	-0.4864392469
H	-2.4790682067	-0.0030904016	-0.6932072796
H	-1.2293880157	-2.1326818315	-0.3394748871
H	-1.1428295646	-0.5293178589	0.5527199626
H	2.386463579	0.1938955076	-0.573371659

Frequencies

984.4739i	265.9603	375.4741
571.6704	663.6181	693.4994
794.8957	907.3305	925.5698
978.8283	1022.0935	1043.5917
1091.2923	1110.5681	1192.2137
1206.4869	1297.0351	1336.0182
1388.8011	1439.5591	1521.4565
1542.1443	2127.4152	3104.2441
3110.2876	3119.4962	3124.6703

i2"-i4"

N	0.447705	1.268685	-0.097589
C	1.318133	0.328559	0.147543
C	-0.879491	1.185405	-0.021674
C	-1.468721	-0.790466	-0.054879
C	-0.326253	-1.308930	-0.036847
C	1.008127	-1.054571	0.000558
H	2.359587	0.630364	0.199084
H	-1.430536	1.798085	-0.730169
H	-1.330611	1.124103	0.962949
H	-2.414591	-0.885348	0.440463
H	1.771443	-1.707985	-0.397406

Frequencies

483.9000i		
231.6835	374.8444	449.4055
543.3739	580.9336	618.0123
708.9049	783.6927	829.0423
909.9062	939.2935	1035.2837
1070.2840	1133.6327	1164.7793
1185.4140	1379.4966	1414.7602
1517.7165	1558.4816	1933.6978
3076.5727	3137.3913	3150.1708
3184.3964	3303.3200	

i2"-i6"

N	-0.7541836711	0.9890895214	-0.507972708
C	0.6022291704	0.9939240544	-0.2225501258
C	-1.5991613344	0.4044279674	0.2275606569
C	0.0557365408	-2.2996578152	-0.6580911179
C	0.9792412558	-1.4210863491	-0.4953744998
C	1.4222060188	-0.0696518451	-0.2475579502
H	1.0254065748	1.983008726	-0.0917032418
H	-2.6429619236	0.3974958752	-0.0730054516
H	-1.337386265	-0.0912024403	1.1652806573
H	1.7196395267	-2.2592935695	-0.6486581563
H	2.4814831068	0.0945908748	-0.1199250629

Frequencies

127.0088i
 64.8564 162.3611 242.3091
 298.3166 436.1732 546.6085
 620.9449 761.7136 795.3058
 897.5876 945.0907 958.6717
 1035.6192 1089.4206 1216.2248
 1251.5165 1418.3948 1508.8004
 1642.5657 1729.8938 1848.4707
 2803.0816 3033.3127 3150.8521
 3160.3521 3203.9121

i10"-i11"

N	-0.444685	-0.867740	-0.321104
C	0.834555	-1.051887	0.112151
C	-1.776126	0.109972	0.293374
C	-0.610590	0.517316	-0.373715
C	0.567706	1.186996	-0.086393
C	1.509443	0.165200	0.148696
H	1.225669	-2.047826	0.246317
H	-1.961729	0.392996	1.328565
H	-2.581395	-0.385763	-0.225241
H	0.716542	2.250176	-0.006463
H	2.563786	0.299013	0.339869

Frequencies

510.0623i
 276.2802 561.5614 635.0294
 739.8253 776.4670 805.6227
 827.4376 868.1204 921.7999
 993.3516 1012.8552 1055.1752
 1071.8298 1120.4874 1127.7848
 1219.5432 1303.9035 1428.9981
 1432.2758 1488.7863 1618.9560
 3082.7307 3203.4112 3223.9921
 3226.3824 3244.6997

i5"-i10"

N	-0.3281884203	1.0022300262	0.3386926469
C	0.9492721532	1.1342290372	0.1813712608
C	-1.8532734018	-0.8650108212	0.1640959777
C	-0.6264119276	-0.345721007	0.0753319442
C	0.650556238	-1.0236631995	-0.2682703303
C	1.7353302345	-0.1143207551	-0.1242035523
H	1.4161451936	2.1020795433	0.3155808302
H	-2.0368305342	-1.9067179139	-0.058465936
H	-2.6883116304	-0.2500767159	0.468736374
H	0.756428008	-2.098327109	-0.3539890357
H	1.1603800871	-0.6237950851	-1.3055021795

Frequencies

823.6594i
 206.4253 357.9444 451.3212
 615.5658 706.6333 765.6990
 832.2671 868.9730 923.3707
 937.8860 961.7153 982.5912
 986.8373 1128.9701 1250.4627
 1272.3529 1325.6540 1350.6624
 1437.2171 1530.0035 1702.8866
 2232.2943 3153.9825 3170.5719

3177.7586	3246.5108		
i1"-i13"			
N	0.804389	0.942175	-0.242806
C	-0.476865	1.185473	0.030847
C	1.534532	-0.234598	0.160068
C	0.414415	-1.146191	-0.051484
C	-0.889111	-1.121377	-0.116120
C	-1.443001	0.219432	0.109431
H	-0.753873	2.235674	-0.007950
H	1.875904	-0.269505	1.206533
H	2.397325	-0.361857	-0.491395
H	-1.513253	-2.002622	-0.174604
H	-2.476647	0.386657	0.370605

Frequencies		
609.9614i		
152.8741	430.7562	511.3330
549.3905	716.7450	787.8045
824.1657	858.9552	894.7317
972.5747	985.5300	1028.1509
1102.4835	1177.2104	1184.2307
1243.2821	1322.4975	1399.3943
1482.2799	1539.9813	1727.5092
2914.6931	3074.4913	3129.1524
3184.1367	3212.4858	

i3"-i5"			
N	0.128095	-1.190535	0.191607
C	1.374042	-0.698548	-0.050657
C	-2.048294	-0.046466	-0.140871
C	-0.767044	-0.252393	0.131438
C	0.337592	1.350720	0.148631
C	1.417188	0.644632	-0.351435
H	2.210719	-1.381935	-0.030989
H	-2.556026	0.850752	0.179251
H	-2.594527	-0.750697	-0.756582
H	-0.104376	2.180273	-0.391465
H	0.266642	1.447685	1.235898

Frequencies		
620.2095i		
215.8097	280.0213	385.6445
493.2943	545.7355	655.7528
708.6902	831.9449	849.0103
902.3089	946.9508	985.4724
1018.0446	1073.2442	1116.6834
1241.9815	1344.4161	1413.4911
1455.0751	1493.2451	1756.4769
3047.7192	3137.2244	3160.3225
3204.1172	3231.1628	

i1"-i7"			
N	1.299595	0.083652	-0.033481
C	1.611732	-1.146235	-0.014653
C	-0.331664	1.797774	-0.032381
C	-0.050377	0.490400	-0.042975
C	-1.069929	-0.533077	-0.055827
C	-1.823915	-1.538248	-0.061569
H	2.666081	-1.404399	-0.012551
H	0.892154	-1.968111	0.004005

H -1.346976 2.163663 -0.054981
H 0.480227 2.508016 0.005797
H -2.326924 -0.453438 0.298615

Frequencies

624.0383i
80.8279 138.9801
183.6088 260.4162 343.9896
491.7323 539.0984 656.2537
728.8609 757.8705 812.8737
925.6964 946.9996 1071.9757
1205.0256 1261.4851 1419.3536
1500.6093 1663.2089 1695.0736
1976.2048 2400.5993 3036.6145
3156.3335 3166.4134 3263.4356

i7"-i9"

N 0.159230 -1.085745 -0.150579
C 1.418469 -0.785867 0.121612
C -2.033610 -0.199974 0.026385
C -0.694278 -0.012904 0.051494
C 0.054219 1.248544 0.019838
C 1.354922 1.037245 -0.181517
H 2.201440 -1.416951 -0.282216
H 1.640833 -0.369585 1.105946
H -2.721748 0.604627 0.237347
H -2.430004 -1.167166 -0.245101
H -0.403461 2.227026 0.011209

Frequencies

506.3992i
162.1764 284.8884
366.9635 478.7418 608.6932
642.1583 677.7601 773.1673
840.3596 883.2086 911.9406
957.6467 1006.7173 1120.5869
1159.8832 1268.4322 1381.9846
1414.5680 1492.7266 1559.7357
1611.4110 3035.4619 3161.9136
3170.4109 3200.0188 3259.0737

i19"-i10"

N 0.108101 -1.145932 0.057211
C 1.393474 -0.607452 0.016444
C -2.041287 -0.127032 -0.052805
C -0.683640 -0.047723 0.126298
C 0.079186 1.215639 0.042190
C 1.387977 0.836734 -0.005274
H 1.733076 -0.277583 -1.095438
H 2.222314 -1.208042 0.372627
H -2.688902 0.702817 0.195559
H -2.479371 -1.003081 -0.510769
H -0.358081 2.186417 -0.123578

Frequencies

1223.9527i
212.2061 332.5372
486.6764 561.9663 620.5464
724.3827 737.8804 784.1763
829.6455 922.5950 977.8802
991.2115 1070.2856 1138.4339

1198.3232	1235.5216	1264.6527
1357.1576	1390.9710	1424.5058
1566.1711	2214.7166	3148.0133
3159.8449	3226.4216	3248.1124

i2"-i6"

N	-1.402010	0.054007	-0.433495
C	-0.607963	1.112078	-0.019583
C	-1.577486	-0.978437	0.273678
C	1.662133	-1.370576	-0.157882
C	1.530726	-0.102189	0.000712
C	0.724602	1.086395	0.147127
H	-1.129543	2.059697	0.047197
H	-2.174491	-1.793833	-0.124592
H	-1.166451	-1.094000	1.279258
H	2.658213	-0.047607	0.009059
H	1.234274	2.014070	0.359230

Frequencies

127.8968i

65.3399	161.8648	
242.0683	297.9304	435.4351
546.5696	620.8126	761.7367
795.0518	897.5472	944.9988
958.9305	1035.5865	1089.5311
1216.2505	1251.4941	1418.2637
1508.7561	1642.4265	1730.0720
1848.6106	2803.4078	3032.6111
3149.9418	3159.2550	3202.9243

i6"-i13"

N	-1.425127	0.171991	-0.292627
C	-0.567226	1.181268	0.062069
C	-1.212839	-1.010942	0.143086
C	1.085189	-1.413302	0.039375
C	1.493097	-0.172289	-0.145401
C	0.779907	1.062098	0.123249
H	-1.014793	2.164059	0.143310
H	-1.783178	-1.849488	-0.238690
H	-0.583207	-1.219152	1.019103
H	2.519116	-0.129859	-0.518400
H	1.369189	1.949503	0.308799

Frequencies

100.3633i

188.8648	282.1239	
365.6946	454.3269	558.3478
620.5991	725.6281	827.5343
860.9662	954.4602	969.6213
980.1788	1063.0984	1093.1024
1179.5801	1241.7563	1419.8230
1468.0994	1544.8990	1641.5659
1656.6295	2951.4970	3073.3248
3164.0261	3171.1129	3188.0267

i14"-i15"

C	-0.5227327936	1.4416933854	0.3256776329
N	0.459948118	2.1713911602	0.4920282343
C	-1.4646019172	-0.8950287856	0.3578159668
C	-0.4000074048	-0.0947348604	0.1786418035
C	0.9547469314	-0.5011627192	0.0802840368

C	1.8488380325	0.4980646055	0.1013355964
H	-1.5469705193	1.8251682021	0.3083947464
H	-1.3392591739	-1.9634713727	0.4507506692
H	-2.4621856154	-0.4887216617	0.4677948342
H	2.8127930641	0.5163095111	0.5905451525
H	1.7300352782	1.2101045353	-0.721024673

Frequencies

542.7095i	183.1602	329.1198
354.0124	469.4557	548.5387
585.5548	631.3610	699.5581
758.6110	815.6566	880.2329
926.8376	955.8403	1003.0608
1121.4964	1202.7870	1327.9573
1430.6953	1520.3686	1645.5225
1721.8899	3039.5087	3050.5593
3145.9408	3206.2362	3245.0780

i14"-i16"

C	-0.1516478096	1.1813518377	0.0861964656
N	0.7422073939	2.0667764641	-0.0533892499
C	-0.8041270658	-1.1706571343	0.1787567741
C	0.1669842457	-0.2599826738	0.0268624365
C	1.5432961357	-0.5979408145	-0.1976616067
C	2.7684650825	-0.7966607408	-0.3977027114
H	-1.2117102432	1.3921548477	0.2585329625
H	0.3519905428	3.0048546127	0.0144227473
H	-0.6145761297	-2.2331855768	0.1423225833
H	-1.8238302005	-0.8535312471	0.3451870565
H	2.0345820482	-1.8046075749	-0.285599458

Frequencies

528.4077i	158.6675	180.6082
224.0290	249.4671	330.7306
490.0488	514.7200	699.0250
733.9271	744.3921	860.0363
943.9258	954.6506	1107.0266
1180.1954	1325.4396	1404.3688
1454.1944	1652.7855	1696.6834
1989.0840	2394.4376	3026.2291
3156.1486	3244.5552	3472.4704

i15"-i17"

C	-0.4077111759	1.3258789691	0.3712711844
N	0.7860547157	1.7924282893	0.3282077467
C	-1.5312309674	-0.932486732	0.3319088841
C	-0.448447023	-0.1465889081	0.306526473
C	0.9548073351	-0.6435897836	0.2924879956
C	1.6332598613	0.6066314721	0.2332184303
H	-1.2701610801	1.978852972	0.4459742258
H	-1.422005582	-2.0077531889	0.2936155434
H	-2.534031468	-0.5271026423	0.3986413571
H	2.6974054006	0.7493056632	0.3757201634
H	1.5769229837	0.0432948894	-0.8337370036

Frequencies

778.5130i	174.8821	348.8342
497.3210	625.3309	689.6693
743.9506	820.8871	903.0989
916.2146	937.5223	966.2530
986.3258	1040.7438	1151.5230

1247.9383	1283.0094	1299.9517
1345.3133	1440.4076	1607.1233
1689.1518	2286.1880	3134.6856
3160.2462	3176.4009	3229.5280

i16"-i17"

C	-0.5340479111	1.3657262918	0.086686808
N	0.660088614	1.8131410311	-0.0394297857
C	-1.5832513487	-0.8804428804	0.1425765879
C	-0.4954996831	-0.1046452682	0.0386014142
C	0.9135236328	-0.4481434729	-0.1374160414
C	1.6752443328	0.6673072867	-0.1940313856
H	-1.412234361	1.9875189605	0.2076679387
H	-1.5154928253	-1.9594223186	0.1027155537
H	-2.5696812251	-0.4545491293	0.2701738072
H	1.2755238836	-1.4617867001	-0.2110136949
H	1.7726958913	2.0712331994	-0.165188202

Frequencies

1747.5421i	203.2439	292.5521
338.8882	500.7453	502.9330
691.5440	701.6129	723.6302
816.1373	838.0993	896.1263
938.3769	964.8599	988.4943
1174.6297	1229.5614	1303.7706
1450.3940	1505.5322	1554.8849
1687.5697	2340.3095	3141.8278
3176.1959	3214.1982	3227.1200

i17"-i18"

C	-0.5533879297	0.9731757766	0.3627605873
N	0.6265676738	1.4771251491	-0.164679678
C	-1.5784600551	0.2353825743	-0.336283154
C	-0.5326337629	-0.8360206406	-0.1451161193
C	0.7794116579	-0.8354885137	-0.3946630564
C	1.3951160106	0.5079837449	-0.5058040835
H	-0.6495943936	1.0382747845	1.4411746654
H	-1.7422078752	0.3907970982	-1.4010403665
H	-2.5108433038	0.1173279055	0.2016229461
H	1.3295501428	-1.7252626484	-0.6769404541
H	2.3606738353	0.6886937697	-0.971706287

Frequencies

357.4599i	302.4777	364.4092
540.3283	617.5787	728.8100
796.3015	863.5285	898.6433
922.8999	943.0836	980.3104
1029.6752	1130.0441	1167.6498
1213.1153	1288.1895	1329.0774
1418.2280	1470.3824	1571.1092
1630.9910	3079.9162	3127.9383
3142.5133	3157.2658	3164.6470

i18"-i12"

C	-0.5422846877	1.3240639182	0.1917898833
N	0.7536567187	1.4019201134	0.1835143141
C	-1.2535808293	0.1436960673	-0.2540835041
C	-0.5804758336	-1.0083274556	-0.8193083461
C	0.8456512415	-0.8405617981	-0.7294204149
C	1.4356381778	0.3116365449	-0.2888290385
H	-1.0919508343	2.1889371903	0.555569303

H	-2.3345941818	0.2153916853	-0.3433631944
H	-1.1358486946	-0.7942516994	0.488719585
H	1.486095014	-1.6404162087	-1.0849538497
H	2.5149699091	0.4245926425	-0.2905917379

Frequencies

825.0431i	139.9434	378.1615
589.2691	660.5656	689.2255
708.1031	850.3268	932.2789
962.0216	1000.2415	1033.1316
1036.1066	1072.2329	1204.4380
1220.9683	1251.5625	1378.1322
1409.4713	1462.2296	1495.6016
1624.1832	2290.8575	3105.9597
3119.8209	3130.5138	3149.7789

i15"-HCN+H₂CCCH₂

C	0.007081362	1.4528025668	0.0588489816
N	1.1013558129	1.9185963374	-0.028091573
C	-1.6618568785	-0.673699202	0.1423114169
C	-0.3729523829	-0.3963789386	0.0320441694
C	0.8417024568	-0.9531537204	-0.0995394027
C	2.0545870523	-0.5713498804	-0.2004365054
H	-0.9964670588	1.8397381794	0.1662454968
H	1.9729668183	0.6341643964	-0.1520629223
H	-2.0211236302	-1.6928743182	0.1413475936
H	-2.3983010503	0.1133121094	0.2370518413
H	3.0140804983	-1.0434035297	-0.3066800964

Frequencies

696.7617i	195.7327	287.6803
341.5982	374.8231	492.1994
558.2464	580.0716	636.2786
743.8294	785.0965	787.6248
915.2549	957.0779	1000.1851
1013.7941	1111.2220	1222.7913
1460.8072	1703.1057	1729.9712
1937.3021	1964.0841	3141.6899
3197.7531	3225.8634	3281.0164

i19"-i20"

N	-0.9801232382	-0.9325469824	0.1887475933
C	-1.1567458335	0.3385719994	0.0375967676
C	-0.0961255378	1.3038567605	0.1043590036
C	1.2053126358	0.9815382047	0.333703847
C	1.6192772609	-0.365664579	0.5286046559
C	0.9033271464	-1.401065194	0.5210904701
H	-1.8331651923	-1.4834544107	0.1132252601
H	-2.1573151274	0.727926731	-0.1525020577
H	-0.3798853387	2.3382020711	-0.0399028638
H	1.9382365823	1.7819511448	0.3668022304
H	0.8144426424	-2.4607097453	0.6112950935

Frequencies

490.5713i	128.6913	278.8504
465.8367	480.9345	529.4874
682.5611	754.6480	863.1571
865.0361	963.6902	1000.1250
1011.2771	1055.2631	1088.9702
1220.6487	1231.8653	1394.2724
1457.8980	1540.0757	1641.0578

1835.4571	3066.8451	3120.2639
3172.7505	3373.1448	3451.4963

N	1.165125	0.759353	-0.062444
C	-0.039077	1.339556	-0.003682
C	-1.215073	0.597450	-0.018973
C	-1.167638	-0.792813	0.012075
C	0.033719	-1.542344	0.008087
C	1.157350	-0.687025	-0.058128
H	-0.045416	2.421133	0.049163
H	-2.162868	1.124500	-0.026206
H	-2.117262	-1.321955	0.031080
H	2.162051	-1.065734	-0.222593
H	1.391927	0.037647	0.969389

Frequencies

1376.2607i	206.5639	302.3420
595.6909	639.4869	678.7745
742.0762	808.3860	867.6760
966.5842	1007.0874	1031.2324
1045.3807	1078.6972	1120.7959
1185.4206	1275.8015	1330.6463
1375.7140	1435.9655	1536.7964
1567.7601	2207.5112	3103.9866
3128.3889	3146.7702	3169.5060

i20"-i22"

N	-0.6478737264	-0.9362165864	0.0335144308
C	-0.9774899602	0.3580048357	-0.182205058
C	0.0036786339	1.3239816252	-0.1775349726
C	1.3246784757	0.9572606443	0.1194962274
C	1.6812375897	-0.3905748365	0.120134031
C	0.6486610889	-1.3640838135	0.0519435046
H	-1.3913589649	-1.6142492139	0.1324963667
H	-2.0237621704	0.5813484766	-0.3344502976
H	-0.2823440101	2.3547062327	-0.3417349259
H	2.0480214866	1.7359207599	0.3404862334
H	1.766378557	-1.6955951241	0.5435994602

Frequencies

1840.4806i	185.7124	345.6135
539.0098	615.3002	651.6884
721.4421	767.6630	834.0252
940.8491	987.7462	991.7127
1035.6979	1065.0289	1087.8393
1171.3313	1225.6197	1288.4484
1426.1310	1481.0634	1557.6322
1609.1425	2206.0680	3128.9077
3168.3820	3195.7131	3550.9804

i21"-i12

N	-0.5966716891	-0.9935343628	-0.3501708129
C	-0.9376234098	0.2562706444	-0.3450135871
C	-0.0226860314	1.3294715269	-0.1034076215
C	1.3062922478	1.0619223772	0.0458469568
C	1.8178781781	-0.285563968	0.1450701924
C	0.7400995779	-1.2546531332	0.0150104246
H	-1.9697368999	0.4901185561	-0.5915625419
H	-0.4013007561	2.3452753621	-0.1121000854
H	2.0168259114	1.8811195357	0.0708764482
H	0.9267919678	-1.0167882606	1.1446747729

H 1.0021759033 -2.3051872777 -0.062202146

Frequencies

549.0483i 197.9336 371.0080
597.1815 624.1241 700.5998
777.7706 873.7003 918.1706
996.7244 1005.5194 1026.4455
1041.0760 1062.1776 1144.8915
1213.6423 1241.8732 1371.0963
1397.7505 1448.2743 1527.0615
1630.7215 2479.0396 3121.3574
3134.8728 3135.4084 3159.4758

i22"-i12

N -0.6416910639 -1.1907736718 -0.0507401067
C -1.0188492551 0.0847203285 -0.2422182174
C -0.0535309706 1.0676127657 -0.2185455554
C 1.2810447696 0.7050463064 0.0023532786
C 1.640506914 -0.618740669 0.1956261562
C 0.6532278703 -1.6147150693 0.1710962825
H -0.482660909 -2.3525108584 0.0960769645
H -2.0687487005 0.2850330466 -0.4071146268
H -0.3282424294 2.1020764834 -0.3690232347
H 2.0381097308 1.48014171 0.0204911084
H 2.6752350437 -0.885179372 0.3646379508

Frequencies

2021.0910i 157.9261 401.0930
462.2959 617.0285 653.9794
734.4975 775.1464 915.1157
974.5024 996.3221 1028.6738
1045.0948 1061.1920 1110.3685
1180.3987 1187.6122 1240.9620
1437.8159 1458.0739 1565.0642
1614.5544 2405.9157 3151.7609
3177.6916 3180.2558 3196.3608

Products

ortho-C₅H₄N

N -0.8052586645 1.3487655046 0.
C 0.4738599752 1.3391442365 0.
C -1.4658591521 0.175798094 0.
C -0.7747361548 -1.02423758 0.
C 0.6207982594 -1.002375505 0.
C 1.2899162394 0.2161618929 0.
H -2.5475007783 0.2145866708 0.
H -1.3151371905 -1.9605094773 0.
H 1.1801732349 -1.9297520623 0.
H 2.3678182313 0.2796332259 0.

Frequencies

386.4512 427.6511 578.2906
663.7073 716.6818 755.9484
894.0024 956.8675 974.8163
1011.9991 1037.4618 1074.9040
1110.6484 1167.9487 1261.9472
1332.1845 1427.1609 1503.2466
1571.3300 1664.1018 3163.0009
3172.6225 3195.2661 3202.6968

meta-C₅H₄N

N -0.8285418085 1.363456887 0.

C	0.5136657578	1.3906806876	0.
C	-1.4393610315	0.1797228983	0.
C	-0.771496371	-1.0404845127	0.
C	0.6249629432	-1.0280134795	0.
C	1.2132000748	0.2083194404	0.
H	0.9884640476	2.3631723026	0.
H	-2.523118012	0.2070303206	0.
H	-1.323226523	-1.9715969041	0.
H	1.1967559225	-1.9471426402	0.

Frequencies

390.7281	424.5636	580.7812
662.5875	692.6503	788.5788
927.0698	950.9567	991.2707
998.8739	1047.7995	1066.2773
1109.8340	1203.9497	1260.5414
1331.6211	1440.5374	1471.8003
1542.3851	1612.8164	3150.1283
3166.5417	3171.4924	3183.6070

para-C₅H₄N

N	-0.828993529	1.3586896001	0.
C	0.5011375049	1.3699871214	0.
C	-1.447473975	0.181108184	0.
C	-0.7753871027	-1.0486822913	0.
C	0.5898289438	-0.9667174251	0.
C	1.2872584859	0.2097682587	0.
H	0.979766716	2.3438109947	0.
H	-2.532388077	0.2010170088	0.
H	-1.3238796952	-1.9805952863	0.
H	2.3668537283	0.2711618349	0.

Frequencies

380.1911	446.7267	618.8660
645.2008	717.2548	772.4021
832.1109	968.6583	982.5181
991.0188	1041.5333	1075.5029
1080.5928	1230.0602	1265.5323
1322.6611	1409.1523	1476.3033
1539.0335	1617.6045	3139.1489
3141.6232	3183.9297	3185.6157

Reactants

C₃H₃

C	1.335257	0.000000	0.
C	-1.248944	0.000000	0.
C	0.115295	0.000000	0.
H	2.396116	0.000000	0.
H	-1.802881	0.928035	0.
H	-1.802881	-0.928035	0.

Frequencies

354.6849	407.3892	463.8420
632.8663	691.1253	1033.7510
1090.2007	1459.7879	2011.1814
3142.9117	3231.8145	3462.5430

H₂CCN

N	-1.353539	0.000000	0.0
C	1.189313	0.000000	0.0
C	-0.187231	-0.000000	-0.0
H	1.731142	-0.9333625	0.0

H	1.731142	0.9333625	0.0
Frequencies			
384.6883	435.8502	677.7500	
1035.1990	1058.8252	1447.2572	
2130.2879	3162.0467	3264.3476	
<i>n</i> -C ₄ H ₃			
C	0	0.000000	0.653495
C	0	-0.501531	1.745923
C	0	0.614632	-0.632781
C	0	-0.057593	-1.762773
H	0	-0.947673	2.708670
H	0	1.702598	-0.652455
H	0	-1.087974	-2.079399
Frequencies			
214.9481	344.5614	512.5788	
648.1910	680.2621	707.9643	
855.3546	875.0441	991.7645	
1269.5155	1624.6148	2198.7835	
3096.4447	3240.8951	3470.1950	
<i>i</i> -C ₄ H ₃			
C	-0.000060	-0.752647	0.000000
C	-0.000192	-1.981606	0.000000
C	0.000000	0.562640	0.000000
C	0.000193	1.865203	0.000000
H	-0.000204	-3.042414	0.000000
H	-0.922684	2.440573	0.000000
H	0.923245	2.440295	0.000000
Frequencies			
84.5647	230.5300	272.9127	
379.8248	544.4460	636.5348	
891.6670	901.8948	980.5452	
1438.3278	1800.7049	2014.6555	
3067.5758	3126.4778	3461.1248	
H ₂ CN			
H	0.000005	-1.075995	-0.934650
H	0.000005	-1.075995	0.934650
C	-0.000001	-0.500874	-0.000000
N	-0.000001	0.736747	0.000000
Frequencies			
934.6859	994.8119	1378.3835	
1724.6088	2959.8511	3012.2841	

References

- 1 Sun, B. J. *et al.* Theoretical study on reaction mechanism of ground-state cyano radical with 1, 3-butadiene: prospect of pyridine formation. *J. Phys. Chem. A* **118**, 7715-7724 (2014).
- 2 Parker, D. S. N. *et al.* On the formation of pyridine in the interstellar medium. *Phys. Chem. Chem. Phys.* **17**, 32000-32008 (2015).
- 3 Parker, D. S. N. & Kaiser, R. I. On the formation of nitrogen-substituted polycyclic aromatic hydrocarbons (NPAHs) in circumstellar and interstellar environments. *Chem. Soc. Rev.* **46**, 452-463 (2017).
- 4 Morales, S. B. *et al.* A Crossed Molecular Beam, Low-Temperature Kinetics, and Theoretical Investigation of the Reaction of the Cyano Radical (CN) with 1, 3-Butadiene (C₄H₆). A Route to Complex Nitrogen-Bearing Molecules in Low-Temperature Extraterrestrial Environments. *Astrophys. J.* **742**, 26 (2011).
- 5 Loison, J. C. *et al.* The neutral photochemistry of nitriles, amines and imines in the atmosphere of Titan. *Icarus* **247**, 218-247 (2015).
- 6 Recio, P. *et al.* A crossed molecular beam investigation of the N(²D) + pyridine reaction and implications for prebiotic chemistry. *Chem. Phys. Lett.* **779**, 138852 (2021).
- 7 Loison, J. C., Dobrijevic, M. & Hickson, K. M. The photochemical production of aromatics in the atmosphere of Titan. *Icarus* **329**, 55-71 (2019).
- 8 Vuitton, V., Yelle, R. V. & Cui, J. Formation and distribution of benzene on Titan. *J. Geophys. Res.* **113** (2008).
- 9 Anicich, V. G. An index of the literature for bimolecular gas phase cation-molecule reaction kinetics. (2003).
- 10 Bolovinos, A., Tsekeris, P., Philis, J., Pantos, E. & Andritsopoulos, G. Absolute vacuum ultraviolet absorption spectra of some gaseous azabenzene. *J. Mol. Spectrosc.* **103**, 240-256 (1984).
- 11 Leach, S., Jones, N. C., Hoffmann, S. V. & Un, S. VUV Absorption Spectra of Gas-Phase Quinoline in the 3.5–10.7 eV Photon Energy Range. *J. Phys. Chem. A* **122**, 5832-5847 (2018).
- 12 Prather, K. A. & Lee, Y. T. The Photodissociation of Pyridine at 193 nm. *Israel journal of chemistry* **34**, 43-53 (1994).

- 13 Lin, M.-F. *et al.* Photodissociation dynamics of pyridine. *J. Chem. Phys.* **123**, 054309 (2005).
- 14 Benne, B., Dobrijevic, M., Cavalié, T., Loison, J.-C. & Hickson, K. M. A photochemical model of Triton's atmosphere with an uncertainty propagation study. *Astron. Astrophys.* **667**, A169 (2022).